A Model of Selected Human Forearm Muscles: Estimation, Scaling and Application

by

Stephan Riek

B.Sc. (Kinesiology), Simon Fraser University, 1990
M.Sc. (Kinesiology), Simon Fraser University, 1991

THESIS SUBMITTED IN PARTIAL FULFILLMENT OF
THE REQUIREMENTS FOR THE DEGREE OF
DOCTOR OF PHILOSOPHY

in the School of Kinesiology

SIMON FRASER UNIVERSITY

April, 1996

APPROVAL

NAME: Stephan Riek

DEGREE: Doctor of Philosophy

TITLE OF THESIS: A Model of Selected Human Forearm Muscles: Estimation, Scaling and Application

EXAMINING COMMITTEE:

Chair: Dr. John Dickinson

Dr. Arthur Chapman
Senior Supervisor
Professor, School of Kinesiology

Dr. Ted Milner
Assistant Professor, School of Kinesiology

Dr. Tom Calvert
Professor & Director, Centre for Systems Science

Dr. James Morrison
Professor, School of Kinesiology
Internal Examiner

Dr. Stuart McGill, Associate Professor
Departments Kinesiology/Mechanical Engineering
University of Waterloo
External Examiner

Date Approved: April 16th 1996

PARTIAL COPYRIGHT LICENSE

I hereby grant to Simon Fraser University the right to lend my thesis, project or extended essay (the title of which is shown below) to users of the Simon Fraser University Library, and to make partial or single copies only for such users or in response to a request from the library of any other university, or other educational institution, on its own behalf or for one of its users. I further agree that permission for multiple copying of this work for scholarly purposes may be granted by me or the Dean of Graduate Studies. It is understood that copying or publication of this work for financial gain shall not be allowed without my written permission.

Title of Thesis/Project/Extended Essay

A Model of Selected Human Forearm Muscles: [redacted] Estimation, Scaling and Application

Author: _____
(signature)

STEPHAN RIEK
(name)

11 March, 1996
(date)

ABSTRACT

In general, only net torque about a joint can be measured experimentally. This torque, however, is often made up of contributions from several muscles that cross the joint. Currently, there is no non-invasive method to measure individual muscle forces in a complex musculoskeletal system. The general purpose of this thesis was to construct a model to estimate force of a single muscle which is part of a more complex multiple-muscle, multiple-degree of freedom system.

Muscle specific parameters for a Hill-type model of a single-muscle, single-degree of freedom system (flexor pollicis longus (FPL) acting on the distal phalanx of the thumb) were determined in several experiments designed to establish the isometric force-length relationship of the contractile component (CC), force-velocity relationship of the CC and force-length relationship of the series elastic component (SEC) for one subject. These relationships were incorporated into an iterative process which resulted in a computer simulation of the force producing capabilities of FPL with muscle activation, from electromyography (EMG), as input. The force outputs from the simulation were compared with experimental results of both isometric and dynamic voluntary contractions of FPL.

Using magnetic resonance images, the relationships obtained for FPL were scaled according to muscle size and shape and were used to develop a computer simulation of the extensor carpi radialis brevis (ECRB) muscle. Physiological cross sectional area was used to scale maximum isometric force capability (Po) and fibre length was used to scale maximum shortening velocity (Vmax). The model of ECRB was evaulated by comparing the simulation output with various contractions evoked by electrical stimulation of ECRB in isolation. The model of ECRB was applied to data describing the kinematics and EMG profiles of novice and advanced tennis players so that muscle force in each group could be evaluated. The implications for sustaining lateral epicondular injuries based on predictions of force in ECRB were discussed.

ACKNOWLEDGEMENTS

There are many people I would like to thank for their support, encouragement, insight and friendship over the past several years. These are but a few:

Arthur - for allowing me to explore my own interests and abilities.

Ted - for keeping me honest and helping to make this a better thesis.

Parveen - for her unyielding support as my academic "mother".

Richard - for setting and example of excellence that I've strived to achieve.

Winston - for helping me keep things in perspective with a few jam sessions.

Kines soccer - for always winning the championship whenever I was away.

My lab mates Helen, MA, Andy, Yves - for sharing a cup of coffee and discussion.

My family - for their continuing support, encouragement and love that has meant more to me than I had ever realized.

Sue - when I saw you my life changed and I found the purpose and direction to finish.

TABLE OF CONTENTS

APPROVAL ii

ABSTRACT iii

ACKNOWLEDGEMENTS iv

LIST OF TABLES ix

LIST OF FIGURES x

Chapter 1 1

1.0 General Introduction 1

2.0 General Purpose 4

Chapter 2: Model Parameters for Flexor Pollicis Longus 6

1.0 Introduction 6

1.1 The Contractile Component (CC) 7

1.2 Series Elastic Component (SEC) 11

1.3 Parallel Elastic Component (PEC) 13

1.4 Lines of Action 13

1.5 Moment Arm 14

1.6 Purpose 15

2.0 Methods 16

2.1 Morphometric Characteristics 16

2.2 CC Force-Length Relationship 17

2.3 CC Force-Velocity Relationship 18

2.4 SEC Tendon Characteristics 19

2.5 SEC Fibre Characteristics 19

3.0 Results 21

3.1 Morphometric Characteristics 21

3.2 CC Force-Length Relationship 22

3.3 CC Force-Velocity Relationship 23
3.4 SEC Tendon Characteristics 26
3.5 SEC Fibre Characteristics 28
4.0 Discussion 33
4.1 Morphometric Characteristics 33
4.2 CC Characteristics 35
4.3 SEC Characteristics 37
5.0 Summary 40
Chapter 3: Model Development and Scaling 41
1.0 Introduction 41
1.1 Muscle Architecture and Scaling 41
1.2 The Wrist Joint 42
1.3 Wrist Musculature 44
1.4 Functional Studies of Wrist Musculature 44
1.5 Purpose 46
2.0. Methods 47
2.1 Morphometric Characteristics 47
2.2 The Model 48
2.3 The Simulation Routine 50
2.4 Scaling 51
2.5 Model Evaluation 53
2.5.1 Isomteric Contractions of FPL 53
2.5.2 Dynamic Contractions of FPL 54
2.5.3 Electrical Stimulation of ECRB 55
3.0 Results 57
3.1 Morphometric Characteristics 57
3.2 Scaling Relationships to ECRB 57

3.3 Model Evaluation 60
3.3.1 Isometric Contractions of FPL 60
3.3.2 Dynamic Contractions of FPL 66
3.3.3 Electrical Stimulation of ECRB 69
4.0 Discussion 72
4.1 Morphometric Characteristics and Scaling 75
4.2 Model Evaluation 75
4.2.1 Isometric Contractions of FPL 75
4.2.2 Dynamic Contractions of FPL 77
4.2.3 Electrical Stimulation of ECRB 77
5.0 Summary 79
Chapter 4: Force in Extensor Carpi Radialis Brevis During a Backhand Tennis Stroke: Implications for Injury 80
1.0 Introduction 80
1.1 Purpose 81
2.0 Methods 82
3.0 Results 83
3.1 Kinematics 83
3.2 ECRB Muscle Force 85
4.0 Discussion 92
Chapter 5: Limitations 94
Appendix A: Sensitivity Analysis 96
A1.1 Activation Time Constant (τ_{rise}) 96
A1.2 Deactivation Time Constant (τ_{fall}) 97
A1.3 Fibre Stiffness (k_{SECf}) 98
A1.4 Hill's Parameter ***a*** 100
A1.5 Hill's parameter ***b*** 102

A1.6 Summary 104

Chapter 6: References. 106

LIST OF TABLES

Table 2.1 - Characteristics Describing the FPL Muscle and Tendon Obtained from Magnetic Resonance Images 19

Table 3.1 - Morphometric Characteristics of Extensor Carpi Radialis Breivs Determined from Magentic Resonance Images Compared with Values Obtained in the Literature 55

Table A1 - Changes in Peak Force as a Function of Changes in Fibre Stiffness 100

Table A2 - Changes in Peak Force as a Function of Changes in a 102

Table A3 - Changes in Peak Force as a Function of Changes in b 104

LIST OF FIGURES

Figure 2.1 - Normalized Force-Length Relationship for the CC.....20

Figure 2.2 - Torque, Angular Velocity and Angular Displacement Profiles Recorded During a Single Isometric Contraction.....22

Figure 2.3 - Force-Velocity Relationship for the CC for Various Levels of Activation...23

Figure 2. 4 - Stiffness-Force Relationship for FPL Tendon.....25

Figure 2.5 - Stress- Strain Relationship for the FPL Tendon.....26

Figure 2.6 - Stiffness-Force Relationship for Fibre Series Elasticity.....27

Figure 2.7 - The Slope of the Stiffness-Force Relationship as a Function of Length Change.....28

Figure 2.8 - Force-Length Relationship for the SEC_f as a Function of Activation.....29

Figure 2.9 - Stiffness-Activation Relationship for the SEC_f.....29

Figure 2.10 - Total Angular Stiffness Versus Torque for the Distal Phalanx of the Thumb 36

Figure 3.1 - Diagram of Cross Section Through the Right Wrist, Viewed from Distal to Proximal, Drawn from Magnetic Resonance Images.....44

Figure 3.2 - Schematic Representation of the Muscle Model Showing the Contractile Component in Series with Two Elastic Components.....46

Figure 3.3 - Flow Diagram Displaying the Iterative Process for Calculating Muscle Force.....48

Figure 3.4 - Diagram Showing the Placement of Force Transducers for Recording Torque About the Wrist During Electrical Stimulation of ECRB.....53

Figure 3.5 - Force-Velocity Relationship for ECRB Obtained by Scaling the Force and Velocity Axes as Indicated.....56

Figure 3.6 - Force Recorded for a Single, SLOW Rise Isometric Contraction of FPL...58

Figure 3.7 - Force Recorded for a Single, FAST Isometric Contraction of FPL.....59

Figure 3.8 - Muscle Force as a Function of Rectified, Low-Pass Filtered EMG for Experimental and Model Results for SLOW Isometric Contractions.....60

Figure 3.9 - Actual Peak Force as a Function of Peak Force Predicted by the Model for SLOW Contractions.....61

Figure 3.10 - Muscle Force as a Function of Stimulation for Experimental and Model Results for FAST Isometric Contractions 62

Figure 3.11 - Actual Peak Force as a Function of Peak Force Predicted by the Model...63

Figure 3.12 - Angular Position, Velocity, and Acceleration for I_{small} Condition.....64

Figure 3.13 - Angular Position, Velocity, and Acceleration for I_{med} Condition.....65

Figure 3.14 - Angular Position, Velocity, and Acceleration for I_{large} Condition.....66

Figure 3.15 - Extensor and Radial Deviation torque Recorded (b) and Predicted by the Model (c) for ECRB in Response to Electrical Stimulation.....67

Figure 3.16 - Experimental and Model Prediction of the Response of ECRB to a Quick Stretch of the Wrist.....68

Figure 3.17 - Moment Arms of ECRB Determined from the MRI Scans in this Study Compared with Values Reported in the Literature.....70

Figure 4.1 - EMG and Wrist Kinematics of Novice and Advanced Players Performing a Backhand Tennis Stroke.....81

Figure 4.2 - Muscle Force in ECRB Predicted by the Model for Advanced and Novice Groups.....82

Figure 4.3 - Muscle Length Change from Resting Length as a Result of Wrist Kinematics of Advanced and Novice Groups.....83

Figure 4.4 - Effects of Wrist Kinematics on Predicted Muscle Force for the Advanced Group.....84

Figure 4.5 - Effects of Wrist Kinematics on Predicted Muscle Force for the Novice Group 85

Figure 4.6 - Muscle Length (a), Tendon Length (b), Fibre Length (c), Contractile Component Length (d), and Fibre Series Elastic Component Length (e) During Backhand Stroke of Novice Group.....87

Figure 4.7 - Muscle Length (a), Tendon Length (b), Fibre Length (c), Contractile Component Length (d), and Fibre Series Elastic Component Length (e) During Backhand Stroke of Advanced Group 88

Figure A1 - Model prediction of force for activation rise time constant +/- 50% of original.....97

Figure A2 - Model prediction of force for deactivation time constant +/- 50% of original.....98

Figure A3 - Model prediction of force for fibre stiffness +/- 50% of original.....99

Figure A4. - Percent change in peak force as a function of percent change in fibre stiffness..... 100

Figure A5. - Model prediction of force for simulations using values of ***a*** +/- 50% of original..... 101

Figure A6 - Percent change in peak force as a function of percent change in ***a***..... 102

Figure A7. - Model prediction of force for simulations using values of ***b*** +/- 50% of original..... 103

Figure A8. - Percent change in peak force as a function of percent change in ***b***..... 104

Chapter 1

1.0 General Introduction

The complexity and versatility of human movement has captured the attention of investigators for centuries. Humans can demonstrate a wide range of movements from the simple to the complex, all the while controlling the complex interactions between muscles, bones and joints in a seemingly effortless manner. In order to understand such a complex system, the interaction between the neural, mechanical and muscular properties during human movement must be considered.

One avenue of investigation has been to understand better the fundamental aspects of multisegmental motion and intermuscular coordination in human movements. Humans have available to them multisegmental limbs, many muscles crossing single or multiple joints and even subsections of muscles all of which must be controlled in order to perform tasks successfully. As a result, the central nervous system is forced to deal with a vast number of degrees of freedom. It has been suggested that the basic problem in motor control is overcoming this problem of redundant degrees of freedom (Bernstein, 1967). Even though the human system has seemingly endless degrees of freedom, there are likely to be constraints, which can be used by the central nervous system (CNS), to reduce the actual degrees of freedom of the endpoint of a multi-joint limb. These constraints may be biomechanical (biarticular muscles, geometric constraints; see van Ingen Schenau 1989; Zajac and Gordon, 1989) and/or physiological (inter-muscular reflexes, motor unit recruitment order, motor unit task groups). In addition, there may also be constraints yet to be discovered which may lead to a unique solution for a given motor task. How can the CNS choose among the seemingly infinite patterns of control variables which may lead to a desired outcome? Or, perhaps more importantly, how can we establish a window into the human system to help us understand this process?

In order to answer this second question it is often useful to determine how muscles produce torque about a joint. Direct measurement of muscle forces inside the human body are rare because of the obvious invasive nature and requirements of sophisticated instrumentation and recording techniques. In animals however, techniques have been used extensively to determine muscle force and changes in both muscle fibre length and whole muscle length during voluntary contractions in awake animals (Hoffer et al 1989, Herzog and Leonard, 1981).

Inverse dynamics has been perhaps the most widely used method of estimating internal muscle forces in humans. The method is essentially the same for all joints in the body. It is based on the representation of the human body as a set of rigid segments connected by idealized joints. All forces acting between two adjacent segments are represented by a resultant or net force and one resultant or net moment. Using this technique, the forces and moments are inferred from the kinematics caused by them, which is *inverse* to the actual operation of the system. This force or moment represents the sum of all load-carrying structures between two adjacent segments. It is often desirable to separate the resultant force and moment into forces and moments attributed to individual anatomical structures. With the inverse dynamics analysis we often face an indeterminate problem when the equations generated from an inverse dynamic analysis do not provide sufficient information to solve for all unknowns. Hence, alternate techniques must be used to help eliminate the number of unknowns in an equation.

There are at least two methods available to solve this indeterminate problem: reduction and optimization. Using the reduction method, the number of unknowns is simply reduced until it is equal to the number of equations. This can be done by simplifying the anatomical structures, grouping muscles with similar function into single equivalent muscles, or separating the movement into distinct phases. Obviously, this results in a model that is less representative of the actual system.

Optimization has been a popular method of selecting a unique solution to an indeterminate problem. Several optimizing criteria or cost functions have been used such as minimizing muscle fatigue, jerk, muscle force or stress. These static optimization schemes, however, cannot predict the load sharing between synergist muscles during dynamic contractions unless some knowledge of the dynamics of force generation is included. Dynamic optimization uses the mechanical properties of muscle to help solve the indeterminate problem. In this way, the number of possible solutions is reduced to those consistent with physiological and mechanical properties of muscles. The problem is still underdetermined, so optimization criteria must still be used to obtain a unique solution. The optimization criteria selected by investigators may lead to erroneous suggestions that the CNS also uses these criteria. However, a criterion that seems successful in one type of task may be inappropriate in other tasks. It is perhaps more useful to consider that the CNS ultimately optimizes for successful execution of a task rather than optimizing for some arbitrary experimental criterion.

As an antecedent to inverse dynamics, direct or forward dynamics can be used to estimate muscle forces in human movement. In forward dynamics the "experiment" is conducted using a computer model of the human musculoskeletal system. This type of analysis has several advantages because the trials are perfectly reproducible, it provides understanding by inclusion of the underlying causal mechanisms, and it allows precise control of all variables. A computer model must relate the most important parameters of the system but need not necessarily represent more than is required for a satisfactory approximation of its normal mechanical function. Prediction by means of a model should be checked experimentally and the model corrected based on this check. Confirmation of models in human biomechanics is difficult because shapes and material properties cannot be quantified accurately and are subject to continuous changes by metabolic processes (e.g. growth, aging, adaptation to changing loads). Parameters in the model can be adapted in

order to match qualities of the real system. Some parameters of a model may be measured accurately, whereas for others, only the order of magnitude can be estimated.

2.0. General Purpose

In general, only net torque about a joint can be measured experimentally. This torque is often made up of contributions from several muscles which cross the joint. Currently, there is no non-invasive method to measure experimentally individual muscle forces and moments in a complex musculoskeletal system. The general purpose of this thesis was to estimate force in a complex multiple-muscle, multiple-degree of freedom system from measures of electromyography (EMG) and kinematics. To this end, a model of the muscle will be used with muscle specific parameters obtained from one of the few single-muscle, single-degree of freedom systems which can be isolated experimentally.

This thesis was divided into 3 sections, each with a specific purpose. The purpose of chapter 2, was to determine the muscle specific parameters for a Hill type muscle model of a (flexor pollicis longus (FPL) acting on the distal phalanx of the thumb). It was hypothesized that, since FPL is a single-muscle, single-degree of freedom system, the force-length-velocity properties of FPL could be measured directly.

Chapter 3 detailed a computer model of the FPL muscle and evaluated the model by comparing the torque about the distal phalanx of the thumb predicted by the model with the actual torque recorded in isometric contractions. The model's prediction of dynamic contractions was evaluated by comparing the kinematics of the distal phalanx on the thumb predicted by the model with the actual kinematics recorded for contractions against three moments of inertia. Also, it was hypothesized that the relationships describing FPL could be extended to another muscle (extensor carpi radialis brevis(ECRB)) by scaling the

parameters with respect to muscle size and shape to produce a model of ECRB acting at the wrist.

In Chapter 4, the model of ECRB was used to simulate the force produced in ECRB during a backhand tennis stroke for both novice and advanced players. It was hypothesized that the model prediction of muscle force and muscle kinematics would display both qualitative and quantitative differences between novice and advanced player that would help explain why novice players are at greater risk of developing overuse injuries.

Chapter 2

Model Parameters for Flexor Pollicis Longus

1.0 Introduction

The interphalangeal joint of the thumb is a simple, one degree of freedom, bicondylar joint which allows flexion/extension of the distal phalanx of the thumb with an axis of rotation through the centre of curvature of the condylar head of the proximal phalanx (Toft and Berme, 1980). On each side of the joint are collateral ligaments which keep the articular surfaces together and restrain their movements. Any side to side movement is passively resisted by the joint surface and the ligaments (Toft and Berme, 1980). Flexion of the distal phalanx is accomplished by contraction of the flexor pollicis longus (FPL) muscle. FPL is a unipennate muscle situated on the radial side of the forearm. It arises from the grooved anterior surface of the shaft of the radius, just below the radial tuberosity and oblique line. The fibres terminate in a flattened tendon which passes beneath the annular ligament and inserts into the base of the distal phalanx of the thumb. This joint is unusual in that FPL is the sole contributor to flexion of the distal phalanx of the thumb, which affords a unique opportunity to study the mechanical function of this muscle in isolation. Specifically, the mechanical properties of FPL can be determined experimentally and these properties can be used to determine the efficacy of a model representation of this system.

The phenomenological model of muscle proposed by Hill (1938; 1970) consists of a contractile component (CC) that is in series with an elastic component (SEC) and in parallel with an elastic component (PEC). The CC is a theoretical construct that represents the force of contraction in skeletal muscle. Force production by the CC is a function of several factors, namely; activation, length, velocity and history of contraction. In the

SEC, force production is a function of muscle length and activation. In the PEC, force is a function of muscle length only.

1.1 The Contractile Component (CC)

The steady state property of muscle tissue is defined by its isometric force-length (FL) relationship (Zajac, 1989). When a muscle fibre is stimulated under isometric conditions at a variety of lengths, the resulting tension is small at extremes of length and maximal in between these extremes. The result is a characteristic inverted "U" shaped curve between length and tension. This fundamental property of muscle is thought to be due to the amount of overlap between thin and thick filaments as predicted by the sliding filament theory (Gordon et al., 1966).

On the muscle level, additional structural factors such as the fibre length relative to the total muscle length and the arrangement of fibres within the muscle must be considered (Woittiez et al., 1984). On the muscle-tendon level, force-length properties are further influenced by the ratio of fibre length to tendon length and the force elongation properties of tendon contributing to the series elastic elements (Zajac 1989).

The physiological operating range for whole muscle lies well within the range where zero force is produced (Winters, 1990; Herzog et al., 1992) with some muscles operating on the ascending limb of the FL curve while others operate on the descending limb during certain movements (Cutts, 1988; Mai and Lieber, 1990; Herzog et al., 1991). Herzog et al., (1992) demonstrated that isometric forces of cat triceps surae tend to increase for increasing muscle lengths, suggesting that they operate primarily on the ascending limb of the FL curve. In contrast, sarcomeres in the frog semitendinosus muscle operate primarily on the descending part of the FL curve (Mai and Lieber, 1990), which has a decreasing isometric force potential for increasing muscle length. Furthermore, human rectus femoris muscles were found to operate on the ascending limb of the FL curve for high-performance runners and on the descending limb for high-performance cyclists

(Herzog et al., 1991). Although muscles operating on the descending limb of their force length relationship tend to instability, the interaction between length changes and moment arm changes must be considered to understand the effects on resultant joint torque. Also, muscle parallel elasticity must be considered. Although individual sarcomeres may be shown to operate on both the ascending and descending limbs of their force-length curves, the whole muscle may still show a positive slope for its overall force length curve. These results suggest an interrelation between isometric force potential and functional demands. Muscles that tend to operate on the ascending limb of the FL relation have an isometric force potential for increasing muscle lengths, and a decreased isometric force potential for decreasing muscle lengths. Therefore, it appears to be an advantage if a muscle operating on the ascending limb of the FL curve increases its force during a functional task while elongating and decreases its force while shortening and vice versa for a muscle operating predominantly on the descending limb of the FL relation (Herzog et al., 1992).

Although related to muscle energetics by Hill (1938), the CC force-velocity relation is essentially a fit to experimental data. This hyperbolic relationship between force and velocity of shortening can described by the Hill equation:

$$(P+a)(V+b) = (P_0+a)b,$$

where P = force, V = velocity of shortening, P_0 = maximal isometric force, a and b = constants with dimensions of force and velocity respectively.

When empirical FV relations are constructed for lengths less than optimal length (L_0), the velocity at which no tension can be sustained is found by extrapolation to be less than maximum shortening velocity (V_{max}) (Zajac, 1989). However, the sliding filament theory predicts that the velocity-axis intercept should be independent of sarcomere length (Huxley, 1974). Some experiments on single fibres, however, suggest that the velocity-axis intercept is both length and activation dependent, especially when muscle length and

activation deviate significantly from L_O and maximal respectively (Zajac, 1989). Edman (1979) has shown that only at very short lengths does maximum velocity of sarcomere shortening diminish. Similar results were obtained by Hatcher and Luff (1986) on cat flexor digitorum longus and soleus muscles which showed a decline in maximum shortening velocity at extremes of muscle lengths only.

Despite this controversy, many investigators who model muscle to study muscular coordination choose to assume that the velocity-axis intercept is constant (Hatze, 1977; Pierrynowski and Morrison, 1985) while others assume that the intercept decreases with decreasing length and activation (Hof and van den Berg, 1981). It should be noted that some scaling of V_{max} would be expected for muscles of mixed fibre type. Assuming that motor units are recruited according to size (Henneman et al., 1965), slower fibres are active at low activation while faster fibres are recruited with increasing activation. This would result in a overall shift of the force-velocity relationship of the muscle to higher V_{max}, with increasing activation. This issue may not be functionally important at the muscle coordination level since muscle neither produces any power at zero force nor exists in a state near zero force for very long, or may never achieve V_{max}.

The shape of the FV relation during eccentric contractions is also important in simulating human movement since muscle often lengthens during contraction (eg. while descending stairs or decelerating to a stop). The shape of the eccentric portion of the FV curve is quite different than the concentric portion and it has been demonstrated that lengthening muscle can generate forces higher than Po. Harry et al. (1990) performed experiments on isolated frog muscle where shortening and lengthening velocities were imposed and corresponding forces were measured. Maximum force during lengthening was found to be approximately 1.5 times Po, but others have used both higher and lower values (Winters, 1990).

It is clear that muscle can produce force from zero activation to some high level of activation. It has been demonstrated that muscle force is under the influence of the size

principle in a variety of contractions (Henneman et al., 1965; Milner-Brown et al., 1973; Riek and Bawa, 1992) This means that small, slow twitch motor units are recruited first followed by larger, fast twitch motor units. Consequently, a measure of activation which is based upon numbers of active motor units and their frequencies of firing will exhibit a complex relationship to force produced (Chapman, 1985).

One expression of the level of activation is termed "active state" (Hill, 1970). Active state is the amount of force that a muscle can generate when in an isometric contraction (i.e., CC is neither shortening nor lengthening). This implicitly gives a linear relation between active state and force. Active state can be considered as the output of the excitation-contraction coupling dynamics and the input to the CC (Winters, 1990). Others have defined active state as the relative amount of calcium bound to troponin (Ebashi and Endo, 1968). This definition in terms of calcium dynamics, is considered a conceptual assumption for Huxley-type models and, in fact, may be inappropriate in a lumped parameter model.

For physiological temperatures, it has been suggested that activation time is in the order of 10 ms and deactivation time on the order of 50 ms (Winters, 1990). Active state dynamics can be adequately represented by a first-order system such that activation level represents the isometric force produced as a percentage of the maximal isometric force (Caldwell, 1987). The simplest approach for modeling this dynamic process has been to assume unidirectional flow and first-order dynamics in which either the activation/deactivation time constants are the same or there are two time constants; one for activation and one for deactivation (Zajac, 1989, Winters 1990, Pandy et al., 1992). Winters and Stark (1985) suggested that these time constants be scaled to muscle fibre type (longer time constants for slow type fibres) and muscle size (longer time constants in larger muscle volumes). There is also evidence that activation is a function of muscle length (Rack and Westbury, 1969). The reduced response to stimulation at shorter lengths may be a result of diminished transmission of the electrical volley in the T-tubules due to

compression (Rack and Westbury, 1969) or a reduction in the affinity of troponin for calcium at shorter muscle lengths (Lambert et al., 1979).

1.2 Series Elastic Component (SEC)

The series elastic component has been modelled as a spring with either non-linear or linear characteristics, determined by using several experimental techniques. Hill (1970) tetanized isolated frog muscle then allowed it to shorten at a controlled speed while recording force. This force was used to determine the velocity of shortening of the CC from the FV curve. The difference between CC shortening velocity and the velocity of the muscle represented the shortening velocity of the SEC. SEC velocity could then be integrated to determine SEC length which was compared to force.

Jewel and Wilkie (1958) developed a technique of quick release from tetanus to examine the relationship between force and length of the SEC in an isolated muscle. The resulting displacement-time profile showed a rapid acceleration followed by a linear phase whose slope represented the shortening velocity. The linear phase of the shortening was extrapolated back to the ordinate at time of release. The magnitude of the intercept represented the amount of shortening of the SEC for a given load. This procedure was repeated with a variety of loads to yield the length-tension curve for the SEC.

A third technique may be referred to as an isometric calculation method in which the properties of the SEC were determined from the rate of rise of tension during an isometric contraction (Wilkie, 1950; cf. Hill, 1970). Since the CC and SEC are in series, the rate of change of force with respect to time (dF/dt) is equal to:

$$\delta F/dx \bullet \delta x/\delta t + \delta F/\delta a \bullet \delta a/\delta t + \delta F/\delta v \bullet \delta v/\delta t$$

If activation (a) and velocity (v) are held constant, this equation reduced to:

$$dF/dt = \delta F/\delta x \bullet \delta x/\delta t.$$

where the rate of change of force with respect to time is equal to the rate of change of force with respect to length multiplied by the rate of change of length with respect to time.

The instantaneous stiffness of the SEC (dF/dx) could then be calculated if the velocity of shortening of the CC (dx/dt), at the same force, was determined from the force-velocity relationship. Each of these techniques have produced concave upward length-tension curves for the SEC with peak extension between approximately 2% and 8% of SEC length (Winters, 1990).

The structural components of the SEC are thought to reside in the tendinous structures (including intramuscular and extramuscular tendon and aponeurosis) which behave as undamped elastic springs, in the cross bridges whose stiffness is a function of activation, and in the Z-bands and contractile filaments themselves whose stiffness is a function of force (Winters, 1990). Zajac (1990) argues that the SEC of the muscle fibre is negligible when compared with that of the tendon and therefore, can be eliminated for modelling purposes. However, SEC of the muscle fibre is variable with activation and at high activation may become more stiff than the tendon (Hoffer et al., 1989).

The series elasticity attributed to the tendon (SEC_t) can be modelled separately from that of the muscle fibres (SEC_f) and can be characterized by its stress-strain relationship. Carlson et al. (1993) found no significant differences in modulus of elasticity (i.e., the slope of the stress-strain curve) for tendons of human extensor digitorum longus, flexor digitorum profundus, palmaris longus and plantaris between 2.5 and 4.5% strain. This similarity of the modulus of elasticity suggested similarity of tendon material, therefore differences in stiffness were probably related to differences in cross sectional area and length. These stress-strain characteristics are similar to those suggested by Zajac (1989) for 'generic' tendon and those of FPL tendon measure in isolation by Rack and Ross (1984). However, measuring tendon stress at strains beyond physiological range may

have little functional significance. In fact, Loren and Lieber (in press) suggest each tendon of the human upper limb has a unique stress-strain relationship.

1.3 Parallel Elastic Component (PEC)

The PEC is also an elastic component of muscle primarily due to the passive tissue within and surrounding muscle (e.g. epimysium, perimysium, endomysium, sarcolemma). This element is often excluded from models of muscle except when joint ranges of motion approach extremes.

1.4 Lines of Action

The relative accuracies of the resultant muscle and joint forces are proportional to the accuracies of specifying the moment arms and orientations of muscle lines of action. In general, accurate data concerning the muscle orientations and moment arms are required to define the coefficients in the equilibrium equations for force analysis of the muscles (An et al.. 1981). In the past, straight lines or lines joining origin to insertion of muscles were used to define muscle lines of action (Seiring and Arvikar, 1975). The locations of origins and insertions have been measured by radiography (Mcleish and Charnley, 1970), directly from cadaver specimens (Veeger et al., 1991; Hogfors et al., 1987; Chen et al., 1988; Wood et al., 1989a, 1989b), using serial sectioning methods on cadavers (An et al., 1981) or *in vivo* using magnetic resonance imaging (MRI) (Koolstra et al., 1989; Caldwell and Chapman, 1991; Buchanan et al. 1993).

The serial sectioning method allows the path of the muscle to be obtained using the centroid of the muscle and tendon cross-sections. The muscle line of action can be obtained by joining these centroids. This approach assumes that the fibres contract uniformly across each cross-section and their lines of pull are perpendicular to the cross-section. Although this assumption may not always be true, An et al. (1981) suggested that the centroid line still provides the best estimate of the line of action and is more accurate

than a straight line approximation . The curved nature of some muscles makes representation of the line of action by straight lines between origin and insertion less appropriate.

1.5 Moment Arm

The capacity for a muscle to act on an object not only depends on the amount of force the muscle can generate but also how well this linear force is translated into rotational force or torque about the joint centre. The moment arms about a joint are crucial in determining the joint torque produced by a muscle. A muscle moment arm can be defined as the length of the perpendicular segment from the line of action of the muscle to axis of rotation of the joint (Buchanan et al., 1993). Changes in moment arm with joint rotations can be estimated in geometric terms by establishing a model describing the tendon-joint displacement relationship. Armstrong and Chaffin (1978), found that Landsmeer's Model I best represented interdigit tendon-joint mechanics. In this model, the tendon is held securely against the curved articular surface of the proximal bone of the joint with the axis of rotation situated at the centre of the head of the proximal bone. During rotation of the joint, the relationship between tendon excursion and joint angle is given by:

$$E = r\,\theta,$$

where E = tendon excursion, r = the distance from the joint centre to the tendon and θ = joint rotation in radians. The instantaneous moment arm (M) of the tendon can be obtained from the slope of the plot of the tendon excursion vs joint angle, or $M = dE/d\theta$, (An et al., 1983).

1.6 Purpose

The purpose of the first part of this study was to determine the muscular properties required to develop a Hill type model of the flexor pollicis longus muscle of one healthy subject. It was hypothesized that, since FPL is a single-muscle, single-degree of freedom system, the force-length-velocity properties of FPL could be measured directly and an indeterminate problem would be avoided.

2.0. Methods

2.1. Morphometric Characteristics

A series of cross sectional magnetic resonance images (each 5 mm thick) of a single subject's right arm and hand in a fully extended position with the forearm supinated. The distance between each slice was 10% of the slice thickness or 0.5 mm. These images were traced by hand and digitized onto a Macintosh IIsi computer using a *Deskjet* scanner and analyzed using *NCSA Image* analysis software. Muscle area, centroid location, tendon area and centroid location were measured with respect to a fixed set of orthogonal axes whose origin was external to the first slice. The centroid location of the muscle and tendon in each slice was defined by the centre of the best fitting ellipse and confirmed visually. The muscle and tendon centroid location of each slice was used to define the line of action of the muscle, described as a three dimensional data set. The distance (r) from one centroid location to the next was calculated from the distance equation:

$$r = \sqrt{x^2 + y^2 + z^2}$$

The x and y values were measured in reference to an external reference frame. The z value was consistent and represented the distance between each slice (5.5mm). In this way, the muscle's length was accurately reflected even when its course was not parallel to the long axis (z) of the reference frame.

Muscle fibre length was estimated using the fibre length to muscle length ratio of 0.24 suggested by Lieber et al. (1990) as being consistent between specimens. The physiological cross sectional area (PCSA) was define according to Sacks and Roy (1984) as:

$$PCSA = \frac{\text{muscle mass (g)} \bullet \cos\alpha}{\rho\ (\text{g/cm}^2) \bullet \text{fibre length (cm)}}$$

alternatively,

$$PCSA = \frac{(\text{muscle volume (cm}^3) \bullet \cos\alpha)}{\text{fibre length (cm)}}$$

where α = the surface pennation angle and ρ = muscle density. Surface pennation angle was taken from Lieber et al. (1992). The maximum isometric tension (Po) was determined from the maximum torque measured (1.39 Nm) divided by the muscle moment arm (0.0086m) estimated from the MRI. From PCSA and Po, the maximum muscle stress, or specific tension, of this muscle was calculated. The moment arm of the FPL muscle was defined as the perpendicular distance from the line of action to the joint centre of rotation as estimated from the centre of curvature of the condylar head of the proximal phalanx (Toft and Berme, 1980).

2.2. CC Force-Length Relationship

Position and torque were measured using a potentiometer and linear strain gauges coupled to a rotatable shaft. The subject's right hand and forearm were stabilized on a horizontal bar in a position similar to that used for the MR imaging. Only the distal phalanx of the thumb was free to move. The axis of rotation of the interphalangeal joint of the thumb was coaxial with the axis of rotation of the shaft. The subject performed three maximum voluntary contractions (MVC) at joint angles ranging from 0 (full extension) to 60 degrees flexion while isometric torque was measured. The mean torque at each angle was converted to force at each length by dividing by the muscle moment arm (MMA) determined from the magnetic resonance images. The length so obtained was adjusted for stretch of the SEC (force divided by stiffness) at each force.

2.3. CC Force-Velocity Relationship

The torque-angular velocity characteristics of FPL were determined by performing several quick release and quick stretch contractions. The subject first performed an isometric contraction at one of three torque levels (0.25 Nm, 0.75 Nm or 1.25 Nm) which corresponded to 0.18, 0.54 and 0.90 activation. The torque was then quickly reduced (or increased for eccentric contractions) while the subject maintained the same level of effort. The resulting torque, angular velocity and angular displacement were recorded for each torque step. This was repeated for several torque steps until near zero torque was recorded at the highest angular velocity. At least 5 torque steps were performed at each initial level of contraction for concentric contractions and 3 for eccentric contractions. The entire procedure was repeated for 3 starting positions (10, 30 and 40 degrees of flexion). The angular measurements were converted to linear measurements by accounting for the muscle moment arm.

Since the CC and SEC are in parallel, the total velocity of shortening is equal to the velocity of the CC plus the velocity of the SEC,

$$V_{TOT} = V_{CC} + V_{SEC} \text{ therefore,}$$

$$V_{CC} = V_{TOT} - V_{SEC}$$

The velocity of the SEC was estimated from the stiffness and displacement - time profile for each contraction and subtracted from the total velocity to give CC velocity. The force was corrected for muscle length so that the values reflected the muscle force at Lo. The force at peak velocity for each activation level was grouped by starting position and formed points along the force-velocity relationship.

2.4. SEC Tendon Characteristics

The tendon characteristics were determined using values obtain from the literature. Rack and Ross (1984) subjected human flexor pollicis longus tendon, obtained at autopsy, to sinusoidal stretching movements from which estimates of tendon stiffness were derived from measured force and length changes. For the current study, it was assumed that the tendon characteristics per unit length and cross sectional area were identical. This allowed the stiffness-force relationship of the FPL tendon obtained by Rack and Ross (1984) to be scaled by length and cross sectional area to represent the tendon measured in the MRIs. A length-tension relationship was constructed by converting the stiffness (N/mm) into compliance (mm/N) and then integrating this with respect to force (N). This represented the series elasticity attributed to the tendon (SEC_t).

2.4. SEC Fibre Characteristics

The series elasticity attributed to the muscle fibres (SEC_f) was estimated by mathematically removing the series elasticity of the tendon (SEC_t) from the total series elasticity (SEC_{Tot}). The characteristics of the SEC_{Tot} were determined by subjecting the muscle to several quick stretches and quick releases. A torque motor apparatus was used to give isovelocity angle changes to the distal phalanx of the thumb while the subject performed an isometric contraction of FPL. The thumb underwent rotations of 3 degrees, 5 degrees and 10 degrees in 9 ms, 15 ms and 30 ms respectively to either stretch or shorten the FPL muscle. The subject performed initial isometric contractions of 0.25 Nm, 0.75 Nm and 1.25 Nm (representing 0.18, 0.54 and 0.90 activation). Each combination of initial torque, amplitude of rotation and direction of rotation (stretch or release) was repeated 5 times for a total of 45 trials. Also, the passive stiffness (k_p) was determined by repeating the stretches while the FPL muscle was relaxed.

The static stiffness for each trial was calculated as the change in torque divided by the change in angle. The new torque level was determined by an average of the torque over

a period after any transient changes in torque due to acceleration and deceleration of the thumb, but prior to increased torque due to reflex activation. The stiffnesses in angular terms (Nm/deg) were converted to linear terms (N/mm).

Since the SEC_t and SEC_f are connected in series, the total stiffness (k_T) is given by:

$$k_T = \frac{k_t k_f}{k_t + k_f} ,$$

which allows the fibre stiffness to be defined by:

$$k_f = \frac{k_t k_T}{k_t - k_T} .$$

3.0 Results

3.1. Morphometric Characteristics

Results from the MRI measurements of FPL are shown in table 2.1 below. Where applicable, measurements of the same muscle from other studies are shown for comparison. Muscle length was defined as the length from the most proximal muscle fibres to the most distal muscle fibres at the muscle-tendon junction following the muscles line of action. Fibre length was not directly measured from the MRI, but rather calculated using the mean fibre length to muscle length ratio of 0.24 reported by Lieber et al. (1992). Muscle volume was calculated by summing the muscle cross-sectional areas measure from MRI over a slice thickness of 5.5 mm

Table 2.1 Characteristics Describing the FPL Muscle and Tendon Obtained from Magnetic Resonance Images.

Characteristic	MRI	Lieber et al (1992)	Rack & Ross(1984)	Amis et al (1979)	Kilbreath et al (1993)
muscle length	11.24 cm	16.8 cm			
fibre length	2.70 cm	4.5 cm	4.0-5.0 cm	3.8 cm	
PCSA	3.14 cm^2	2.08 cm^2		4.42 cm^2	
tendon length	13.17 cm		10-13 cm		
tendon CSA	0.0842 cm^2		0.091 cm^2		
muscle volume	8.54 cm^3				
pennation angle		7 degrees			
muscle mass	9.02 g	10 g	11.8 g	18 g	
FL/ML		0.24			
moment arm	8.6 mm		7.4-8.0 mm		7.6 mm
Po	161.33 N				131 N

3.2. CC Force-Length Relationship

The CC force-length relationship exhibited a characteristic inverted "U" shape of maximum isometric force versus muscle length. At both very short lengths and very long lengths, the isometric force capability of the muscle was reduced (approx 0.65Po and 0.64Po respectively) with the maximum isometric force (Po) at some intermediate muscle length (Lo). Figure 2.1 shows force (P/Po) as a function of muscle length (L/Lo). The 11 experimental data points were fit with a 4th order polynomial that predicted force (F) from length (L) where:

$$F = 11679L^4 - 46067L^3 + 67883L^2 - 44279L + 10785 \quad (r^2 = 0.955)$$

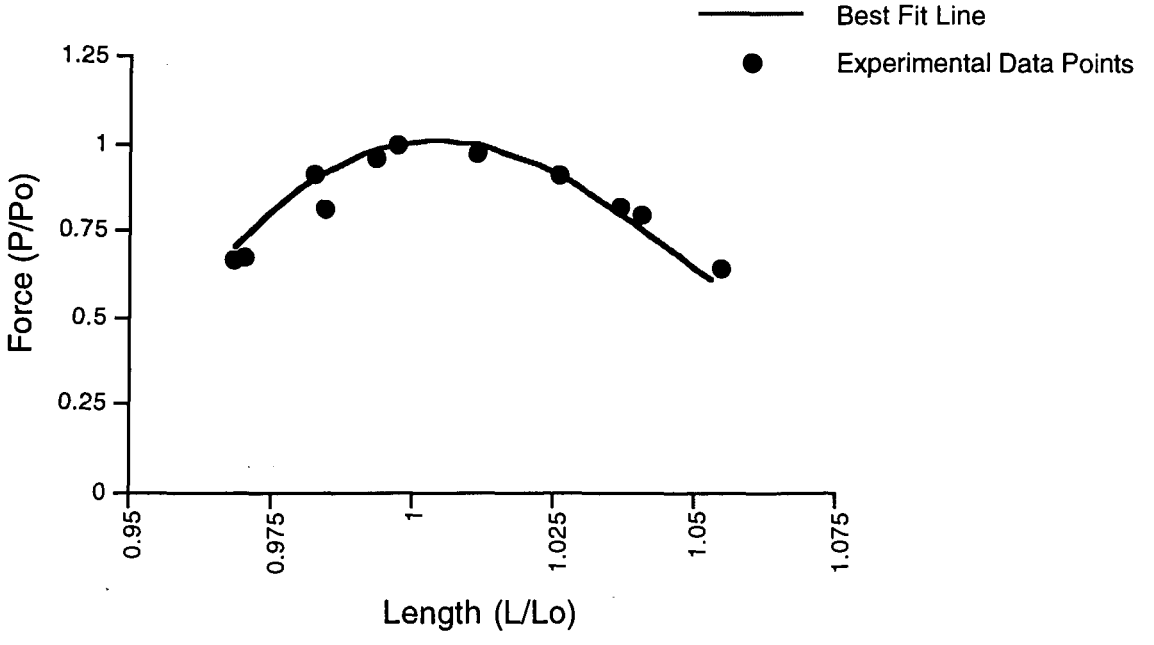

Figure 2.1 Normalized Force-Length Relationship for the CC

Resting length (L_R) was slightly longer than Lo at (1.01Lo) and was defined by measuring the angle of the distal phalanx of the thumb (0.52 radians from full extension) when the joint was relaxed after several passive movements from fully extended to fully

flexed. Muscle length at this angle was determined by calculating the tendon excursion (change in length) from fully extended (position of MRI measurements) using a constant moment arm of 8.6 mm determined from MRI cross sections. Tendon excursion (E) was a function of moment arm (r) and angle (θ in radians) where:

$$E = r\theta.$$

The isometric force-length relationship indicated the relative force producing capability of the muscle at a given length.

3.3. CC Force-Velocity Relationship

Below is a representative record of a single contraction of FPL from a quick release after generating an isometric voluntary contraction (figure 2.2). The line shows the time at peak angular velocity where torque and displacement were measured. These measurements were converted to force and velocity and formed one point on the force-velocity relationship. The force was also normalized to optimal muscle length (Lo).

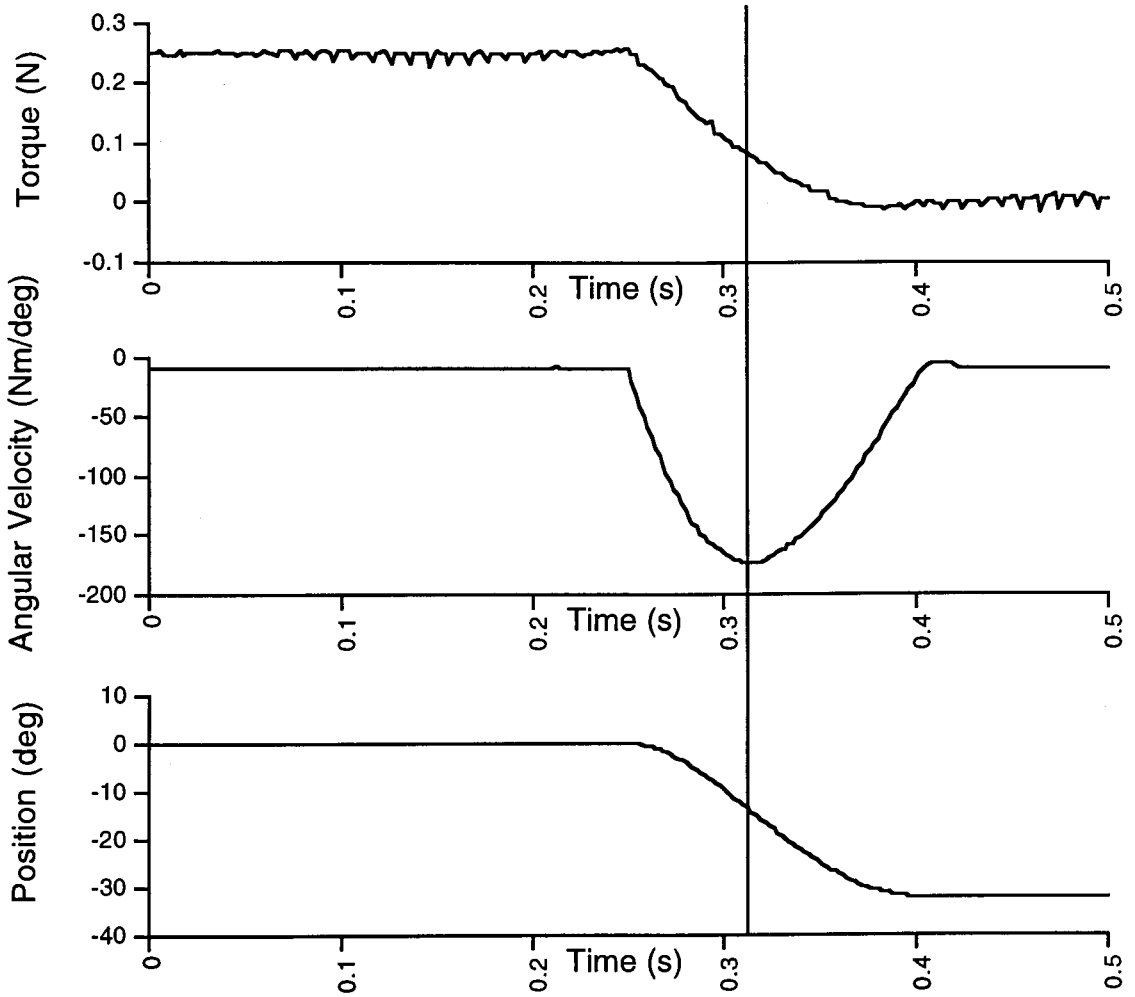

Figure 2.2 Torque, angular velocity and angular displacement profiles recorded during a single isometric contraction.

The CC force-velocity relationship exhibited a characteristic decrease in velocity with increases in load with the maximum force (Po) obtained at zero velocity. Figure 2.3 shows the data points obtained describing the force (P) produced as a function of velocity (V). These points were fitted with Hill's equation where:

$$(P+a)(V+b) = (Po+a)b$$

or

$$V=\frac{(Po+a)b}{(P+a)} - b,$$

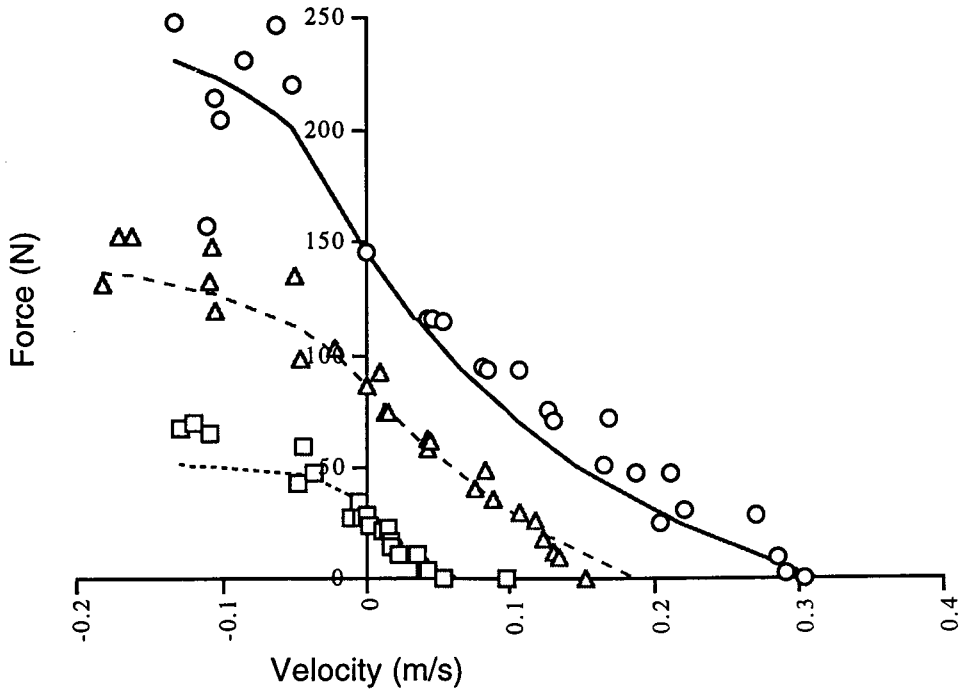

Figure 2.3 Force-velocity relationship for the CC for various levels of activation (open squares = 0.18, open triangles = 0.54, open circles = 0.9).

The eccentric portion of the relationship was predicted using the following equation adapted from Caldwell (1995):

$$Vcc = S \bullet \frac{(Ps - Po)}{(P - Ps)} + S$$

$$S = \frac{0.5 \bullet b(Ps-Po)}{(Po+a)}$$

where: Po = maximum isometric muscle force,

Ps = saturation force in eccentric contraction,

P = instantaneous muscle force,

Vcc = velocity of the CC,

a & b = constants from Hill's equation.

The constants a and b were determined using a public domain, non-linear curve fitting program (Xmgr). Several fits were performed until suitable values of a and b were found such that both the concentric equation and eccentric equation could be scaled by Po alone. The values for a and b were 140.0 N and 0.30 m/s respectively. From the raw data, the maximum force during eccentric contraction was estimated to be 1.72Po.

3.4. SEC Tendon Characteristics

The tendon characteristics obtained from the literature (Rack and Ross, 1984) showed a typical relationship between tendon stiffness and force. Figure 2.4 shows the stiffness-force relationship obtained by Rack and Ross (1984) for a tendon 100 mm long, with a cross sectional area (CSA) of 9.1 mm^2. This relationship was fitted with an equation;

$$\text{Stiffness} = 39.06 \bullet \text{Force}^{0.246} - 39.06$$

Also shown in figure 2.4 is this same relationship scaled to represent a tendon 131.7 mm long with a CSA of 8.42 mm^2 as described by the MRI. Since the MRI tendon is longer and has a smaller CSA it was expected to be less stiff than the tendon examined Rack and Ross (1984). The scaling was accomplished by multiplying the stiffness (k) at each force by the ratios of length and CSA as follows:

$$k_{MRI} = k_{cadaver} \bullet \frac{100mm}{131.7mm} \bullet \frac{8.42mm^2}{9.1mm^2}$$

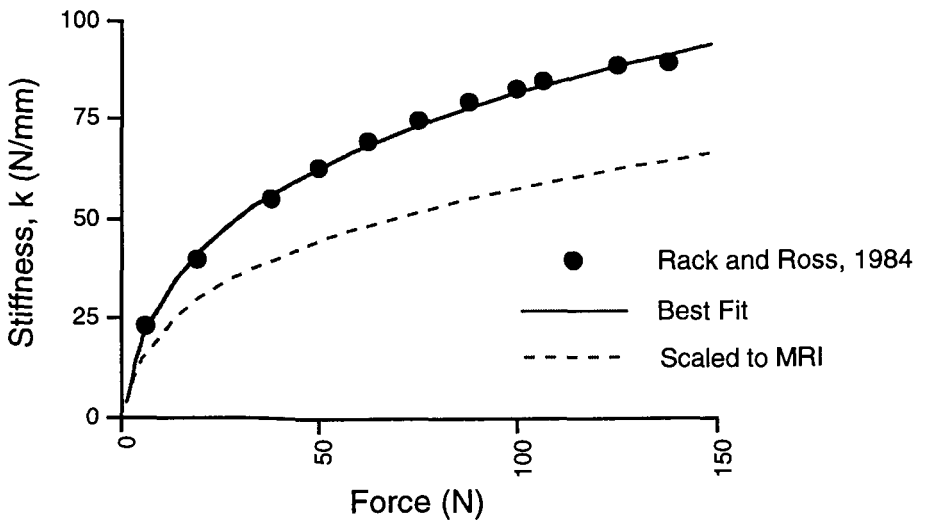

Figure 2.4 Stiffness-Force Relationship for FPL tendon

A force-length relationship was constructed by converting the stiffness to compliance, and then integrating this with respect to force. For tendon, the force-length relationship is commonly reported as a stress-strain relationship. Force was divided by tendon CSA to yield stress (N/mm^2) while length change was reflected as percent extension to give strain (%). The tendon characteristics showed increasing stress with increasing strain (figure 2.5). This relationship was fitted with a line described by the following equation:

$$y = 6.158 \bullet e^{(0.864x)} - 6.158,$$

where y = stress (N/mm^2) and x = strain (%).

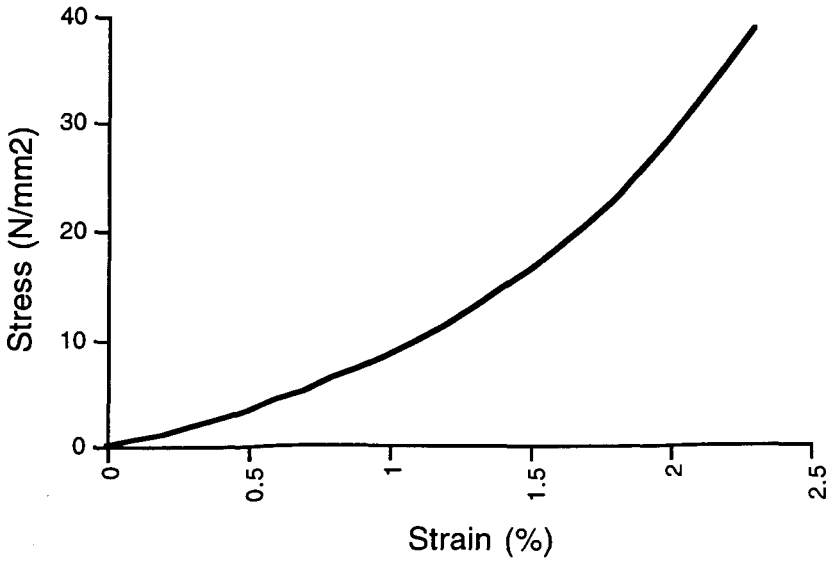

Figure 2.5 Stress-Strain Relationship for the FPL Tendon

3.5. SEC Fibre Characteristics

SEC fibre stiffness was derived from SEC_{Tot} and SEC_t. The stiffnesses calculated for each displacement were collapsed across starting positions to produce the stiffness force relationship seen below (figure 2.6) where stiffness is a function of force and length.

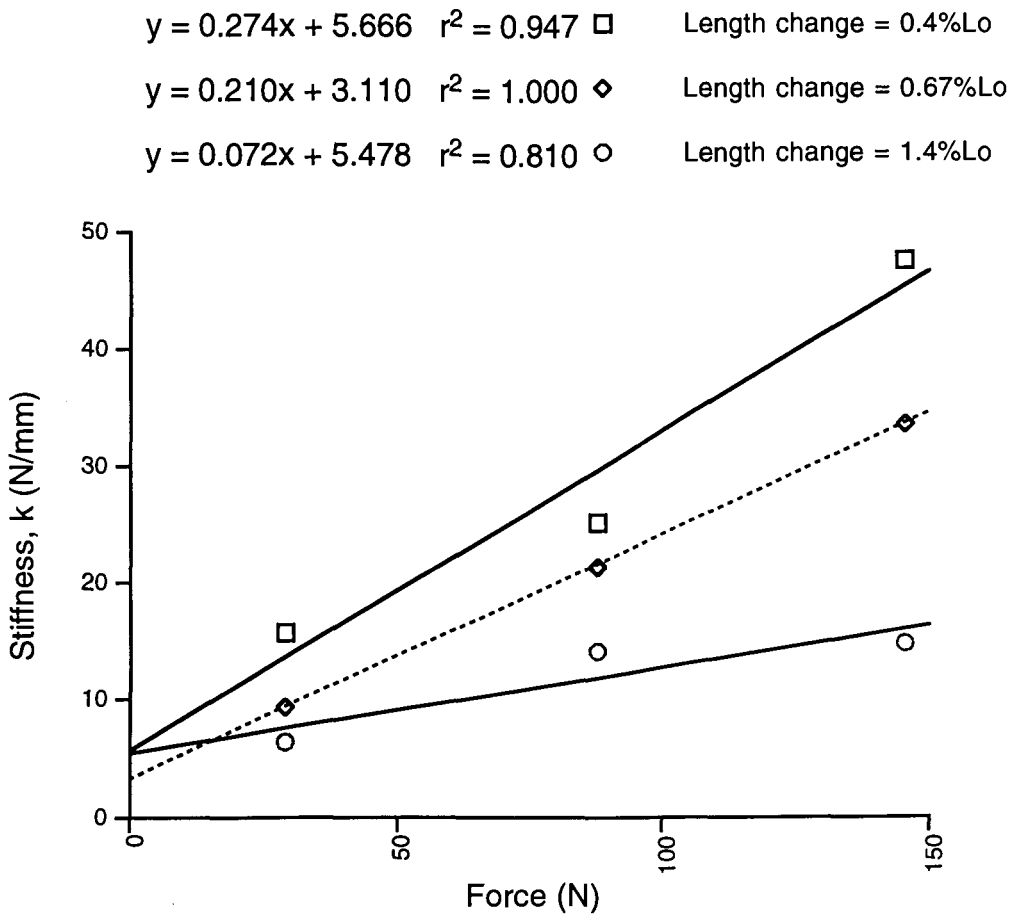

Figure 2.6 Stiffness-Force Relationship for Fibre Series Elasticity (SEC_f)

The stiffness-force relationship was assumed to be linear and was described by an equation of the form:

$$k_{SECf} = S \bullet F + k_p,$$

where F = force (N), S = the slope of the stiffness force relationship as a function of length change and k_p = passive stiffness (2.79 N/mm). The function, S, was determined by fitting a second-order polynomial to the data (figure 2.7).

$$S = 324.82L^2 - 96.71L + 7.033,$$

where L = length change as %Lo.

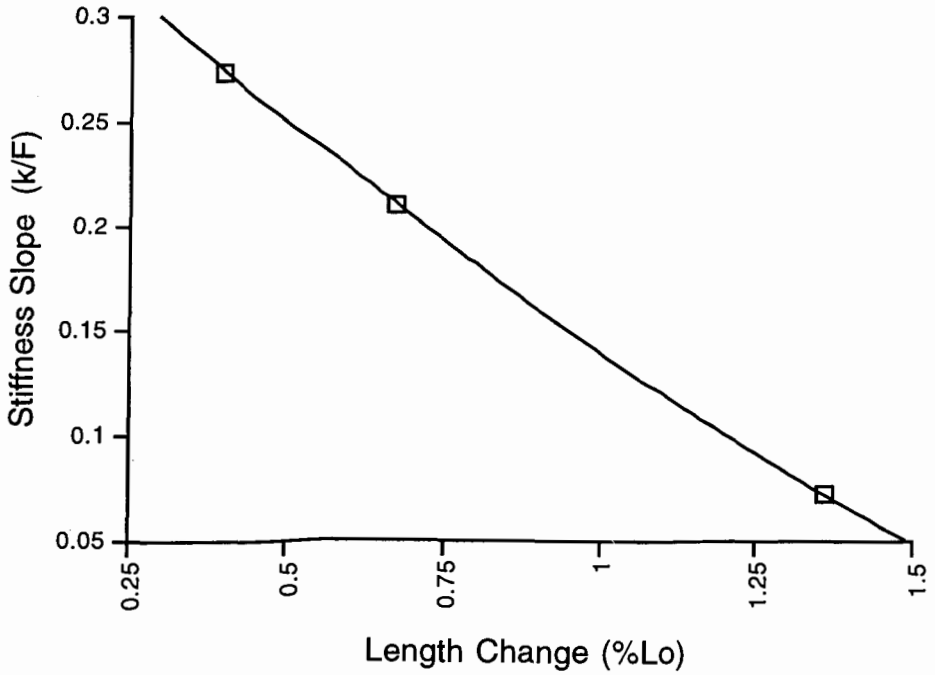

Figure 2.7 The slope of the stiffness-force relationship as a function of length change.

The stiffness-force relationship was converted to a force-length relationship ($F = k \bullet \Delta L$) for the SEC_f that was dependent on activation (figure 2.8). When the SEC_f is at resting length (i.e., no stretch) the force across it must be zero. Therefore, the force-length relationship also had a point at the origin. The slope of force-length relationship (stiffness) was a function of activation described by figure 2.9. The stiffness at zero activation corresponds to the passive stiffness of 2.79 N/mm (17.32 (P/Po)/m).

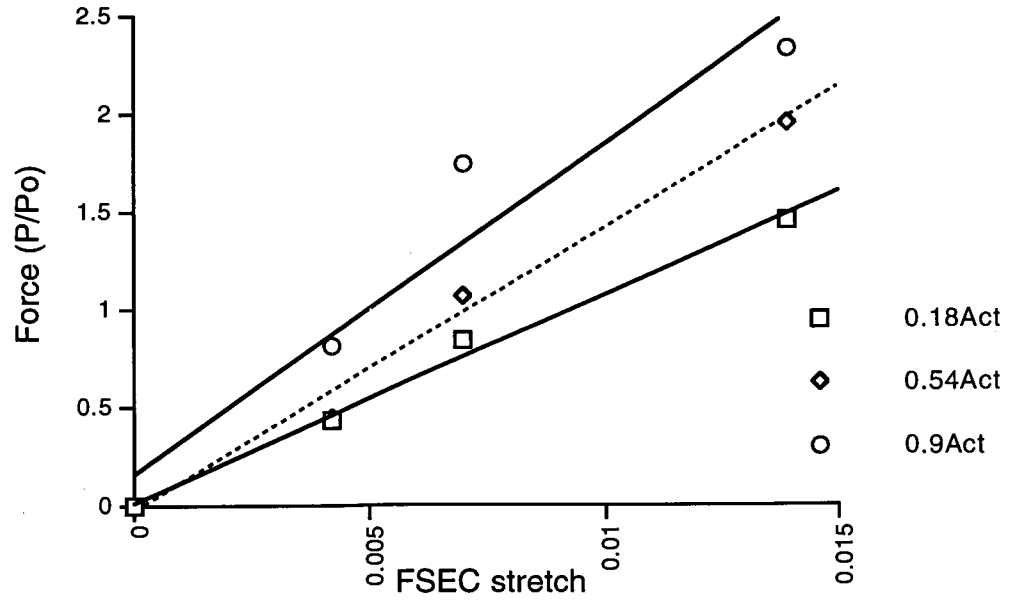

Figure 2.8 Force-length relationship for the SECf as a function of activation.

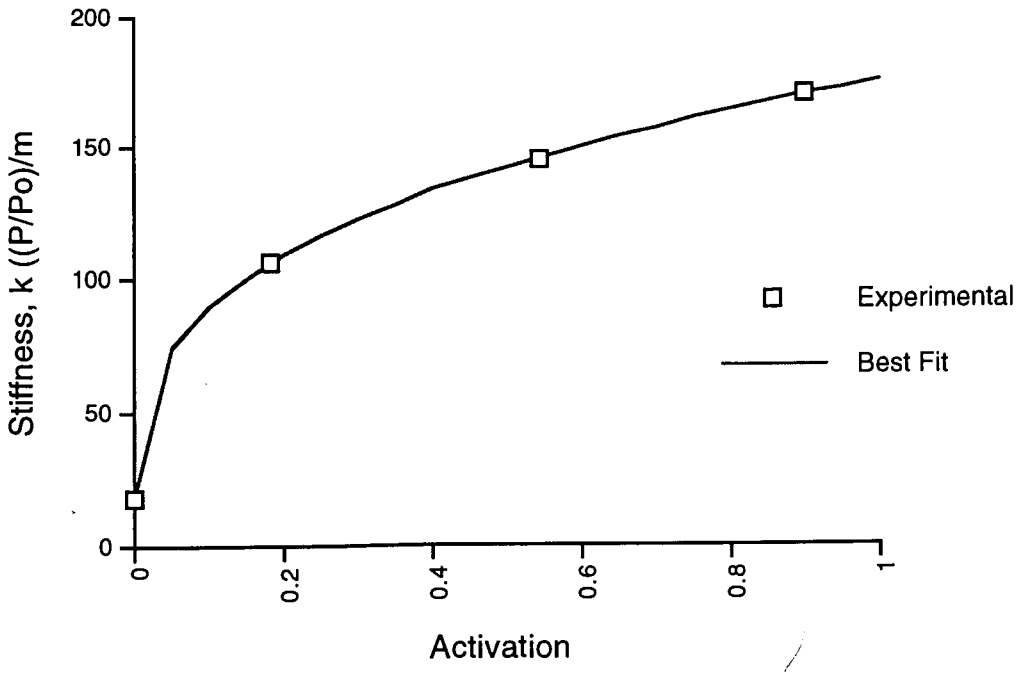

Figure 2.9 Stiffness-activation relationship for the SECf. ($y = 17.32 + 157.82x^{0.399}$ $r^2 = 0.99$)

Combining these two relationships yielded the equation below which described the force of the fibre SEC as a function of length and activation.

$$\text{Force} = (17.32 + 157.82\text{Act}^{0.399}) \bullet \text{Stretch of the SEC}_f$$

4.0 Discussion

Models of the mechanical properties of skeletal muscle allow investigators to study various aspects of movement control and coordination. Many researchers have found Hill's model suitable for examining muscular contraction in human movement because of its balance between simplicity and accuracy (Caldwell and Chapman, 1988; Zajac, 1989; Caldwell, 1995). To implement a Hill model as representative of a specific muscle, morphometric data are needed to transform the model from a dimensionless, generalized form to one specific to the muscle of interest. Most often these morphometric parameters are estimated from the literature. In this experiment, the properties of human flexor pollicis longus muscle required to produce a Hill model were determined from *in vivo* experimental measurements along with a morphometric description of FPL obtained from MR images. The only characteristic that could not be determined experimentally was the isolated tendon stress-strain relationship which was derived from data presented by Rack and Ross (1984) and muscle fibre length from Lieber et al., (1992).

4.1 Morphometric Characteristics

Measurements taken directly from the magnetic resonance images were used in conjunction with values from the literature to produce a morphometric profile of the FPL muscle of one subject. The FPL was described by its total length, fibre length, physiological cross sectional area (PCSA), tendon length, tendon cross sectional area, volume, mass and moment arm. As depicted in Table 2.1, the measurements obtained from the MR images were compared subjectively with values obtained from the literature. It is clear that the values obtained in this study are similar in their description of the morphology of FPL when compared with the studies cited. The advantage of the present study is that these morphometric measurements were acquired from a healthy subject *in*

vivo rather than from cadaver specimens. This allows for the direct comparison and construction of the relationships describing the mechanical properties of FPL.

From the measured torque during maximum voluntary contraction and PCSA, a value for maximum muscle stress was obtained. The conversion from torque to force was accomplished by dividing by the muscle moment arm (8.6 mm) and muscle stress or specific tension was represented as force/unit cross sectional area. For FPL, maximum muscle stress was found to be 51.4 N/cm^2. Despite the fact that maximal muscle stress has been suggested to remain constant across muscle specimens (Loren and Lieber, in press) there is still considerable variation in the values reported in the literature. The value obtained in this study is considerably higher than values obtained in studies of isolated muscle. Many investigators have used a value in the range of 20 - 25 N/cm^2 for maximal isometric stress in mammalian muscle (Lieber et al., 1994; Powell et al., 1984; Loren and Lieber, 1995; Close, 1972; Ettema & Huijing, 1993). Upon direct measurement values from 30 to 38 N/cm^2 have been reported in dog muscle (Jayes & Alexander 1982; Alexander, 1974). Rall, (1985) suggested a maximum force per unit cross sectional area 20 - 35 N/cm^2 for vertebrate skeletal muscle stress although indicated that this may vary considerably while Yoshihuku and Herzog (1990) used 40 N/cm^2 for the human quadriceps. The value obtained in this study was approximately 2 fold larger than the lower values cited in the literature. This may be explained in terms of the FL/ML ratio obtained from Lieber et al (1992) used to determine fibre length. The fibre length reported by Lieber et al (1992) was actually a measure of fibre bundle length and in most cases this is not the same as the actual length of the individual muscle fibres (Loeb et al, 1987). In some cat hindlimb muscles, fascicles are composed of muscle fibres that run only part of the fascicle length and taper to the end as fine strands. These strands are interdigitated with other tapered fibres with the muscle mass (Loeb et al, 1987). This means these long parallel-fibered muscles are actually composed of shorter muscle fibres arranged in series. The result is an increase in effective PCSA. The implications for this study are that the

fascicle fibre bundle) length measured by Lieber et al (1992) may over-estimate fibre length considerably. If for example fibre length were overestimated by 2 fold, PCSA would be underestimated by 2 fold and specific tension would also be overestimated by 2 fold. Should this be the case, the specific tension found in this study would be 25.7 N/cm^2, and would compare well with the literature.

4.2 CC Characteristics

As expected, the isometric force producing capability of FPL depended on the length at which it was allowed to contract. The maximum isometric force capability (Po = 161.3 N) was slightly higher than that estimated by Kilbreath and Gandevia (1993) (Po = 131 N). The latter, however, was estimated from external estimates of moment arm rather than direct measurement using MRI as in the current study. For a better comparison, the direct torque measurements should be used. The peak isometric torque found in this study was 1.39 Nm compared with 1.79 Nm estimated from the data of Capaday et al. (1994), 1.0 Nm found by Kilbreath and Gandevia (1993) and only 0.48 Nm reported by Carter et al. (1993). Clearly the torque at MVC measured in this study is within the range reported elsewhere in the literature.

The force-velocity relationship found in this study showed a characteristic decreasing force potential with increasing velocity of contraction. This relationship was first characterized by A.V. Hill (1938) is his experiments on isolated frog muscle culminating in the equation bearing his name that describes the relationship between force and the velocity of shortening. In determining the constants for this equation, Hill found a mean a/Po of 0.25 for frog sartorius muscle (Hill, 1970). The ratio, a/Po, describes the curvature of the relationship and establishes how quickly the velocity decreases with increasing force. Wilkie (1950) however, found that a/Po ranged from 0.20 to 0.48 for five subjects performing elbow flexion. More recently, a/Po ratios have been shown to vary considerably between muscles of the cat hindlimb ranging from 0.067 for extensor

digitorum longus (EDL) to 0.927 for soleus (Baratta et al., 1995). In the present study, both a and b were fitted using a recursive least-squares algorithm (Xmgr). The best fit was obtained when the relative error in the sum of squares was $\leq 1 \times 10^{-9}$ ($a/Po = b/V_{max} = 0.96$).

The differences in a/Po ratios may be related to differences in muscle fibre composition (Close, 1972). One would expect a lower a/Po ratio for predominantly slow twitch muscles as suggested by Faulkner et al., (1986) who found a/Po was 0.15 for slow twitch muscle fibres and 0.25 for fast twitch muscle fibres. This, however, is contrary to the findings of Baratta et al. (1995) who found that the muscles with the highest velocities (tibialis anterior and EDL in the cat hindlimb) also had the lowest a/Po ratios. Considerations should be made when comparing results from experiments done on isolated animal muscle with those done on intact humans. In experiments with human subjects, it is often more difficult to control accurately load, velocity, activation and limb position in the apparatus. Also isolated muscle can be examined in linear terms whereas for *in vivo* human studies, experimental data are measured in angular terms since muscular contraction usually results in angular motion of a limb segment. Since torque is a function of moment arm, joints in which moment arm change through range of motion may display torque-angular velocity relationships that depart significantly from Hill's hyperbolic relationship. In this study, it was assumed that the moment arm for FPL was constant throughout the range of motion. Small changes in moment arm may have led to errors in converting measured torque values to muscle force. Measurement errors can easily occur when estimating centres of rotation and moment arms required when data in angular terms are related to linear measurements. Also, joint viscosity and segment moment of inertia as well as moment of inertia of the recording equipment should be considered and corrected for. In this study, however, the moment of inertia of the distal phalanx of the thumb was probably insufficient (approximately 7.5 gcm^2) to affect the measured torques.

4.3 SEC Characteristics

Muscle stiffness is reflected by the slope of its length-tension relationship. Stiffness tends to increase as tension and length increase until a maximum value is attained and failure occurs. In normal conditions, the regulation of muscle stiffness in under reflex control, which when combined with central control creates a complex system (Nichols and Houk, 1976). The actual regulation of stiffness may involve both force feedback and length feedback components that constantly update the muscle's stiffness to accommodate load and length changes.

Tendon is situated in series with muscle fibres and each has its own mechanical properties that contribute to muscle stiffness. Experiments on isolated tendon suggest that tendon stress (force per unit cross sectional area) increases with strain (relative change in length) (Rack and Ross, 1984; Lieber et al., 1994; Loren and Lieber (in press)). Typically, the stress-strain (or force-length) relationship for tendon exhibits a curvilinear toe region with small increases in length leading to a linear increase in force with further stretch. This toe region tends to occur within the first 2% of strain with failure at approximately 10% strain and 100 MPa stress. Although the curved toe region is relatively small compared with the entire range of tendon extensibility, it is functionally the most important. Tendon strain when muscle force is maximum is typically 3 to 3.5% with stress around 35 MPa stress (Zajac, 1989).

The tendon of FPL described by Rack and Ross (1984) was subjected to sinusoidal stretches at forces up to nearly 150 N. This force represented a torque of approximately 1.2 Nm if the tendon attached to the distal phalanx of the thumb at a point 7.7 mm from the axis of joint rotation as was estimated in their study. Comparing with the maximum isometric torques produced by FPL found in other studies, suggests that this tendon was examined within its physiological operating range.

The stiffness-force relationship obtained from Rack and Ross (1984) was scaled to represent a tendon of the size and length measured from the MRI. The stress-strain

relationship obtained was similar to those seen for isolated tendons of other forearm muscles. Loren and Lieber presented average load(%Po) - strain(%) relationships for the five prime movers of the wrist (Loren and Lieber, in press). When converted to the same units, the FPL tendon in this study was found to be approximately as stiff as extensor carpi radialis longus, but more stiff than extensor carpi radialis brevis, extensor carpi ulnaris, flexor carpi radialis and flexor carpi ulnaris tendons (Loren and Lieber, in press).

The stiffness-force relationship obtained for the entire series elasticity (SEC_{Tot}) was similar to those reported for the same muscle in other studies. To compare with other studies figure 2.6 must be converted to angular terms to give angular stiffness (Nm/rad) vs torque (Nm). Figure 2.10 shows the angular stiffness-torque relationship for both the data obtained in this study and those obtained by Rack and Ross (1984, their figure 4) for the interphalangeal joint of the thumb. Although at each torque, the angular stiffness calculated in this study was lower than found by Rack and Ross, they are in the same order of magnitude. Compared with Carter et al., (1993) the stiffness obtained here were higher, although again in the same order of magnitude. This is not surprising considering the potential variation in muscle and tendon sizes across subjects.

The increase in stiffness with force is expected and confirmed in many other studies (Carter et al., 1993; Rack and Ross, 1984). With increased activation more cross bridges are formed effectively increasing the number of springs in parallel. Since stiffnesses add for springs in parallel, the overall stiffness increases.

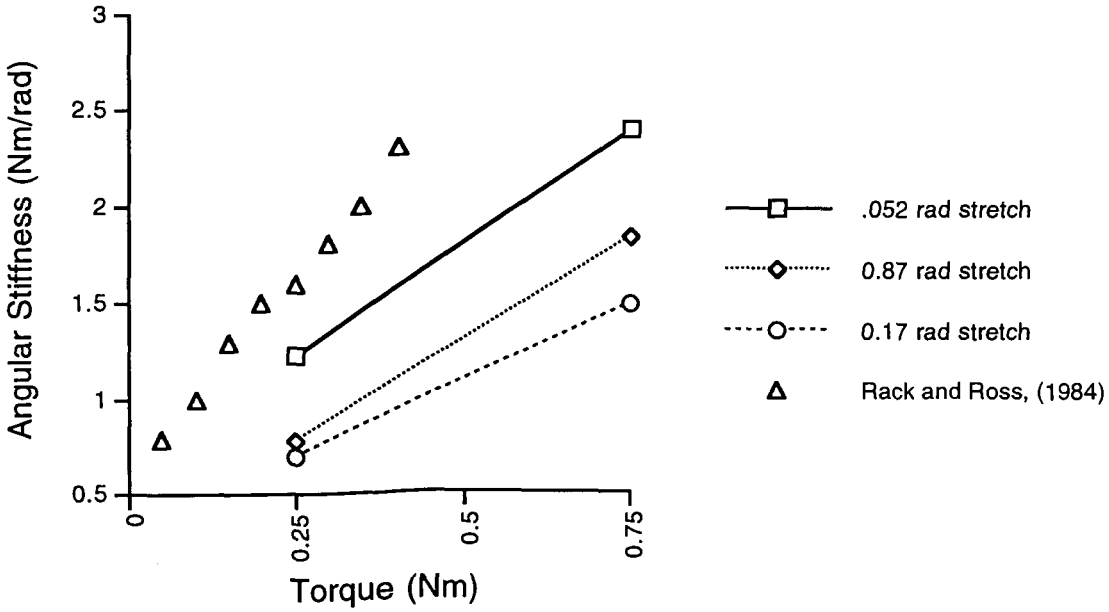

Figure 2.10 Total angular stiffness versus torque for the distal phalanx of the thumb. The data of Rack and Ross (1984) are compared with the experimental data from this study for the three stretches (3 degrees = 0.52 radians, 5 degrees = 0.087 radians, 10 degress = 0.17 radians).

The stiffness of springs in series add as their reciprocals so that the overall stiffness of springs in series is less than any of the constituents. This fact was used to determine the stiffness attributed to the muscle fibres themselves as outlined in the methods. Strictly speaking the SEC_f represents not only the elasticity of the muscle fibres and cross-bridges, but also any tendinous structures that may reside in the muscle in the form of an aponeurosis. Experimental results of Rack and Westbury (1984) indicate equal normalized stiffness values for tendon and aponeurosis. However, others have suggested that tendon and aponeurosis may display different elastic properties, perhaps being related to the junction between the aponeurosis and muscle fibres (Huijing and Ettema, 1989; Ettema and Huijing, 1993).

The passive properties of the muscle fibres were represented as a pure elasticity. Recently however, Lin and Rymer (1993) showed that the mechanical response of muscle to stretch exhibits not only length dependence but also velocity dependence. They argue

that the traditional descriptions of short-range stiffness and yield are inadequate and that the change in force that has typically been called muscle yield reflects a transition between short-range, transient elastic behaviour to steady-state viscous behaviour. However, in the model used in this study (presented in Chapter 3), the viscous properties of the muscle were contained solely in the force-velocity relationship.

5.0 Summary

The relationships obtained in this study describing the mechanical properties of the flexor pollicis longus muscle appear to be appropriate when compared with available information in the literature. These relationships were used in a computer simulation describing force production of FPL as presented in Chapter 3.

Chapter 3

Model Development and Scaling

1.0 Introduction

It is often useful and indeed desirable to estimate individual muscle forces in a multimuscle system. When individual muscles are modelled, their parameters are often estimated from the body of literature available. Although the efficacy of a model derived from estimated parameters can always be questioned, it is of little consequence to model only those muscles for which all parameters can be measured directly. The power of a muscle model is realized when it is modified to represent those muscles that can not normally be isolated *in vivo.* This section details a muscle model based on the relationships described in chapter 2 and the extension of those relationships to produce a model of extensor carpi radialis brevis (ECRB) so that its contribution to net torque at the wrist can be estimated.

1.1 Muscle Architecture and Scaling

Skeletal muscle architecture is important in determining the functional properties of muscle (Gans 1982; Gans and Gaunt, 1991; Lieber and Brown, 1992). It has been shown that the maximal tension developed by skeletal muscle (P_O) is proportional to its physiological cross-sectional area (PCSA) in spite of the wide variability in muscle size and shape (Powell et al., 1984). Gans (1982) suggested that PCSA and fibre length were the primary determinants of a muscle's isometric force and isotonic velocity respectively. The architectural features of 21 different muscles in the human forearm and upper arm were determined by Lieber et al.. (1990, 1992). Measurements included muscle length, muscle mass, surface fibre pennation angle, and fibre bundle length and PCSA. Generally, digital

extensors were similar in design and characterized as long fibred, small PCSA muscles while digital flexors were characterized as long fibred muscles with intermediate PCSA.

The greater the PCSA, the better suited a muscle is for force production. With this information force per unit cross-sectional area (specific tension) can be used to estimate the muscles maximum force producing capability.

Fibre length is also an important factor that affects muscle function. The speed capacity of a muscle (i.e. its maximum shortening velocity) is proportional to its fibre length (Zajac 1992; Gregor, 1993). The shortening velocity of a fibre is proportional to its length because muscle fibre velocity is the sum of all the velocities of the in-series sarcomeres. Thus the velocity capacity of the fibre is proportional to the number of its sarcomeres or, equivalently, to fibre length. As a result, muscles with long fibres have the potential to shorten faster than muscles with short fibres. The length range over which a muscle can generate active force is also proportional to its fibre length (Zajac, 1992). The excursion range of a muscle is identical to the range of a single muscle fibre if the fibres have a small and constant pennation angle. Therefore, fibre length, not muscle length, is the relevant parameter in estimating velocity and excursion potential. It has been suggested that fibre length and PCSA are the most important musculotendon architectural parameters in discriminating muscles of the forearm (Lieber et al., 1992; Zajac 1992).

1.2 The Wrist Joint

Wrist motion is the result of a complex interaction of carpal kinematics occurring at the different levels of the joint. None of the muscles acting on the wrist insert on the proximal carpal row. Instead, they attach distally either to the base of the metacarpals or to the bones of the distal carpal row (Garcia-Elias et al., 1991). In normal wrist motion, there is very little motion between the individual bones of the distal carpal row which can be thought of as one functional unit (Ruby et al., 1988, Savelberg et al., 1993). In flexion, the distal carpal bones not only rotate about an axis implying flexion but also ulnar

deviation. Conversely, in extension they slightly radial deviate (Ruby et al., 1988). The bones of the proximal carpal row appear to be less tightly bound to one another than in the distal row (de Lange et al., 1985). However, all the bones in the proximal row rotate in the same direction no matter what wrist motion occurs (Ruby et al., 1988, Savelberg et al., 1993). Therefore, the proximal carpal row can also be considered as a functional unit articulating with the radius and ulna proximally and with the distal row of carpal bones. This finding leads to the concept of the carpal mechanism which considers the proximal row of carpals as a segment whose total outline is adjustable to the space left between the radius and the relatively rigid distal row of carpals (Ruby et al., 1988, Savelberg et al., 1993). In such a concept, the distal row of carpals should be considered as part of the hand. Models of the wrist joint, then, should focus on determining the rules governing the equilibrium between the total outline of the proximal row of carpals and the position of this joint (i.e., the position of the hand relative to the radius) (Savelberg et al., 1993). As such, an anatomically based coordinate system originating in the distal radius and oriented in such a way that the x-axis was directed in the radioulnar direction, the y-axis in the palmardorsal direction and the z-axis longitudinally, has been used to describe the motion of this joint (de Lange et al., 1985). Similarly, Ruby et al. (1988) used a set of orthogonal axes based on the bone structure of the distal radius with the longitudinal axis lying along the shaft of the radius to describe global wrist motion based on motion of the capitate with respect to the distal radius.

In a recent study by Buchanan et al. (1993), the wrist was model as a non-orthogonal, skewed universal joint based on the experimental data of Andrews and Youm (1979), Bumbaugh (1982) and Sommer and Miller, (1980) which showed a separation between the radial-ulnar deviation axis and the flexion-extension axis. Both axes were found to pass through the capitate with the radial-ulnar deviation axis 4-9 mm more distal than the flexion-extension axis. Despite this separation of the axes, Buchanan et al.

(1993) found that force analysis was insensitive to changes in these parameters over the range of 0 to 2.0 cm of skew.

1.3 Wrist Musculature

Of the 15 muscles whose tendons cross the wrist joint, 5 are thought to be prime wrist extensors or flexors. They are: extensor carpi ulnaris (ECU), extensor carpi radialis longus (ECRL), extensor carpi radialis brevis (ECRB), flexor carpi ulnaris (FCR) and flexor carpi radialis (FCR). The other muscles whose tendons cross the wrist joint are the long finger flexors and extensors. Although these muscles insert distally to the wrist, they may still contribute some torque at the wrist joint.

Lieber et al. (1990, 1992) performed detailed studies on the architectural features of several muscles of the forearm. For the prime wrist extensors and flexors fibre length to muscle length ratio ranged from 0.19 (+/- 0.01) to 0.82 (+/- 0.01)(mean = 0.40) and pennation angle ranged from 2.5 (+/- 0.7) to 12.1 (+/- 0.6)(mean = 6.02) degrees in the five sets of cadaver muscles. In the long finger flexors and extensors fibre length to muscle length ratio ranged from 0.28 (+/- 0.012) to 0.69 (+/- 0.062)(mean 0.40) and pennation angle ranged from 2 (+/- 0.06) to 10 (+/- 0.08)(mean 5.5) degrees. Clearly the architectural features of the prime wrist extensors and flexors are similar to the long finger flexors and extensors.

1.4 Functional Studies of Wrist Musculature

In an effort to understand better the functional contributions of each of the main wrist moving muscles, several studies have been performed using both cadaver and *in vivo* specimens. In a study by Horii et al. (1993), the excursion of the tendons of prime wrist movers in seven cadavers was measured in response to angular displacements of the wrist joint. From these relationships, instantaneous moment arms of each tendon were calculated on the basis of the slope of the curve between tendon excursion and joint angular

displacement. Tendon moment arms were found to be consistent throughout the full range of motion in both flexion-extension and radial-ulnar deviation. It was suggested that, based on moment arm calculations, the more effective working muscles were the FCR and FCU for flexion, the ECRB for extension, the ECRL for radial deviation and the ECU and FCU for ulnar deviation. The FCR was found not to work efficiently as a radial deviator by virtue of its small moment arm.

Use of electrical stimulation has allowed some researchers to investigate the isometric action of forearm muscles, *in vivo* (Nathan, 1992). Electrical stimulation can, however, lead to erroneous results since it is difficult to ensure that only one muscle is being stimulated (i.e., no stimulation "overflow"). Also, the mechanical response of electrically stimulated muscle tends to be of high gain since large, fast-twitch fibres are recruited first, contrary to the orderly recruitment of motor units seen in voluntary contractions. Although, the direction of the resultant moment vector for a stimulated muscle may be determined (Nathan, 1992), electrical stimulation does not address the question of the magnitude of the moment produced by individual muscles during voluntary contraction.

In an effort to estimate isometric muscle forces, Buchanan et al. (1993) used EMG signals from five muscles acting at the wrist during a series of isometric contractions in flexion, extension, ulnar deviation and radial deviation. With this method, force-EMG coefficients, in units of Newtons per normalized EMG unit, were calculated and used in conjunction with the necessary anatomical data, to predict individual muscle forces. There are, however several limitations with such a method. The force-EMG coefficients are not applicable across subjects or even within the same subject on different days. This method also assumes a linear force-EMG relationship and that the EMG describes the average activity of the entire muscle (i.e., no functional compartmentalization)(Buchanan et al., 1993).

1.5 Purpose

The purpose of this chapter was to construct a model and computer simulation of the FPL muscle using the relationships described in chapter 2 and to evaluate the model by comparing its output with experimental data recorded during voluntary contractions. A further purpose was to scale the relationships according to PCSA and fibre length so that a model of the ECRB muscle could be constructed.

2.0 Methods

2.1 Morphometric Characteristics

The morphometric characteristics of ECRB were measured from serial, cross-sectional magnetic resonance images of one subject taken at 5.5 mm intervals. See section 2.1 for details on the measurements taken. The wrist was modelled as a two degree of freedom hinge joint, and ECRB has a moment arm for flexion/extension motion as well as radial-ulnar deviation motion. The moment arm was defined as the perpendicular distance between the axis of rotation to the line of action of the muscle. Both the flexion/extension and radial-ulnar deviation axes were defined as running through the head of the capitate bone of the wrist (figure 3.1)

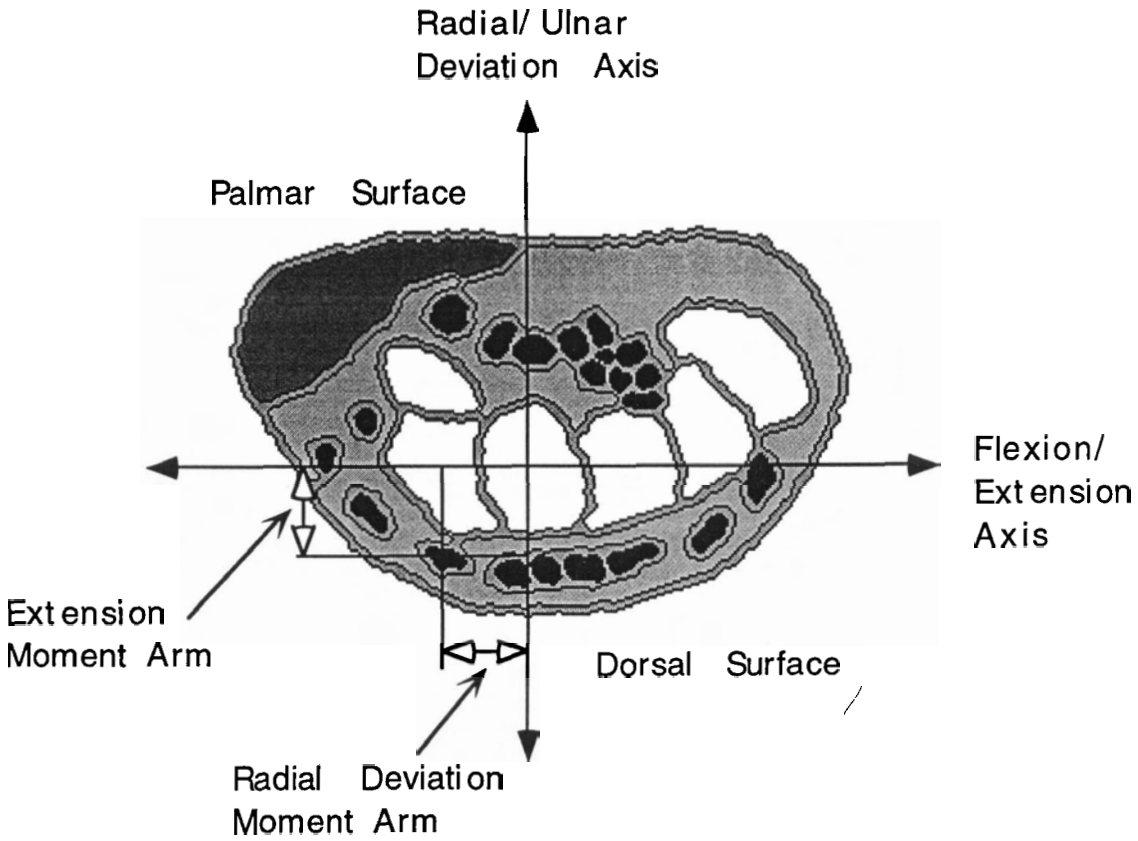

Figure 3.1 Diagram of cross section through the right wrist, viewed from distal to proximal, drawn from magnetic resonance images. Origin of axes is the head of the capitate. Extension and radial deviation moment arms are shown in relation to the ECRB tendon.

The two most important measurements for scaling the relationships describing the mechanical properties of FPL to describe the mechanical properties of ECRB were PCSA and fibre length. PCSA was calculated according to Sacks and Roy (1982), in which

$$PCSA = \frac{\text{muscle mass (g)} \bullet \cos\alpha}{\rho\ (\text{g/cm}^2) \bullet \text{fibre length (cm)}}$$

alternatively,

$$PCSA = \frac{(\text{muscle volume (cm}^3) \bullet \cos\alpha)}{\text{fibre length (cm)}}$$

where α = the surface pennation angle and ρ = muscle density. If the angle of pennation is small its cosine is close to 1.0 and the PCSA is approximately muscle volume over fibre length. This approximation was used since the surface pennation angle for ECRB is less than 10 degrees (Lieber et al., 1990). Fibre length was calculated using the ratio of fibre length to muscle length of 0.38 described by Lieber et al. (1992, 1994) and Loren and Lieber (1995) as being consistent across specimens.

2.2 The Model

The muscle model consisted of three components; an active contractile component (CC) in series with two passive elastic components; one whose stiffness was variable with activation representing the elasticity of the muscle fibres (SEC_f) and one representing the elasticity of the tendon (SEC_t). The characteristics of each component were described by the relationships obtained for FPL in chapter 2.

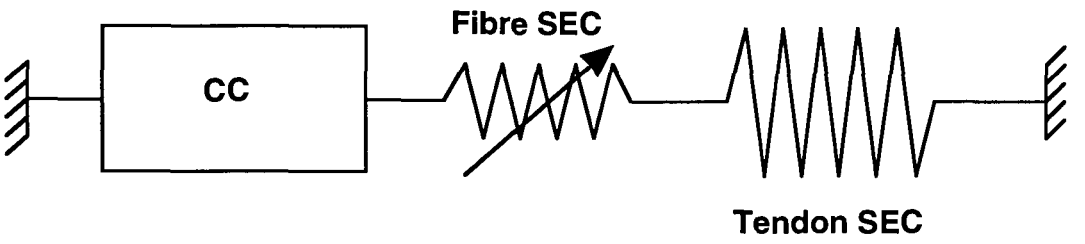

Figure 3.2 Schematic representation of the muscle model showing the contractile component in series with two elastic components. The arrow signifies a stiffness that is variable with activation.

The movements of interest in this study did not occur near the extremes of joint range or muscle length so the parallel elastic component used in other Hill models was ignored.

The inputs to the model were activation and muscle kinematics. Activation was a function of stimulation defined by rectified, low-pass filtered EMG adapted from Pandy et al. (1992).

$$\frac{da(t)}{dt} = \left(\frac{1}{\tau_{fall}}\right)(u(t)-a(t))u(t) + \left(\frac{1}{\tau_{rise}}\right)[u(t)-a(t)-(u(t)-a(t))u(t)]$$

where $a(t)$ = muscle activation at time t.

$u(t)$ = neural input between 0 and 1.

τ_{rise} = activation time constant

τ_{fall} = deactivation time constant

This is a first order differential equation for muscle excitation-contraction dynamics that is nonlinear in the control of $u(t)$ (Pandy et al., 1992). The advantage of this equation is that it models muscle activation ($a(t)$) at any value of ($u(t)$) between 0 and 1 and is not constrained to an on or off type of activation. The rise and decay time constants were

determined by comparing the rising and falling phases of the model output with the tension recorded during a twitch-like contraction of FPL. Activation and deactivation time constants of 45 and 90 ms respectively with a fixed delay of 50 ms seemed to best capture the time course of tension development and relaxation. The stimulation input was derived from surface EMG that was rectified and low-pass filtered at a frequency of 3 Hz.

2.3 The Simulation Routine

The simulation routine used in this study was similar to that developed by Baildon and Chapman (1983) and used elsewhere (Caldwell and Chapman, 1989; Caldwell and Chapman, 1992; Edmonstone, 1993; Caldwell, 1995). It consisted of an iterative process which used EMG and muscle kinematics as inputs and calculated muscle force as its output.

The force-time profile of the muscle calculated by the model was determined as follows. For each iteration (time = t), the relative force potential of the muscle was determined from the active force-length relationship and activation. Force was first predicted as a function of SEC_f length according to its force-length relationship. Since the CC and SEC_f are in series, the force across the CC was set equal the force across the SEC_f. The CC velocity at this force was determined from its force-velocity relationship. The velocity was then integrated with respect to time to determine a new CC length. The new SEC_f length was determined from the new CC length. Also, the tendon length was calculated based on the tendon stress-strain relationship that described SEC_t. Tendon stress was calculated as force / tendon cross sectional area. At the next time step (time = t + Δt), this process was repeated with the new set of initial conditions (activation, CC length, SEC_f length). This iterative process is displayed graphically in figure 3.3.

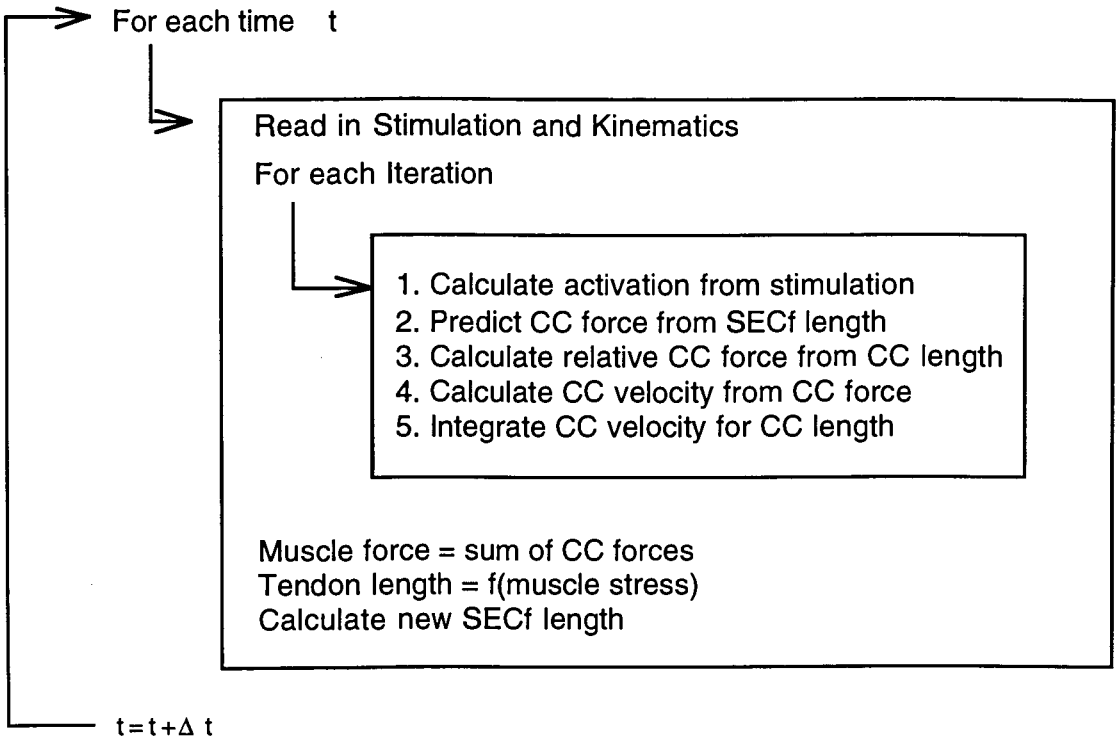

Figure 3.3 Flow diagram displaying the iterative process for calculating muscle force.

For contractions from rest, there are no initial external muscle kinematics from which to predict SEC stretch and therefore muscle force. However, since the muscle in this model was under very little load, only a small amount of activation was needed for the CC to shorten. A very small load allowed the CC to shorten at a very high velocity. Integration of the CC velocity with respect to time determined the CC shortening at the expense of SEC fibre stretch. From then on, the iterative process is identical to when the muscle was exposed to an external influence causing a change in kinematics.

2.4 Scaling

To extend the model to ECRB, the force-velocity relationship describing the CC and stiffness-force relationship describing the SEC_f and the stress-strain relationship describing the SEC_t of FPL were scaled according to the morphometric measurements

obtained for both muscles. The morphometric characteristics of the ECRB muscle were measured in the same manner as FPL (see Methods, chapter 2). Since the isometric force-length relationship describing the CC had been normalized with respect to maximum isometric capacity (Po) and muscle length at Po (Lo) the same relationship was used for both muscles.

The force-velocity relationship was scaled on both the force and velocity axes. The maximum force (Po) was scaled by the ratio of PCSAs while maximum velocity (Vmax) was scaled to ratio of fibre lengths. In order to maintain a/Po = b/Vmax constant, Hill's constant 'a' was also scaled by the ratio of PCSA and 'b' by the ratio of fibre lengths (FL) as indicated below.

$$a_{ECRB} = a_{FPL} \cdot \frac{PCSA_{ECRB}}{PCSA_{FPL}}$$

$$b_{ECRB} = b_{FPL} \cdot \frac{FL_{ECRB}}{FL_{FPL}}$$

The SEC relationships were scaled by these parameters also. Muscles with larger PCSAs tend to be more stiff (i.e.. more springs in parallel) while muscle with long fibres tend to be less stiff (i.e.. more springs in series). The stiffness (k) of the SEC fibre was scaled by the ratios of PCSA and fibre length as shown below:

$$k_{ECRB} = k_{FPL} \cdot \frac{PCSA_{ECRB}}{PCSA_{FPL}} \cdot \frac{FL_{FPL}}{FL_{ECRB}}.$$

The stress-strain relationship describing the tendon of FPL was scaled by the tendon cross-sectional area and length. The same principle applies as for scaling SEC fibre. It was assumed that tendon characteristics per unit length and cross sectional area were the same for both FPL and ECRB tendons.

2.5 Model Evaluation

The efficacy of the model was evaluated by comparing model results to experimental results of a number of different contractions; isometric contractions of FPL, dynamic contractions of FPL and electrical stimulation of ECRB.

2.5.1 Isometric Contractions of FPL

Torque during isometric contractions of FPL was recorded using the force transducer apparatus described in chapter 2. Instead of the elastic link, a rigid link was used to connect the force transducer to the disk so that the disk was unable to rotate. Electromyographic (EMG) signals were recorded using silver-silver chloride electrodes placed on the surface of the skin over the FPL muscle. The EMG signal was amplified and bandpass filtered (32Hz - 3.2 kHz), digitized at 2000 Hz sampling rate and stored on computer (DataQ Data Acquisition Software) for later analysis. The subject performed several isometric contractions of various intensities at the optimal joint angle (established in chapter 2). The subject performed two series of 16 isometric contractions categorized as "FAST" (those with fast rise times) or "SLOW" (those with slow rise times). The first three and last three contractions in each series were of maximum intensity. The EMG recorded during each contraction was full-wave rectified and 3 Hz low-pass filtered (2nd order, dual pass Butterworth) to establish a linear envelope. The mean peak EMG recorded at maximum intensity (first 3 and last 3 contractions) for each condition was used to scale all other EMG (within each condition) so that it could be express as a value between 0 and 1. This established the stimulation input to the model simulation. The stimulation profile of each contraction in each of the two conditions was used as input to the simulation. The output, in the form of a force-time profile, was compared with the force-time profile established experimentally. The measured torque was converted to muscle force using the moment arm measure as described in Chapter 2.

2.5.2 Dynamic Contractions of FPL

During the dynamic contractions of FPL, the angular position of the interphalangeal joint of the thumb was measured using the apparatus described in chapter 2. EMG was recorded from the FPL muscle as described above. Both angular position and EMG were digitized (2000 Hz sampling rate) and recorded on computer. The subject performed maximum flexion contractions of the interphalangeal joint of the thumb in three load conditions. In the first condition (I_{small}), 12 contractions were performed against a small moment of inertia (2.45×10^{-4} kgm^2) introduced by fixing a 50 g mass a distance of 7 cm from the axis of rotation . In the second condition (I_{med}), a 100 gram mass was fixed to the apparatus at a distance of 7 cm from the axis of rotation increasing the moment of inertia to 4.9×10^{-3} kgm^2. Twelve contractions were performed. The third condition (I_{large}), consisted of 12 contractions against a moment of inertia of 9.8×10^{-2} kgm^2 (200g mass at 7 cm). The angular position records for each condition were averaged then differentiated to give angular velocity and double differentiated to give angular acceleration. The EMG was full wave rectified, low pass filtered (3 Hz), scaled to the maximum and then averaged to give the average stimulation profile for each condition. These procedures resulted in a single stimulation and kinematic profile for dynamic contractions against each of the three moments of inertia.

The stimulation profile in each condition formed the input to the model. The output, in the form of joint kinematics, was based on the muscle force predicted by the model. The joint kinematics were calculated in a separate subroutine as an impulse-momentum problem. The angular impulse about the axis of rotation of the distal phalanx of the thumb is equal to the change in angular momentum as reflected by:

$$M_o \Delta t = I_o \omega_2 - I_o \omega_1.$$

The time over which the moment (M_o) was applied was equal to the iteration time of the model (Δt). The resulting angular velocity (ω_2) was calculated by:

$$\omega_2 = \frac{M_o \Delta t + I_o \omega_1}{I_o}$$

The angular position (θ) was determined by numerical integration of the angular velocity over the iteration time,

$$\theta = \omega_2 \Delta t.$$

This procedure was repeated for each iteration of the simulation.

2.5.3 Electrical Stimulation of ECRB

The ECRB muscle was electrically stimulated (Grass S48 stimulator and Grass SIU5 stimulation isolation unit) through bipolar stimulating electrode (Ag-AgCL, 1cm diameter contacts, 2cm centre to centre separation) with a train of 0.2 ms pulses at 60 pps for 800ms. The best location from stimulation was found by moving the stimulator to various locations over the surface of ECRB. The best site was one which produced the largest contraction of ECRB but with no overflow to the neighbouring muscles. The intensity was set high enough to evoke contraction of ECRB but with no overflow to neighbouring muscles. Overflow to other muscles was examined by visual inspection as well as gentle palpation of the tendons of the muscles, particularly extensor carpi radialis longus (ECRL). Extensor torque and radial deviation torque were measured simultaneously using two force transducers similar to the one described in chapter 2. With the hand in a position similar to when the magnetic resonance images were taken, the rigid bar of one force transducer was placed against the dorsum of the hand 5.5 cm from the wrist. The other transducer was placed against the radial side of the hand 6.7 cm from the

wrist (figure 3.4). A train of pulses was used rather than single pulses to provide a better signal to noise ratio for recording torque with the torque transducers. Single pulses evoked only very small torques that were difficult to record over background fluctuations in torque. The train of stimuli were recorded with surface electrodes placed over the ECRB. This signal was later treated in the same manner as the EMG recorded from FPL during voluntary contractions and formed the basis of the stimulation input to the model.

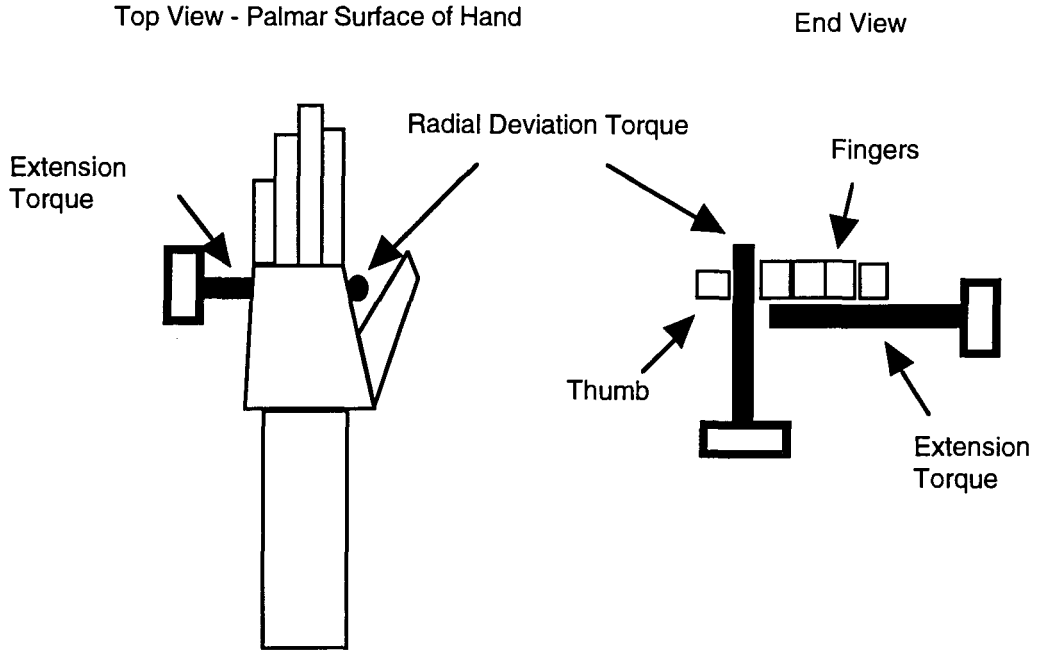

Figure 3.4 Diagram showing the placement of force transducers for recording torque about the wrist during electrical stimulation of ECRB.

Since the stimulation intensity as a ratio of maximum (ie.between 0 and 1) could not be determined accurately for the stimulation trials, only the time course of the resulting twitch-like contractions were compared, not the amplitude.

The ECRB was also subjected to perturbations consisting of a quick stretch. The ECRB was electrically stimulated to produce approximately 0.3 Nm torque then stretched either 3 degrees or 10 degrees in 100 ms by a torque motor apparatus. The torque, angular velocity and angular position were recorded later compared with model predictions.

3.0 Results

3.1. Morphometric Characteristics

Results from the MRI measurements of ECRB are shown in table 3.1 below. Where applicable, measurements of the same muscle from other studies are shown for comparison. Muscle length was defined as the length from the most proximal muscle fibres to the most distal muscle fibres at the muscle-tendon junction following the muscles line of action. Fibre length was not directly measured from the MRI but rather, calculated from muscle length and the fibre length:muscle length ratio of 0.38 reported by Lieber et al. (1990). Muscle volume was calculated by summing the muscle cross-sectional areas measure from the MRI over a slice thickness of 5.5 mm. Muscle mass was calculated from muscle volume and muscle density (1.056 g/cm^3). Maximum isometric force (Po) was estimated by multiplying the PCSA by specific tension (51.4 N/cm^2 calculated in chapter 2).

3.2 Scaling Relationships to ECRB

The effects of scaling the force-velocity relationship for FPL to ECRB by the ratios of PCSAs and fibre lengths are shown below in figure 3.5. The new force-velocity relationship maintained its general shape and is described by Hill's equations where a = 173.6 N and b = 0.873 m/s (a/Po = b/Vmax = 0.87). The maximum isometric capacity (Po) was calculated to be 199.4 N (Po for FPL multiplied by 1.24 (ratio of PCSAs, ECRB:FPL). The maximum shortening velocity (Vmax) for ECRB was calculated to be 2.91 times that of FPL (ratio of FLs, ECRB:FPL).

Table 3.1. Morphometric characteristics of extensor carpi radialis brevis determined from magnetic resonance images compared with values obtained in the literature.

Characteristic	MRI	Loren et al (1995)	Lieber et al (1994)	Lieber et al (1990)	Brand et al (1984)	An et al (1981)	Amis et al (1979)	Horii et al (1993)
muscle length	20.68 cm	18.64 cm	17.6 cm	12.7 cm				
fibre length	7.86 cm	7.08 cm	7.08 cm	4.77 cm	6.1 cm	5.3 cm	4.9 cm	
total length	30.25 cm	28.91 cm	27.87 cm					
PCSA	3.88 cm^2	2.40 cm^2	2.40 cm^2	2.73 cm^2		2.9 cm^2	4.72 cm^2	
tendon length	9.57 cm	10.27 cm	10.27 cm					
tendon CSA	0.115 cm^2	0.146 cm^2						
muscle volume	28.7 cm^3					15.8 cm^3		
pennation angle				8.9 degrees				
muscle mass	30.3 g		11.8 g	13.8 g			24.5 g	
FL/ML		0.38	0.40	0.38				
Moment arm: Ext	1.24 cm	1.5 cm			1.2			1.2 cm
Moment arm: RD	0.97 cm	1.5 cm			1.6			1.3 cm
Po	199.4 N	58.8 N						

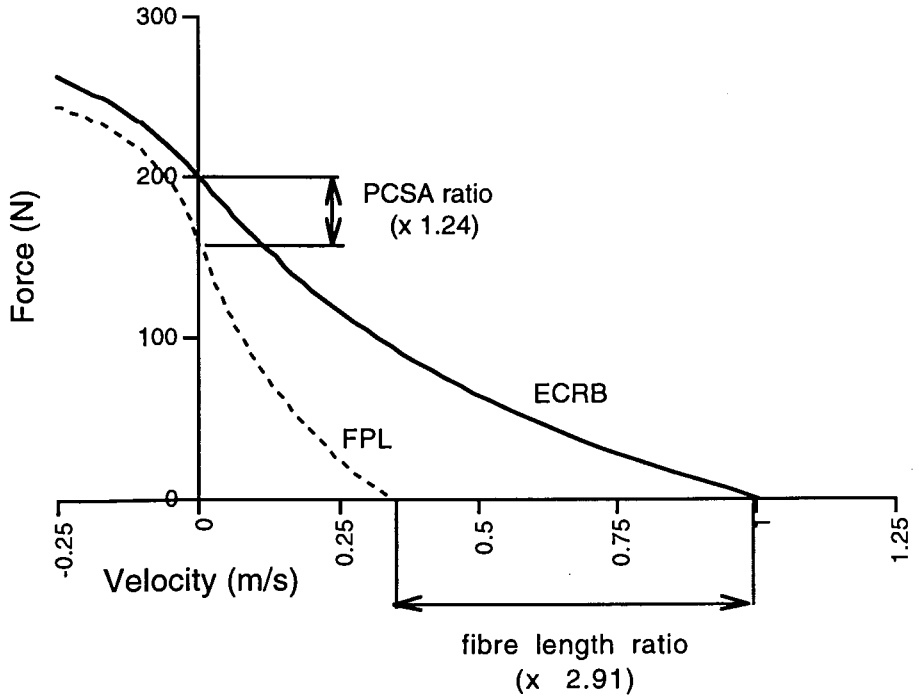

Figure 3.5 Force-velocity relationship for ECRB obtained by scaling the force and velocity axes as indicated.

The force-stiffness relationship describing the SEC_{fibre} of FPL was scaled by the ratios of PCSAs and fibre lengths. The stiffness portion (slope) of the equation describing the force-length-activation relationship of the fibre SEC of FPL was scaled as below:

$$Force_{ECRB} = (17.32+157.82Act^{0.399}) \bullet \left(\frac{PCSA_{ECRB}}{PCSA_{FPL}} \bullet \frac{FL_{FPL}}{FL_{ECRB}} \right) \bullet \text{Stretch of SECf}$$

This equation has the form $F = k \bullet \text{scaling factor} \bullet x$.

3.3 Model Evaluation

3.3.1 Isometric Contractions of FPL

When comparing single contractions, the model produced an isometric force-time profile that resembled the experimental force-time profile for the same EMG input. Figure 3.6 shows the processed EMG signal (rectified, 3 Hz low-pass filtered) that represented the stimulus input to the model. The stimulus to activation function used in this model (Pandy et al., 1992) had an activation time constant of 30 ms and a deactivation time constant of 180 ms. These time constants were chosen so that the activation profile followed the recorded force profile as closely as possible for a single twitch-like contraction. The muscle force predicted by the model is shown together with the actual force recorded for this contraction (figure 3.6). Of note is the similarity in rise-time and peak tension of the force profile predicted by the model compared with the actual record. It is also important to note that the force profile produced by the model follows the activation process much more closely than the actual muscle, suggesting that the model lacks, somewhat, the low-pass filtering characteristics of muscle.

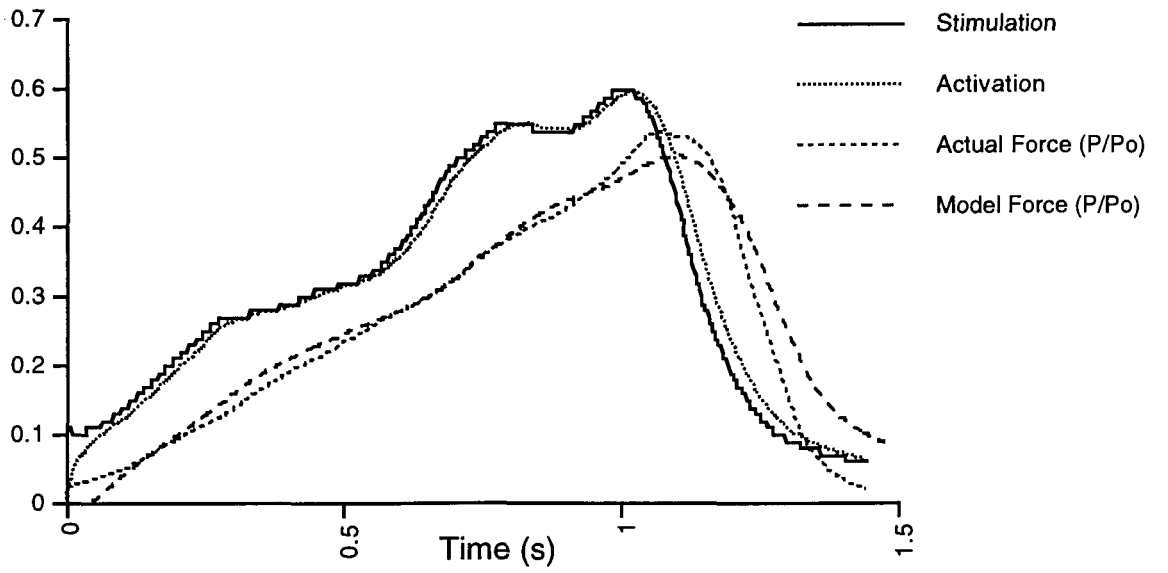

Figure 3.6 Force recorded for a single, SLOW rise isometric contraction of FPL. The processed EMG and model activation are shown for comparison as is the force predicted by the model.

A typical force-time profile of a fast isometric contraction is shown below in figure 3.7. In general, the force profile predicted by the model compared well with the actual force profile. Both the amplitude and time course of tension development and relaxation were predicted well by the model. Of note is the slower rise time of tension compared with stimulation and activation, illustrating the low-pass filter characteristics of muscle captured by the model.

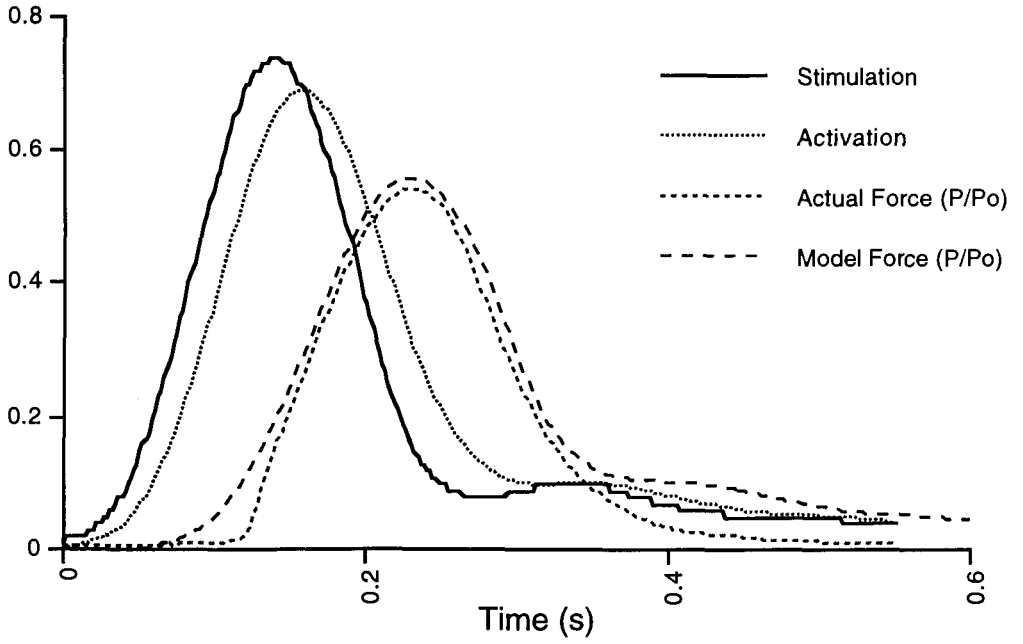

Figure 3.7 Force recorded for a single, FAST isometric contraction of FPL. The processed EMG and model activation are shown for comparison as is the force predicted by the model.

To compare how well the model predicted force from measures of EMG the peak force predicted by the model as well as the peak force recorded experimentally were plotted as a function of peak stimulation (processed EMG). A positive linear correlation for this relationship was expected. Using the rectified, low-passed filtered EMG as input, each voluntary contraction that was recorded was simulated by the muscle model to produce a force-time profile. The peak force predicted by the model was plotted with respect to the peak stimulation determined from the processed EMG. For the SLOW contractions, this relationship was fitted by linear regression and yielded a line with a significant positive correlation ($r^2 = 0.917$, $F(1,9) = 3218$, $p < 0.001$). For the experimental data, the peak torque that was recorded was converted to force and also plotted with respect to the peak stimulation. As with the model results, linear regression resulted in a significant positive correlation ($r^2 = 0.839$, $F(1,9) = 41.84$, $p < 0.001$). When the two EMG-force relationships were compared for SLOW isometric contractions (figure 3.8), the model

appeared to underestimate force more for high intensity contractions than for low intensity contractions.

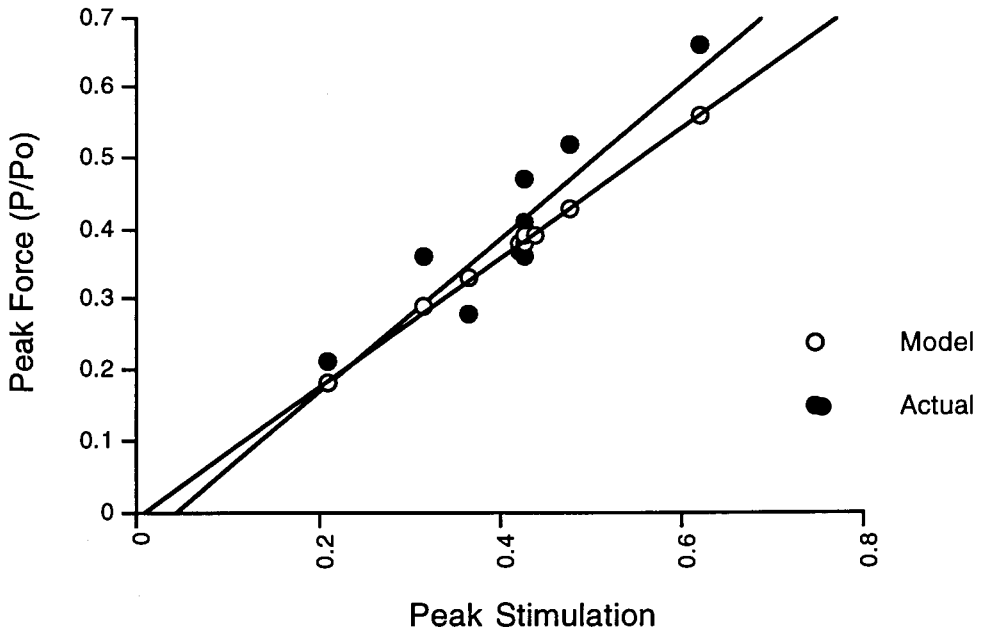

Figure 3.8 Muscle force as a function of rectified, low-pass filtered (3 hz) EMG for experimental and model results for SLOW isometric contractions. (experimental data y = 1.085x - 0.046, $r^2 = 0.839$; model prediction y = 0.917x - 0.007, $r^2 = 0.998$)

Comparison of model results with actual results was accomplished by plotting the actual peak force with respect to the peak force predicted by the model (figure 3.9). If the model prediction were perfect, one would expect a relationship with a perfect correlation, $r^2 = 1$ with a slope of 1. For the SLOW contractions, a significant positive correlation was found ($r^2 = 0.833$, $F(1,9) = 36.96$, $p < 0.001$). The slope of this relationship was 1.177 and y intercept of -0.035 suggesting that the model was a good predictor of force for SLOW isometric contractions.

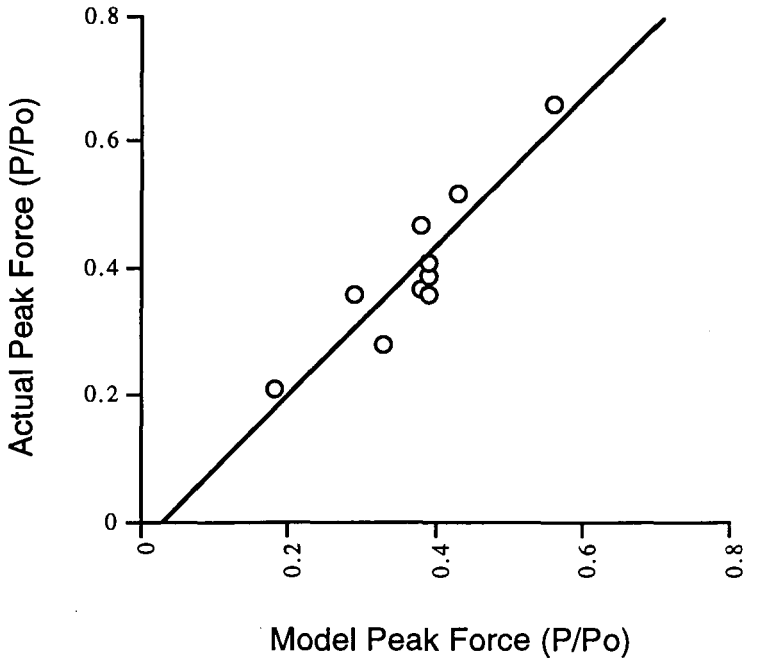

Figure 3.9 Actual peak force as a function of peak force predicted by the model for SLOW contractions. Linear regression $y = 1.177x - 0.035$, $r^2 = 0.833$.

For the FAST isometric contractions, the discrepancy between the model predictions and the actual results was accentuated (figure 3.10). The experimental data showed a larger, although still significant correlation ($r^2 = 0.772$, $F(1,16) = 50.83$, $p < 0.001$) compared with the SLOW contractions. The force-EMG relationship obtained from the model results displayed a significant positive correlation ($r^2 = 0.998$, $F(1,16) = 9627$, $p < 0.001$). The model results appeared to overestimate force for FAST isometric contractions of low intensity contractions but underestimate force for high intensity contractions.

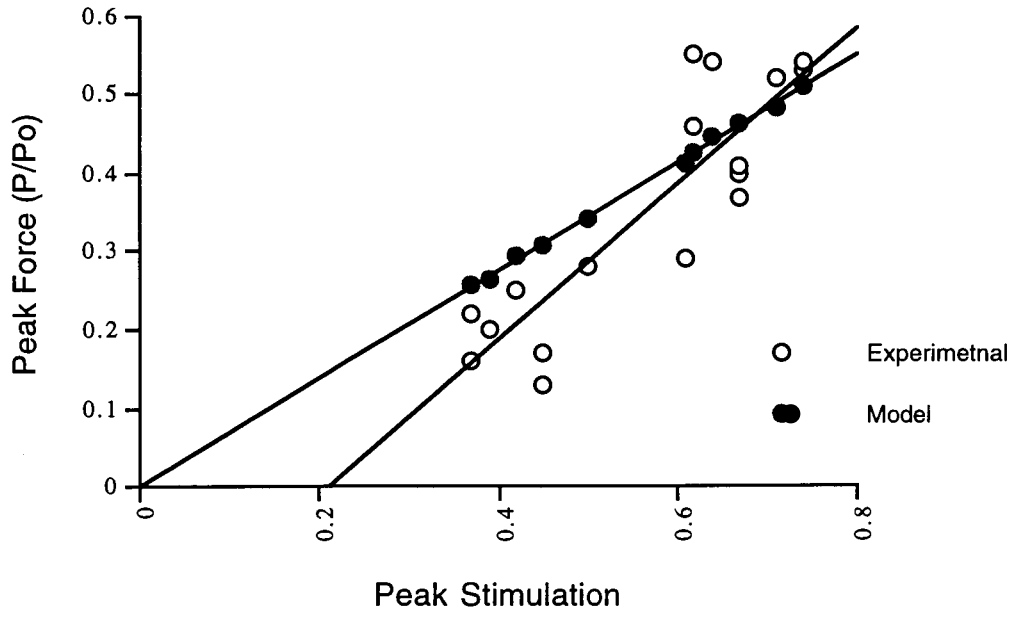

Figure 3.10 Muscle force as a function of stimulation (rectified, low-pass filtered (3 hz) EMG/max EMG) for experimental and model results for FAST isometric contractions (experimental data $y = 0.993x - 0.209$, $r^2 = 0.772$; model prediction $y = 0.684x + 0.003$ $r^2 = 0.998$)

Similar to the SLOW condition, the plot of actual peak force as a function of peak force predicted by the model showed a significant positive correlation ($r^2 = 0.788$, $F(1,16) = 55.65$, $p < 0.001$) in the FAST condition. Also, the slope (1.461) and y-intercept (-0.218) suggest that there is a systematic offset in the model predictions (figure 3.11).

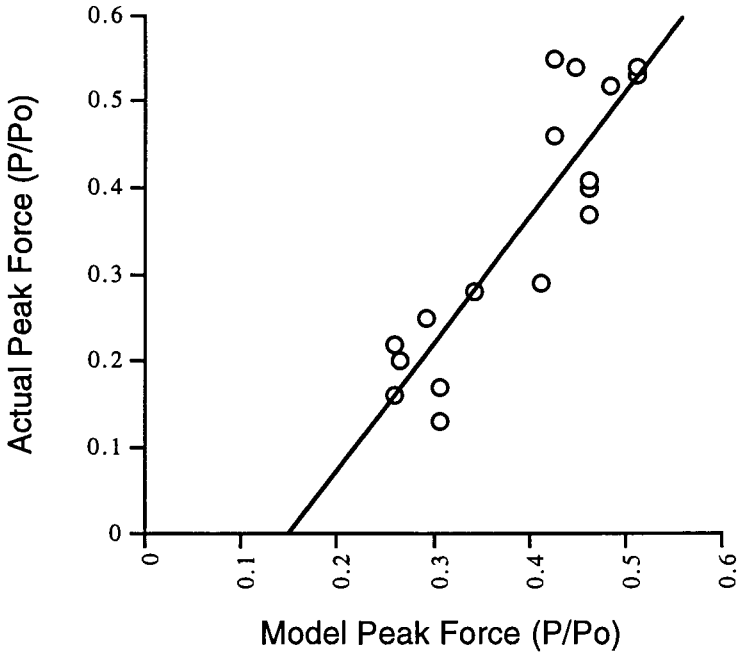

Figure 3.11 Actual peak force as a function of peak force predicted by the model. Linear regression: y = 1.464x - 0.218, $r^2 = 0.788$.

3.3.2 Dynamic Contractions of FPL

The average profiles describing the angular position, angular velocity and angular acceleration of the distal phalanx of the thumb were compared with model results for contractions against three moments of inertia (figures 3.12, 3.13, 3.14). The model appeared to predict well the kinematic characteristic of contractions against each moment of inertia. In each case, however, the model predictions appeared to fluctuate more when compared with the experimental trials. This is not surprising since each experimental condition was an average of ten trials. As the moment of inertia was increased, the kinematics predicted by the model were advanced in time compared with the actual results.

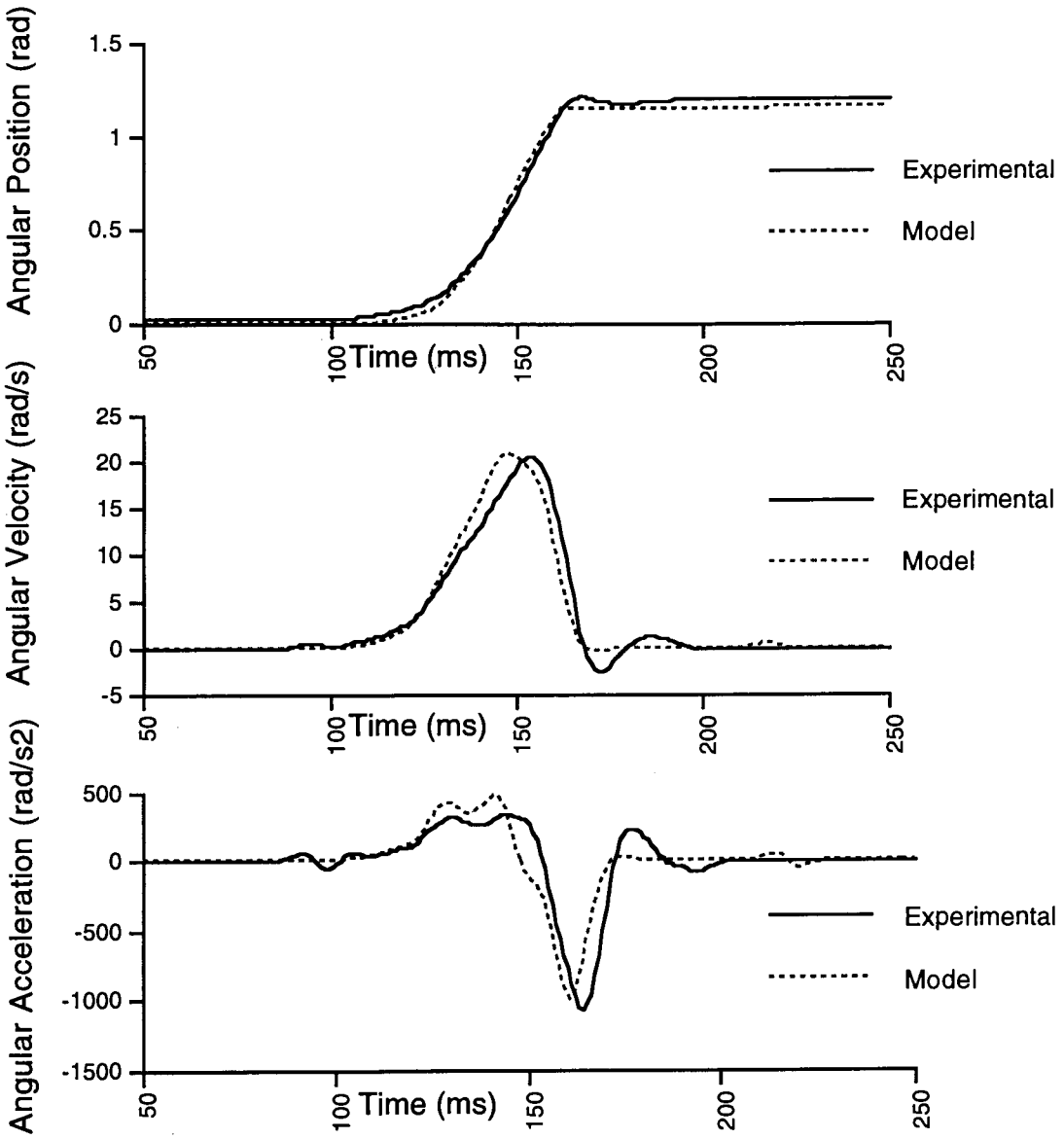

Figure 3.12 Angular position, angular velocity and angular acceleration for I_{small} condition.

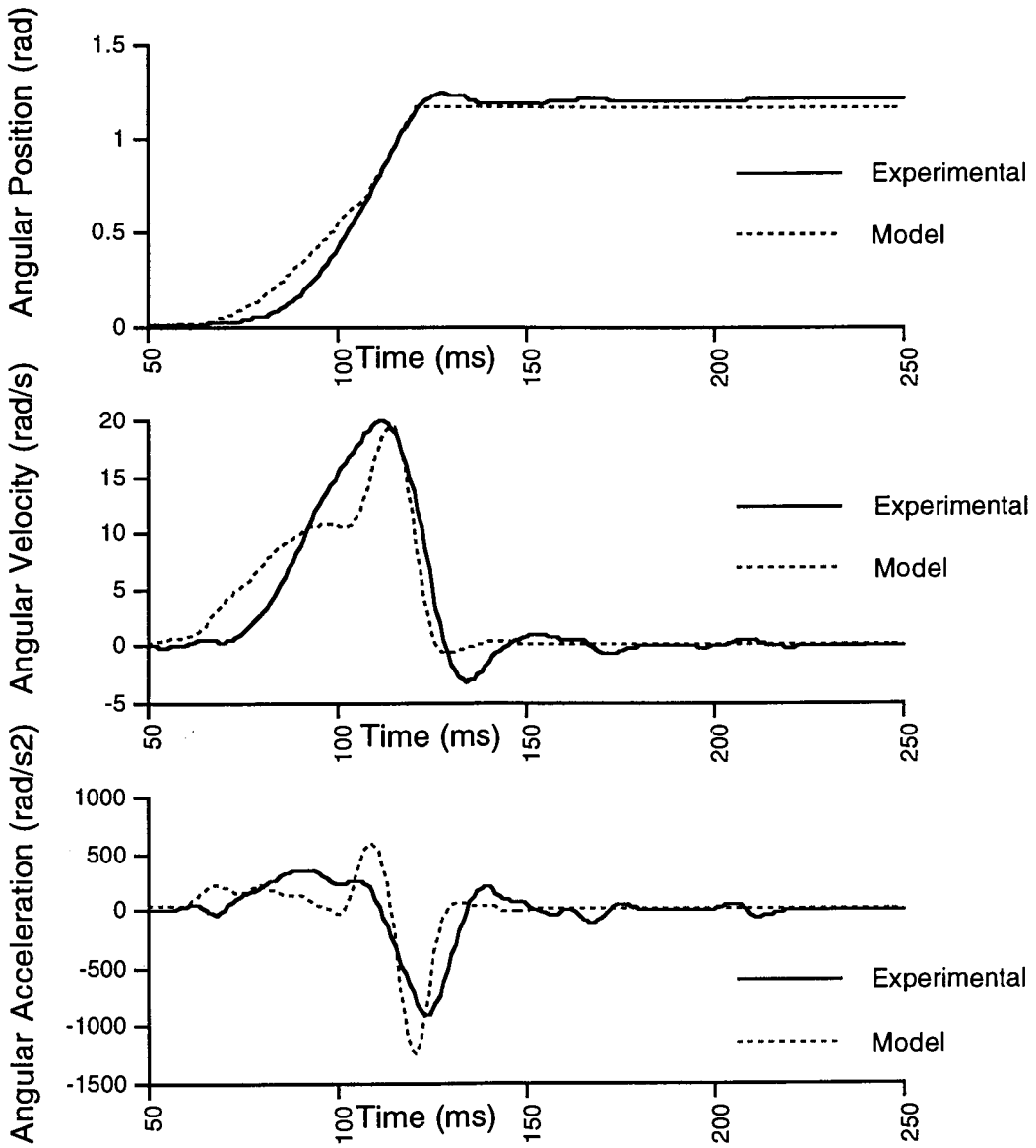

Figure 3.13 Angular position, angular velocity and angular acceleration for I_{med} condition

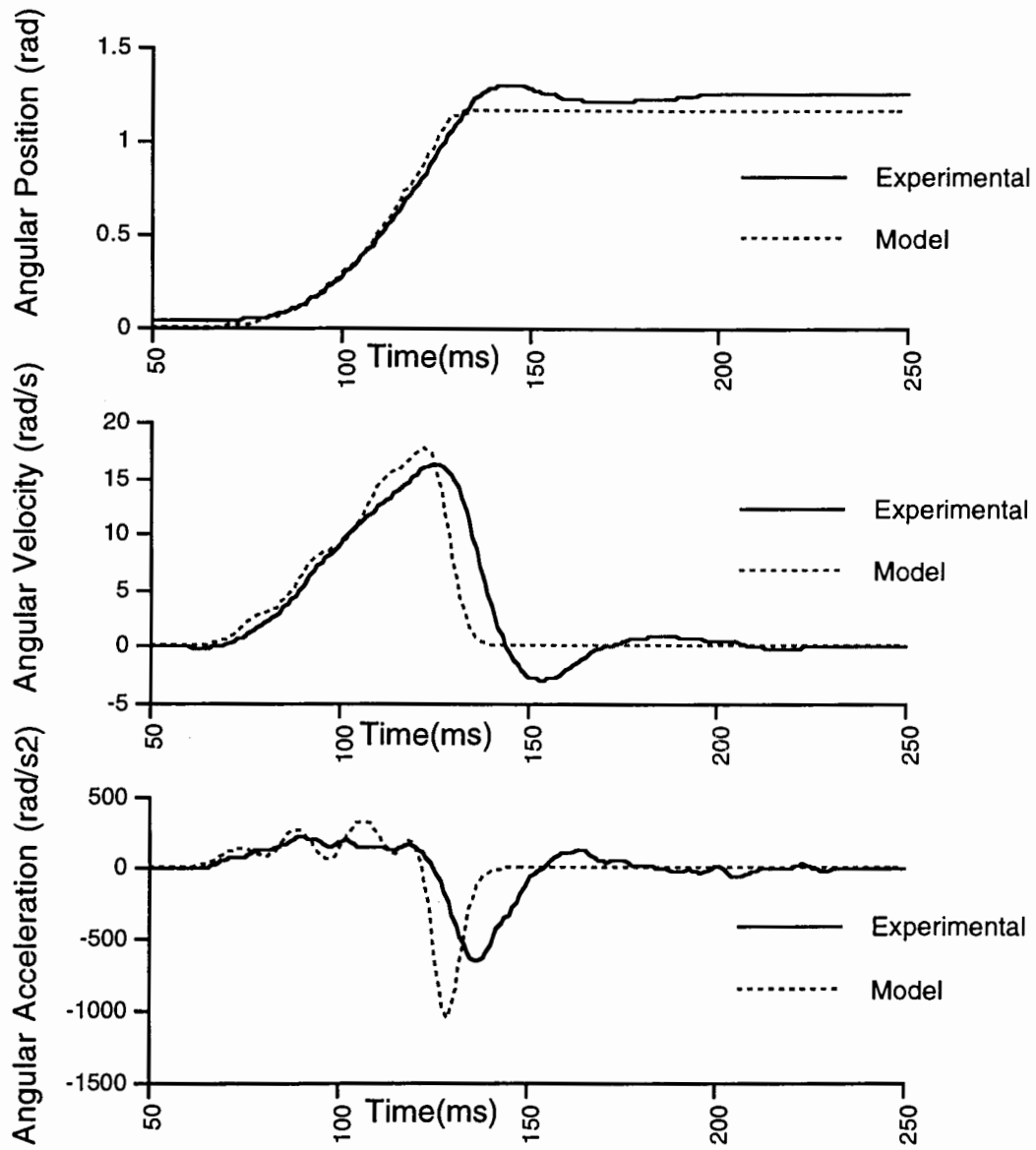

Figure 3.14 Angular position, velocity and acceleration for I_{large} condition

3.3.3 Electrical Stimulation of ECRB

Extensor torque and radial deviation torque recorded during electrical stimulation of ECRB are shown below in figure 3.15. These values were displayed as joint torque rather than converted to muscle force so that the relative magnitude of the muscle moment arms for ECRB could be easily observed.

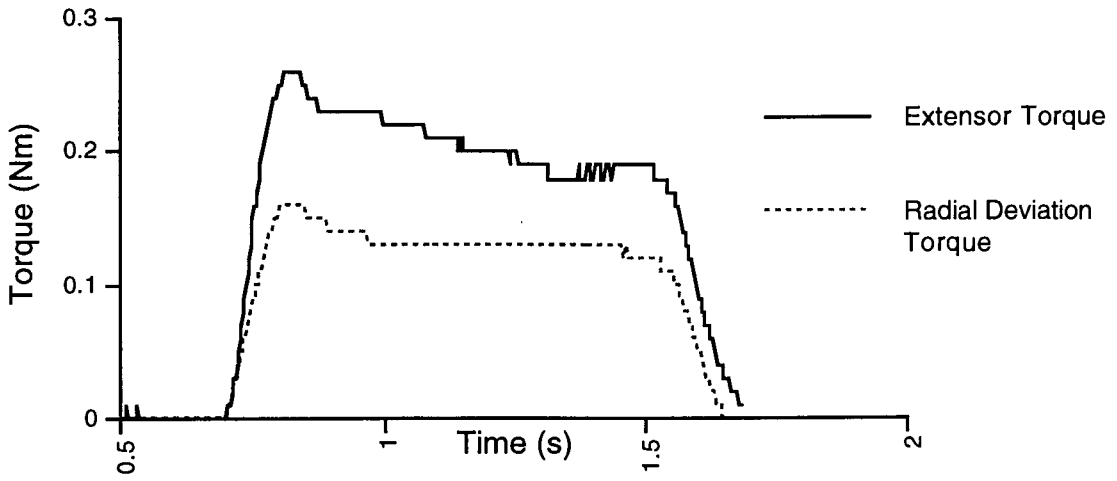

Figure 3.15 Extensor and radial deviation torque recorded for ECRB in response to electrical stimulation (800 ms train, 60 pps, 0.2 ms pulse)..

For the experimental data, the peak torque in the extension direction was 1.6 times higher than in the radial deviation direction in response to the same muscle stimulation. The ratio near the end of the stimulation train dropped to 1.46 times. Extension torque predicted by the model would be 1.28 times greater than radial deviation torque since the moment arm measured in the MRI cross-sections was 1.28 times greater for extension than for radial deviation.

When subjected to a quick stretch perturbation, the model prediction showed an increase in torque as a result of the stretch. In the experimental trial, there was a large transient torque due to acceleration and deceleration of the hand and the apparatus. The moment of inertia of the hand and apparatus was estimated by oscillating the hand and apparatus at a frequency of 20 Hz and recording position and torque. The position trace was double differentiated to give angular acceleration. The moment of inertia was estimated as the average ratio of torque to angular acceleration during the period of oscillation. Also the passive stiffness of the wrist extensors was measured by performing quick stretches while the limb was relaxed. The values for inertia and passive stiffness

were used in the model so that total torque about the wrist could be calculated. The torque due to the passive stiffness was a function of angle while the torque due to the inertia was a function of angular acceleration (angular position double differentiated). These torques were added to the torque contribution of ECRB predicted by the model.

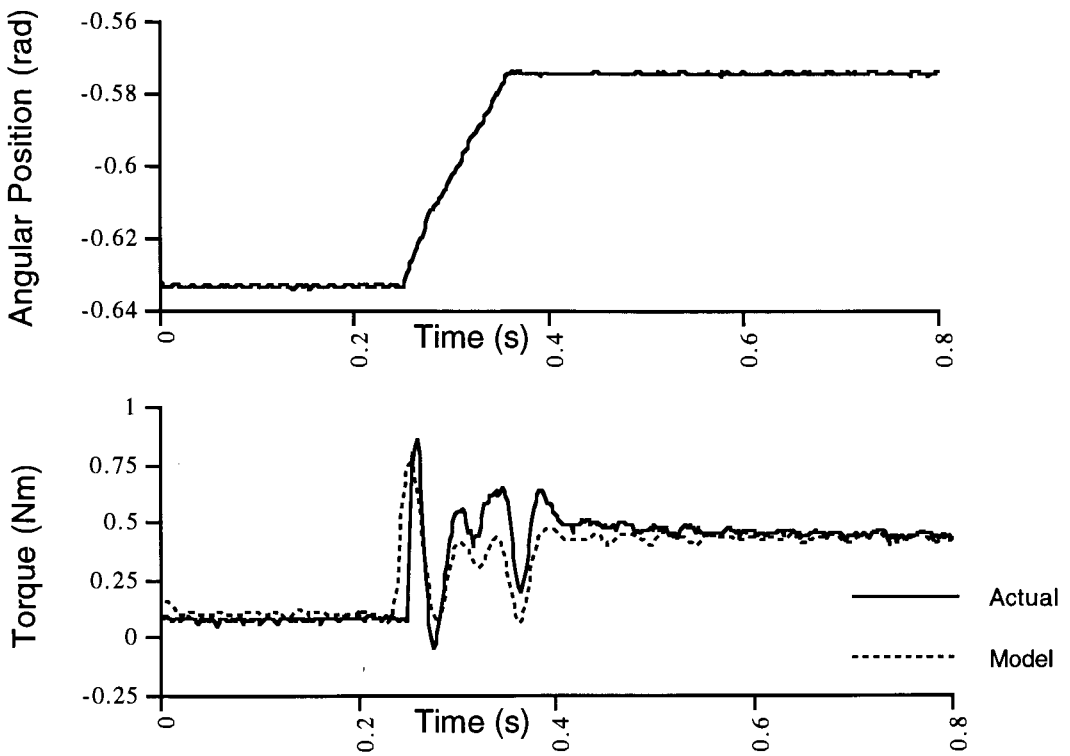

Figure 3.16 Experimental and model prediction of the response of ECRB to a quick stretch of the wrist (3 degree stretch)

4.0 Discussion

In general, the computer simulation of FPL predicted force well for isometric contractions. During dynamic contractions the angular kinematics predicted by the model compared favourably with those recorded experimentally. The model parameters were scaled based on the morphometric characteristics to represent ECRB. The efficacy of the model of ECRB was tested by imposing a quick stretch perturbation. The model predicted the torque response well after inertial effects and passive stiffness were accounted for.

4.1 Morphometric Characteristics and Scaling

As in chapter 2, the morphometric characteristics of ECRB were determined from serial cross sectional magnetic resonance images of the right forearm and hand of one subject. The dimensions describing muscle volume, mass, length, physiological cross sectional area, fibre length, tendon length, tendon cross sectional area and moment arm were displayed in table 3.1 along with measurements available in the literature that described the same dimensions. Although there is a considerable variation in human dimensions, the values obtained in this study were similar to those found in the literature.

When measuring the muscle moment arm, it is vital to have an accurate description of the axis of rotation of the joint. This is particularly difficult for the wrist joint because of the complex interaction between the carpal bones. Also, the precise centres of rotation for the wrist were difficult to measure from only cross sectional scans. Ideally, serial longitudinal scans in conjunction with kinematic data could be used to determine the centres of rotation. In addition, each MR cross-sectional image portrayed a surface that was separated from the next by 5.5mm. If the axis of rotation was somewhere in this gap, it could not be measured. Therefore, there could be an error of up to 2.75 mm in estimating the axes of rotation of the wrist. This potential error corresponds to approximately half the distance between the radial-ulnar deviation axis and the flexion-extension axis (Buchanan et

al., 1993). However, using an EMG coefficient method, Buchanan et al. (1993) found that the torque about the wrist was insensitive to changes in the separation of the two axes over a range of 0 to 2.0 cm and suggested that the variability of the EMG activity overshadowed any variability in the length of separation of the two axes. Since EMG forms the basis of the activation input to the model, this study would face the same insensitivity. Therefore, for ease of measurement, the axial position of the centres of rotation of both the flexion/extension axis and radial-ulnar deviation axis were set to coincide at the head of the capitate.

The magnitude of the moment arms of ECRB for radial deviation and extension (figure 3.17) found in this study compared favourably with those reported previously (Horii et al., 1993; Buchanan et al., 1993; Tolber et al., 1985; Loren et al., in press). There is, however, some controversy as to which is larger.

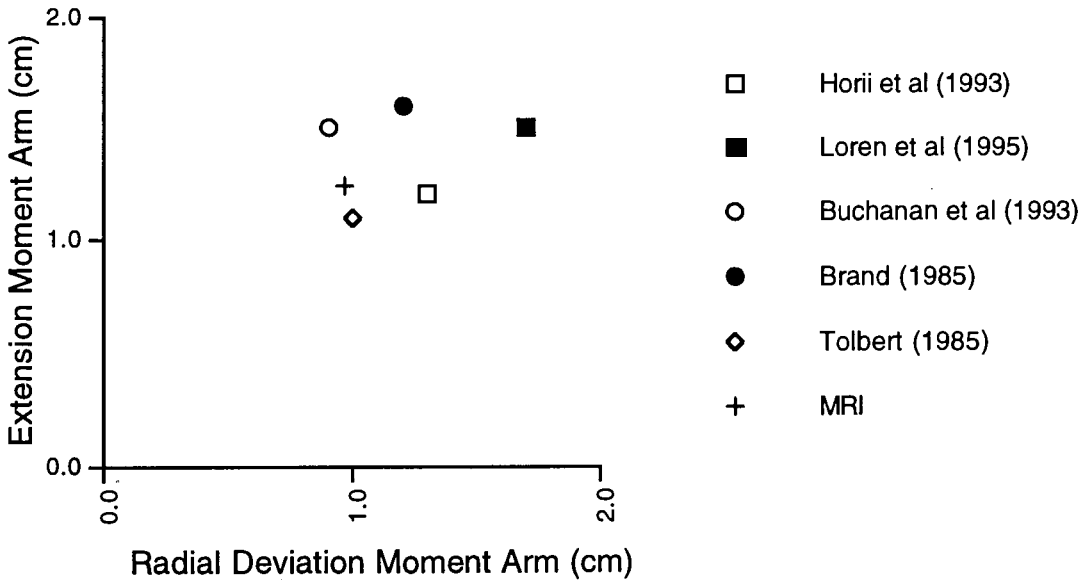

Figure 3.17 Moment arms of ECRB determined from the MRI scans in this study compared with values reported in the literature.

After examining the tendon excursion of ECRB in human cadavers Horii et al. (1993) suggested that the moment arm for radial deviation was 1.3 ± 0.2 cm and for

extension 1.2 ± 0.2 cm and that these values remained constant through the range of motion. Loren et al.. (in press) however, suggested that the moment arms vary with joint angle, particularly for extension. With the wrist in neutral position the moment arms of ECRB were approximately 1.7 cm for radial deviation and 1.5 cm for wrist extension but reached its maximum of 1.9 cm at 30 degrees of extension (Loren et al., in press). The radial deviation moment arm varied less. Using MR images, Buchanan et al. (1993) found that the moment arm for wrist extension (1.5 cm) was considerable larger than for radial deviation (0.9 cm). These are similar to the values reported here and were confirmed by electrical stimulation of ECRB which resulted in greater extensor torque than radial deviation torque.

The effects of scaling the force-velocity relationship of FPL to represent ECRB were shown in figure 3.5. This scaling was based on the ratio of physiological cross sectional areas and the ratios of fibre lengths between the two muscles. The maximum isometric tension of a muscle is proportional to its physiological cross sectional area (Powell et al., 1984) and so the relative tension of muscles can be compared by comparing their PCSA (Brand et al., 1981). The PCSA calculated in this study for ECRB was 1.24 times greater than the PCSA of FPL, suggesting that the maximum isometric potential of ECRB was 1.24 times greater. Brand et al. (1981) estimated that the ECRB could produce 1.56 times the tension of FPL based on measurements taken from cadaver specimens. These measurements were based on comparisons of PCSA of each muscle as a percentage of the total PCSA for all the muscles of the limb. The resulting term, "tension fraction" was only a proportional measure and made no numerical statement of the tension, but rather allowed for comparison of the relative capability of each muscle. Lieber et al. (1990, 1992) also measured morphometric characteristics of several forearm muscles of five human cadavers. The PCSA measured was 1.31 times greater for ECRB than for FPL. In examining the MRIs, there was some difficulty in delineating individual muscles,

particularly the proximal fibres of ECRB from extensor carpi radialis longus. This could have lead to an underestimation of the volume of ECRB and subsequently the PCSA.

It has been suggested that the speed at which a muscle can contract is proportional to its fibre length (Zajac, 1992). Assuming that individual sarcomeres have similar maximum shortening velocities, a muscle fibre with more sarcomeres in series would have a larger maximum shortening velocity. The fibre length in this study, calculated as a portion of muscle length measured from the MR images was 7.86 cm. Lieber et al. (1992, 1994) has shown that there is a remarkable consistency in the muscle length to fibre length ratio. For ECRB this ratio is 0.38 and was used to calculated the fibre length of ECRB. When compared with the data of Lieber et al. (1994), the muscle length measured in this study compares well. Obviously using the muscle length to fibre length ratio suggested by Lieber et al. (1992, 1994) would result in a good comparison of fibre length as well. Other studies have measured fibre lengths in ECRB of 4.9 cm (Amis et al., 1979), and 5.3 cm (An et al., 1981). Although the fibre lengths described by Lieber et al (1992) are actually measures of fascicle length (see Chapter 2), they are still useful in scaling the velocity axis of the force-velocity relationship to represent muscles of various lengths assuming there is a consistent relationship between fibre length and fascicle length.

4.2 Model Evaluation

In general, the model predictions of force in isometric contractions compared well with experimental results whereas the kinematics of dynamic contractions was less well predicted.

4.2.1 Isometric Contractions of FPL

The force-time profile for isometric contractions of FPL were compared with model predictions for contractions of both fast rise times and slow rise times. Although the overall range was similar, the SLOW contractions appeared to underestimate force

particularily for high intensity contractions. Linear EMG-force relationships for isometric contractions have been well documented (Seyfert and Kinkel, 1974; Carter et al., 1993; Jensen et al., 1993) and have formed basic assumptions in estimating muscle forces (Buchanan et al., 1993). The force estimate of the model for isometric contractions is a linear function of stimulation (rectified and low-pass filtered EMG) and so the explanation for the error may be expressed in terms of the EMG. The rectified EMG was low-pass filtered at 3 Hz, similar to the 20 ms rise time used by Hof and van den Berg (1981a,b) and suggested by Zajac (1989). Filtering would result in a bias toward low frequency, type S (slow) motor units. That is, the higher frequency fast motor units would be attenuated more than lower frequency slow motor units. According to the size principle (Henneman et al., 1965) small, slow motor units are recruited before large, fast motor units. Filtering would reduce the amplitude of the EMG, more at higher intensities than at lower intensities because the high frequency units would be more attenuated. The greater attenuation of the signal at higher intensities could be a direct contributor to the underestimation of force since the stimulation input to the model was attenuated. This may contribute to the overestimation of force at low intensity contraction also. Since the stimulation input to the model was expressed relative to the maximum rectified, low-pass filtered EMG for a given condition, an underestimate of this maximum due to the biased attenuation of the filtering would lead to an overestimation of the submaximal stimulation, particularly at the lowest intensities of contraction.

For the FAST isometric contractions, force predicted by the model was overestimated at the lowest intensities and underestimated at the high intensities of contraction compared with the force determined from experimental trials. The explanation offered above would explain this observation as well. A further explanation is that the EMG-force relationship for FPL is non-linear. Infact, an exponential relationship may provide a good fit to the experimental data.

4.2.2 Dynamic Contractions of FPL

Dynamic contractions of FPL against various moments of inertia were performed while angular position of the thumb and EMG were recorded. The model predictions compared well with the actual kinematics recorded for position, velocity and acceleration. Although in some cases EMG-force relationships have been found to be highly non-linear during dynamic contractions (Guimaraes et al., 1995) others have found have found linear relationships, but only using EMG recordings from areas of high signal amplitude (Jensen et al., 1993). Reasonable predictions of instantaneous force during dynamic voluntary contractions have been made using models that use processed EMG along with force-velocity and force-length properties of muscle (Hof and van den Berg, 1981a,b; van den Bogert et al. , 1988). One possible explanation for the variability in EMG during dynamic contractions may be movement of the electrodes with respect to the active motor units. Given that each contraction was of maximum effort and there was little variability in the peak angular velocity obtained, one might expect a more consistent peak amplitude of the processed EMG.

As the moment of inertia against which FPL was contracted was increased the model predictions became more advanced in time. A constant time delay was introduced between stimulation and activation in order to approximate any electromechanical delay. There are data, however, that would suggest that the phase lag between integrated EMG and tension increases with the frequency (Soechting and Roberts, 1975). Therefore it may have been more appropriate to have a delay that was a function of the input frequency (command) rather than a constant delay.

4.2.3 Electrical Stimulation of ECRB

Stimulation of ECRB was used to examine the mechanical properties of the muscle in isolation and compare the responses with the model predictions. Specifically, the stimulation profiles were used to examine the extension and radial deviation moment arms

as well as the muscle's response to a perturbation. The difference between extensor torque and radial deviation torque was simply a function of the magnitude of the moment arm in each of these two directions since muscle force should be the same. The ratio of extensor torque to radial deviation torque for the electrical stimulation contraction of ECRB was 1.6 to 1.46 depending on where it was measured and suggested the moment arm for extension was at least 1.46 times greater than for radial deviation. The model, however, predicted that the torque in extension should be only 1.28 times greater based on the comparison of moment arms. The decreasing torque during the stimulation suggested that some form of accomodation may have been present. As the stimulation continued, the muscle fibres may have been less likely to respond to their full capacity. Also, the torque values did not drop by the same ratio (extension torque decreased more than radial deviation torque), suggesting that the experimental set may have been at fault. Despite this, the stimulation suggested that the moment arms determined from the MR images were at least the correct order of magnitude as well as direction (i.e., extension greater than radial deviation). There may also have been some stimulation overflow to other muscles. Given the location of the stimulating electrodes, it was likely that overflow stimulated a portion of the finger extensors, which would contribute to wrist extensor torque also, rather than the flexor carpis radialis (also a radial deviator). This would explain the greater extensor torque seen during the stimulation trials compared with the extensor torque predicted by the moment arm ratios.

In response to a sudden perturbation about the wrist joint consisting of a stretch of the extensor muscles, torque about the wrist increased markedly. The magnitude of the torque increase was predicted well by the model, including the torque fluctuations during the stretch. This suggested that the model adequately reflected the muscle's response to a sudden perturbation and would be useful in simulating conditions in which the muscle is subjected to a sudden, small perturbation.

5.0 Summary

The model and simulation of FPL presented in this chapter accurately predicted muscle force for isometric contractions as well as joint kinematics for the dynamic contractions. When the parameters were extended to ECRB, the model captured the general force producing characteristics of this muscle. These results suggested that the model would prove useful in simulating a wide variety of contractions of ECRB.

Chapter 4

Force in Extensor Carpi Radialis Brevis During a Backhand Tennis Stroke: Implications for Injury

1.0 Introduction

Lateral Epicondylitis or Tennis Elbow is manifested by pain over the region of the lateral epicondyle of the humerus (Roetert et al., 1995). One prime etiological factor for Lateral Epicondylitis (LE) is thought to be over exertion of the Extensor Carpi Radialis Brevis (ECRB) muscle resulting in microtrauma (Morris et al., 1989). At greatest risk of injury are those persons performing repetitive wrist movements in sports such as tennis or occupations such as keyboard entry.

It appears that novice tennis players in particular are at risk of developing LE and often report pain on performing a backhand stroke. Lateral Epicondylitis occurs in up to 50% of recreational tennis players, most of whom are over 30 years of age (Morris et al., 1989). Examination of the kinematics of the backhand stroke initially led investigators to suggest that skilled players maintain a constant wrist position, whereas novice players are likely to use more wrist motion to produce the stroke (Bernhang, et al., 1974). Increased grip pressure has also been suggested as an expert-novice difference that may contribute to over exertion of the ECRB muscle (Bernhang et al., 1974). More recently, Ingelman (1991) and Blackwell and Cole (1995) investigated the kinematic and EMG profiles of expert and novice tennis players performing the backhand stroke and showed distinct differences between the two groups. Experts performed the stroke with the wrist extended while novices performed the stroke with the wrist flexed. Furthermore, at ball contact, experts increased the amount of wrist extension while novices increased the amount of

wrist flexion (Blackwell and Cole, 1995). The wrist flexion patterns observed in the novice players may indicate conditions that promote wrist extensor injury. This eccentric contraction of the ECRB may lead to injury through at least two possible mechanisms. First, eccentric muscle contraction has been shown to result in muscle injury (Lieber et al., 1991) characterized by muscle fibre degeneration. The second possible mechanism concerns the muscle's isometric force-length relationship. The kinematic profile of the novice group suggests and increased lengthening of the ECRB muscle at the point of impact of the ball. This lengthening may move the ECRB beyond the plateau of its force-length relationship, to a position that is less advantageous in counteracting the large loads experienced during the imposed stretch resulting from ball impact (Blackwell and Cole, 1995). Until now, muscle forces and internal muscle kinematics could not be assessed in order to confirm or refute the speculative nature of the potential injury mechanisms.

This section offers a practical application of the model of ECRB to predict muscle force using the EMG and kinematic data of Ingelman (1991) as inputs. These data were used because the kinematics describing not only the motion about the flexion/extension axis, but also motion about the radial/ulnar deviation axis were available.

1.1 Purpose

The purpose of this chapter was to apply the model of ECRB using established kinematic and EMG data describing the backhand tennis stroke. It was expected that both qualitative and quantitative differences in the action of ECRB in advanced and novice players would be predicted and that these differences would help to explain why novice players are more at risk of developing lateral epicondylitis.

2.0 Methods

The typical EMG and kinematic profiles of advanced and novice tennis players as reported by Ingelman (1991) were used as input to the model simulation. The figures summarizing the EMG (rectified, low-pass filtered) and wrist joint kinematics (figures 9, 10 and 11 from Ingelman, 1991) of advanced and novice tennis players performing a backhand stroke were scanned onto a Macintosh computer and digitized using *NCSA Image* software. This process resulted in time series data describing each profile at a resolution equivalent to sampling at 143 Hz. The EMG was expressed as a fraction of maximum (0 to 1). Kinematics were described by the changes in wrist joint angle about both the flexion/extension axis and the radial/ulnar deviation axis. From the kinematics, the length change or excursion of the ECRB muscle was calculated based on the equation, $E = r\theta$, where r is the moment arm and q the joint angle. The total excursion was calculated as the sum of the excursion due to both flexion/extension motion and radial-ulnar deviation motion. For a full description of how these data were collected and processed, see Ingelman (1991). The iterative model developed in Chapter 3 was used to predict the muscle force in ECRB in both the novice and advanced groups.

3.0 Results

3.1 Kinematics

The time series data describing the EMG and joint kinematics of advanced and novice tennis players performing a backhand stroke are shown in figure 4.1. For a full description of these data see Ingelman (1991). Briefly, the advanced and novice groups show similar patterns of activation and joint kinematics although the amplitude of activation and angular position were significantly different (Ingelman, 1991). Both groups began the movement with the wrist extended. The novice group began movement toward wrist flexion well before ball impact and reached a peak wrist flexion angle of approximately 10 degrees approximately 200 ms before ball impact. Just before impact, the novice group began a rapid extension movement. Immediately after impact, the wrist angular position in the novice group increased sharply toward flexion due to the collision of the ball with the racquet. This transient and abrupt change in angle lasted approximately 50 ms, after which wrist extension continued in the follow through phase of the motion.

In contrast, the advanced group exhibited little change in flexion angle until approximately 400 ms before impact. At this point, the advanced players began wrist flexion, however the angular position of the wrist always remained in extension. Just before ball impact, the advanced group began a rapid extension movement. The transient flexion after ball impact was markedly diminished in the advanced group compared with the novice group.

The angular position about the radial deviation axis showed differences between the advanced and novice groups as well. Novice players began the motion with the wrist ulnar deviated. Just before impact, they rapidly increased ulnar deviation angular position. Immediately after impact there was a sudden slowing of the ulnar deviation before increasing again to reach a peak of approximately 24 degrees about 100 ms after impact. Following this, the wrist underwent radial deviation toward neutral. The advanced group

displayed a similar kinematic pattern but began the movement with the wrist radially deviated. The rapid movement to ulnar deviation began approximately 100 ms before impact. At impact there was a brief change in direction from ulnar deviation to radial deviation before ulnar deviation continued to a maximum angle of approximately 15 degrees about 150 ms after impact.

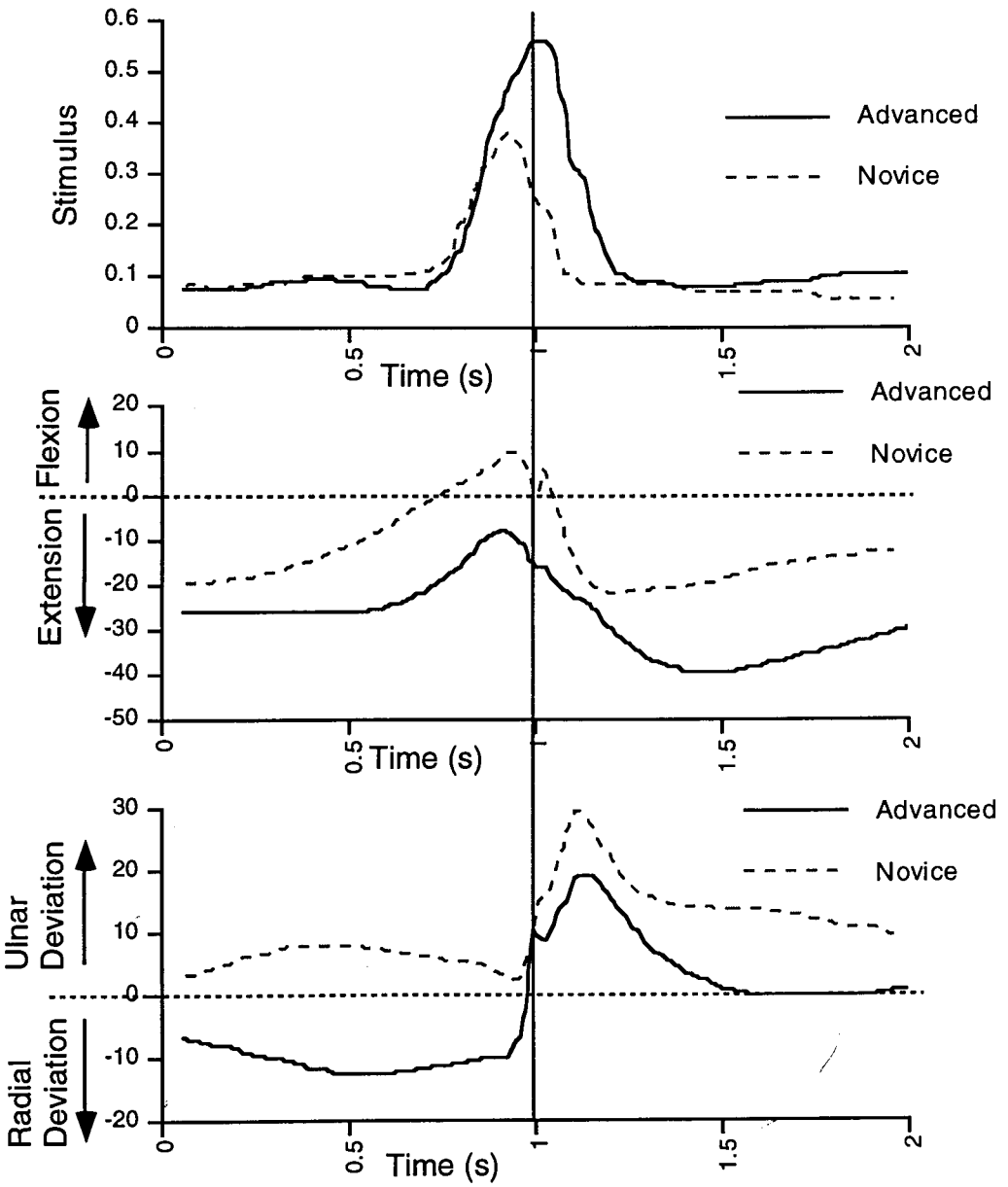

Figure 4.1 EMG and wrist kinematics of novice and advanced players performing a backhand tennis stroke. Stimulation (a), flexion/extension kinematics (b) and radial/ulnar kinematics (c) shown are from Ingelman (1991).

3.2 ECRB Muscle Force

The force-time profiles predicted by the model for advanced and novice players are shown in figure 4.2 below. The advanced group exhibited a larger peak force (89.9 N, 162 ms after impact) compared with the novice group (65.33N, 3 ms after impact). In the advanced group, impact occurred well before the peak force but for the novice group impact nearly coincided with peak force. The greater muscle force seen in the advanced group compared with the novice group may have been predicted from the greater magnitude of stimulation (EMG), however, kinematics also play an important role in determining muscle forces.

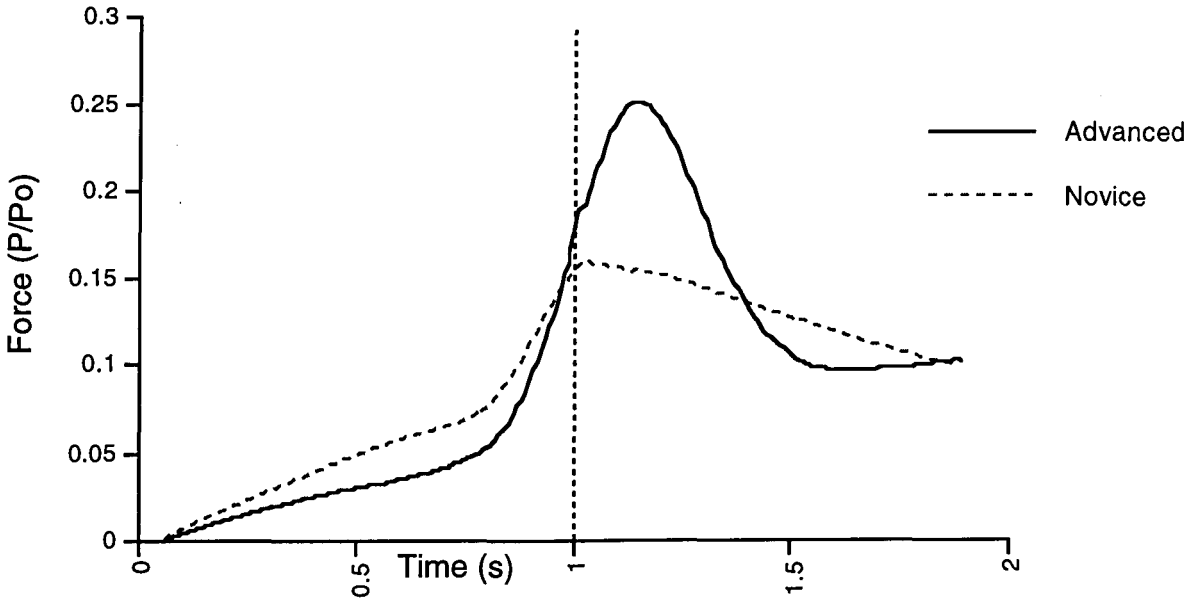

Figure 4.2 Muscle force in ECRB predicted by the model for advanced and novice groups. Ball impact is at time = 1.0 s.

The change in length of ECRB resulting from the wrist kinematics during the backhand stroke of the advanced and novice groups is illustrated in figure 4.3. Although in both groups the muscle lengthened during the first half of the movement (until ball impact) then shortened during the follow-through, there also were striking differences between the

two profiles. In the novice group, ECRB moved from a length shorter than resting (negative values) to a length longer than resting (positive values) at impact. However, in the advanced group, ECRB remained shorter than resting length throughout the entire course of the movement. At impact it was closest to resting length, but remained slightly shorter.

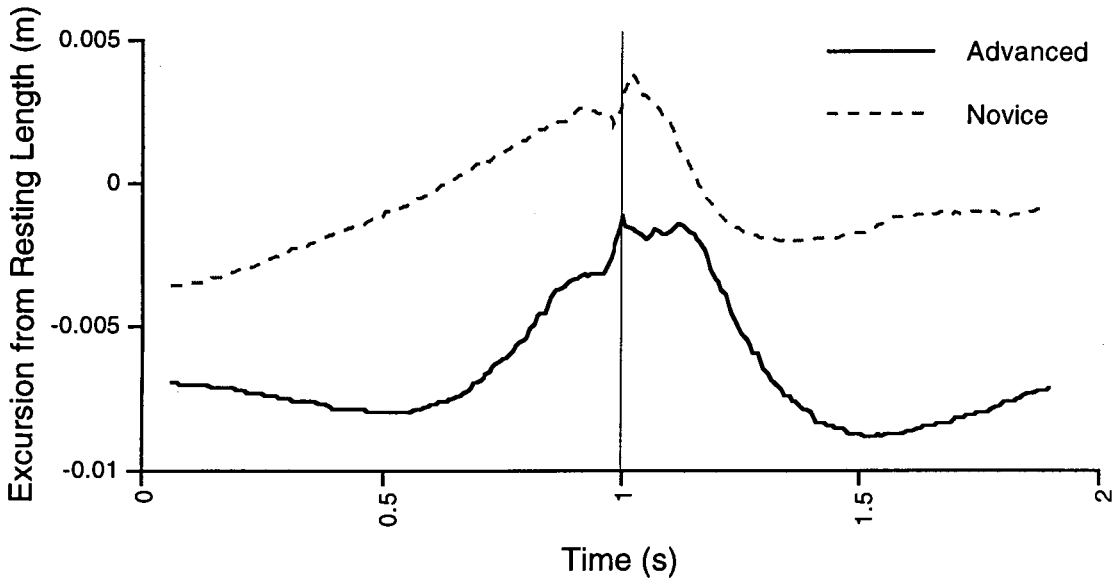

Figure 4.3 Muscle length change from resting length as a result of wrist kinematics of advanced and novice groups. Solid vertical line designates ball impact.

To demonstrate the importance of the wrist kinematics in determining muscle force, the model was used to predict force for an isometric contraction from the same activation profile as the dynamic contraction (Figure 4.4). Muscle length was set to the same length as the initial conditions of the dynamic contraction and remained constant. In the advanced group the peak tension was considerably lower in the isometric contraction compared with the dynamic contraction.

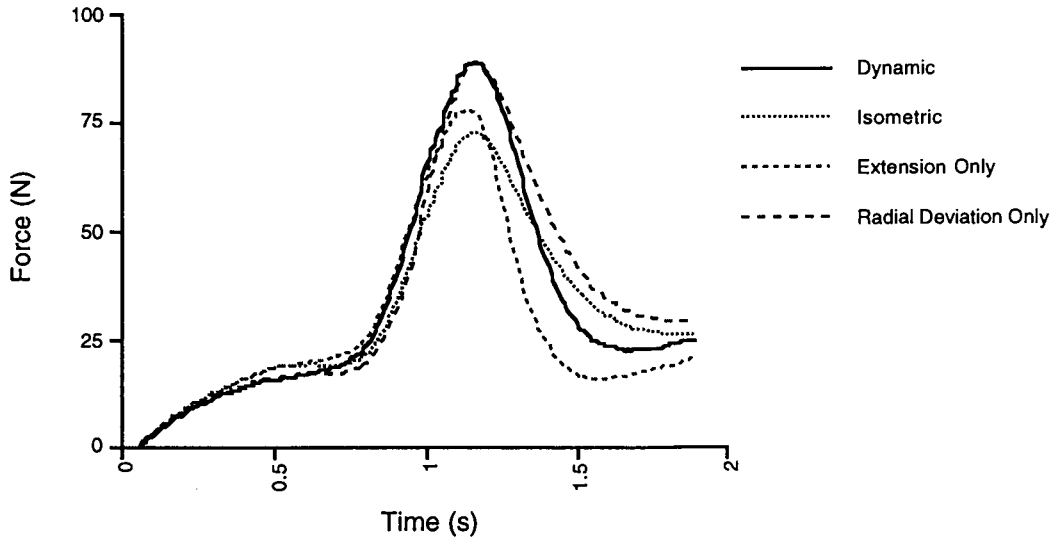

Figure 4.4 Effects of wrist kinematics on predicted muscle force for the advanced group.

When radial/ulnar deviation movement was removed, the tension was also lower than the normal dynamic condition and the shape of the later phase of the force-time profile was altered. When flexion/extension movement was set to zero, the force-time profile was nearly identical compared with the normal condition until impact after which the force profile was altered.

For the novice group, kinematics seemed to play a minor role in determining muscle force. The tension under normal dynamic conditions, theoretical isometric conditions, radial/ulnar deviation kinematics alone and flexion/extension kinematics alone were predicted by the model and shown in figure 4.5.

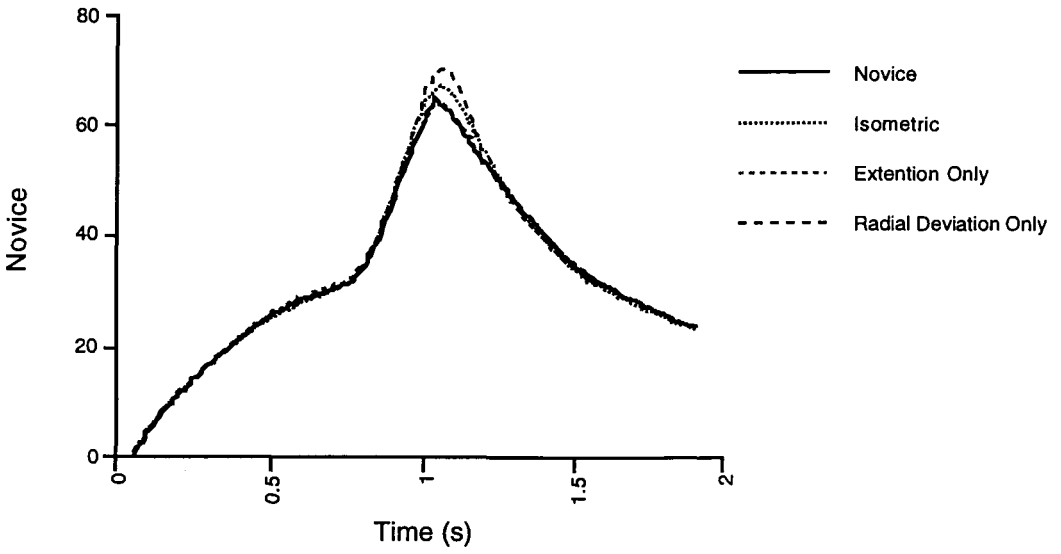

Figure 4.5 Effects of wrist kinematics on predicted muscle force for the novice group.

The isometric contraction showed a small increase in force compared with the normal dynamic contraction suggesting that the wrist kinematics of the novice group had little effect on determining muscle tension. Not surprisingly neither radial/ulnar deviation kinematics alone nor flexion/extension kinematics alone had a large effect on muscle force.

The length changes of the ECRB muscle brought about by the wrist kinematics were examined more closely in an effort to determine how these length changes were distributed amongst the components of the muscle model. The muscle was made up of part tendon (SEC_t) and part muscle fibre. The sum of the length of these two components was always equal to the length of the muscle. Continuing, the muscle fibre was made up of part contractile component (CC) and part fibre series elastic component (SEC_f). Similarly, the sum of the length of these two components was always equal to the length of the muscle fibre.

In the novice group, the muscle kinematics resulted in a slow stretch of the muscle fibre (figure 4.6c) with little length change in the tendon (figure 4.6b) for the first 750 ms of the movement. Just before ball impact, the muscle fibre underwent little length change

while the tendon was stretched. The ball impact resulted in a sudden lengthening of the muscle which was taken up primarily by the muscle fibre. Closer examination of the components that make up the muscle fibre revealed that the lengthening of the muscle fibre was taken up almost exclusively by the SEC_f.while the CC length remained constant.

In the advanced group, the muscle kinematics showed a slow shortening of the muscle fibre (figure 4.7c) with little change in tendon length (figure 4.7b) for the first 500 ms of the movement. Closer to ball impact, both the muscle fibre and tendon were stretched. Just after impact, the muscle fibre shortened slightly while the tendon continued to stretch. The kinematics of the contractile component (figure 4.7d) and fibre series elastic component (figure 4.7e) showed that the lengthening was taken up by the SEC_f while the CC shortened.

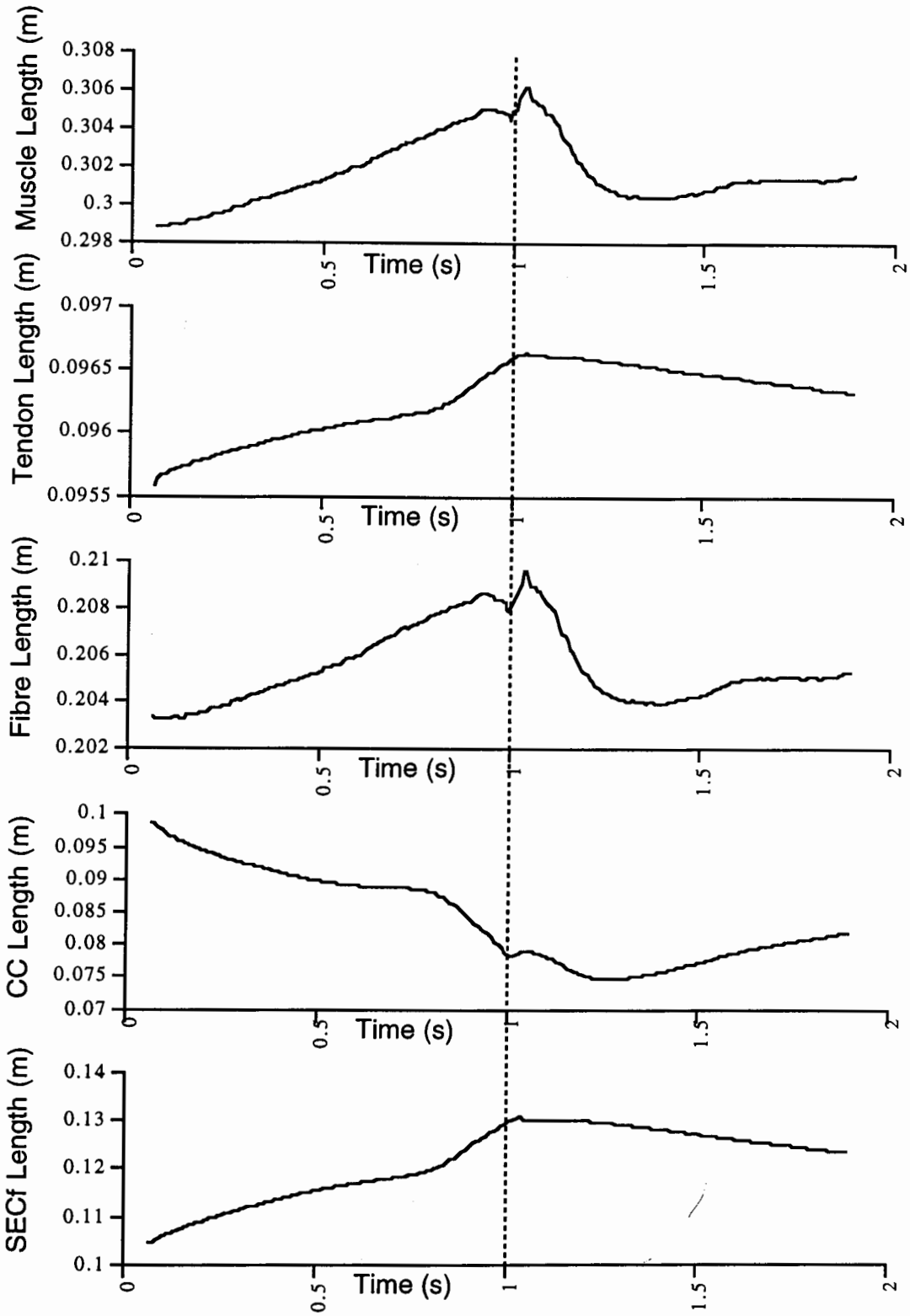

Figure 4.6 Muscle length (a), tendon length (b), fibre length (c), contractile component length (d), and fibre series elastic component length (e) during backhand stroke of novice group.

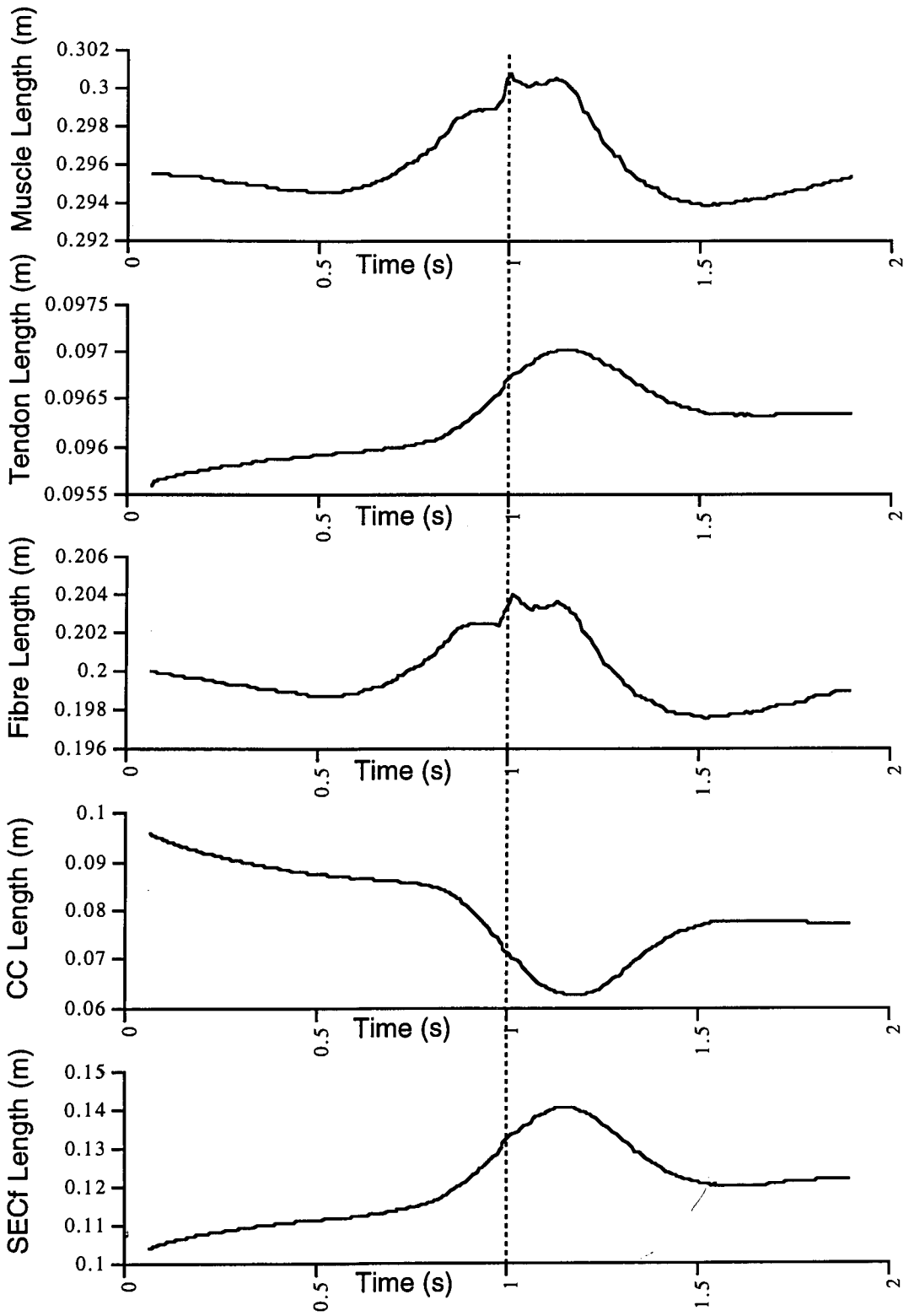

Figure 4.7 Muscle length (a), tendon length (b), fibre length (c), contractile component length (d), and fibre series elastic component length (e) during backhand stroke of advanced group.

4.0 Discussion

The model results suggested that advanced players produced more tension in ECRB during the backhand tennis stroke than did novice players. Perhaps a more important aspect than the amplitude of the tension is where the peak tension occurred with respect to ball impact. In the novice group, the impact occurred at peak force in ECRB. As a result the muscle was in a less advantageous state to deal with the sudden stretch, which occured just after impact. With decreasing activation and tension, stiffness was reduced, particularly in the muscle fibre where a large portion of the impact was taken up (figure 4.6c). This means the muscle fibre underwent a large stretch due to the ball impact which was taken up in primarily by the fibre SEC (figure 4.6e). An additional consideration is the muscle's position along its force-length relationship when impact occurred. For the novice group, the muscle was slightly longer than resting length. The sudden lengthening resulted in movement toward the descending limb of the force-length relationship, toward diminishing force potential for increased lengths. Essentially, the novice group displayed entirely the wrong muscle kinematics and activation pattern to best cope with the sudden lengthening resulting from ball impact.

The advance group, on the otherhand, displayed increasing activation and muscle force leading up to ball impact. The impact resulted in a stretch of the muscle, which was taken up by the tendon and fibre series elastic components. The ECRB muscle length for the advanced group was slightly shorter than resting length at ball impact and therefore, any sudden stretch would push the CC to a more advantageous position on its force-length relationship.

These observations fit with those seen during surgical intervention to treat LE. The tendinous origin of ECRB has been implicated as the site of damage in patients with lateral epicondylitis (Peterson and Renstrom, 1986). Although the maximum tendon stress observed in this study (7.8 N/mm^2 for advanced and 5.7 N/mm^2 for novice) was far from

the estimated ultimate stress (50 - 100 N/mm^2; Zajac, 1989) and would not cause an acute tendon strain, the repetitive nature of tennis could result in a chronic strain due to the repetitive loading or stresses of the tendinous origin of ECRB (Keene, 1985). Indeed, the observations in this study suggest that the novice player is subjected to greater stretch of tendinous components of the ECRB than are advanced players.

Chapter 5

Limitations

The usefulness of a model can be evaluated by asking whether it contributes to the better understanding of a problem or question in science. The model presented in this thesis was a better predictor of muscle force in some contractions than in others. Isometric contractions were predicted well, but dynamic contractions were more variable. The difficulty in predicting force from EMG during dynamic contractions has been experienced by many researchers. Most often, electromyography has been used as an indicator of muscle force in conjunction with some force-length-velocity relationship of muscle to predict force. This seems to work well for isometric contractions, but not dynamic contractions. The major limitations of this type of Hill model is that the relationships were derived from essentially static situations. Even the force-velocity relationship, which by name implies some dynamic component was, essentially a static relationship. Each point was derived from a measure of instantaneous velocity and force and so the relationship lacked the continuous nature of actual muscle. This is also a fundamental limitation of a computer simulation. In this simulation, there was a discrete, serial order of operations that was a quasistatic iteration to determine force.

The simulation also had other limitations that may alter the behaviour of the muscle. There was no distinction of "internal tendon" or aponeurosis which would alter the properties of the muscle Also, pennation angle, although when small may hardly alter muscle force, has been shown to have a considerable effect on muscle compliance.

Despite these short comings, the model performed quite well when used to compare two conditions of muscular contraction as in the tennis stroke. Each parameter was estimated as accurately as possible and appeared to compare well with similar measurements obtained from the literature. Therefore, to obtain results more accurate than

those presented in this thesis it may be necessary to utilize a model of more complex structure. However, this would require more complex interactions between relationships and as a result more computing time and power. One must evaluted the balance between cost and benefit for each application of this and any other model before deciding on potential changes.

There are several advantages of using MRI to establish model parameters. The technique allows parameters to be established on living tissue in an unharmful and non-invasive manner. It is also useful since data from the same subject can be used to perform experiments in the laboratory. However, difficulties arise in determining the precise centres of rotation and orientation of the axes. In this study only cross-sectional images were available to determine the centres of rotation of joints and moment arms of muscles. A better method would have been to use additional scans form other angles in conjunction with kinematic data to estimate better the location of the centre of rotation of each joint.

Appendix 1

Sensitivity Analysis

In many models, certain parameters have a greater influence on the model's outcome than others. In this sense, it is often useful to determine which parameters are the most important. This can be accomplished by assessing changes in the model's output in response to changes in a given parameter. Those parameters for which small changes cause large changes to the model output are thought to be most important and the model is said to be *sensitive* to changes in these parameters. A sensitivity analysis was carried out on the model of FPL by altering several parameters. The activation time constant (τ_{rise}), deactivation time constant (τ_{fall}), muscle fibre stiffness, and the force-velocity parameters ***a*** and ***b*** were each altered by plus or minus 5, 10, 25 and 50 % of their initial value while every other parameter was held constant. The peak force predicted by the model during a single isometric contraction was compared for each change in the parameter of interest.

A1.1 Activation Time Constant (τ_{rise})

Only the largest changes in activation rise time (50%) had a noticeable effect on the force profile predicted by the model (figure A1). Using the fastest rise time (-50% of the initial value) resulted in a highest peak force as well as a fastest rise in tension. Using the slowest rise time (+50% of the initial value) resulted in a lowest peak tension and slowest rise in tension. However in general, the model was insensitive to small changes in activation rise time.

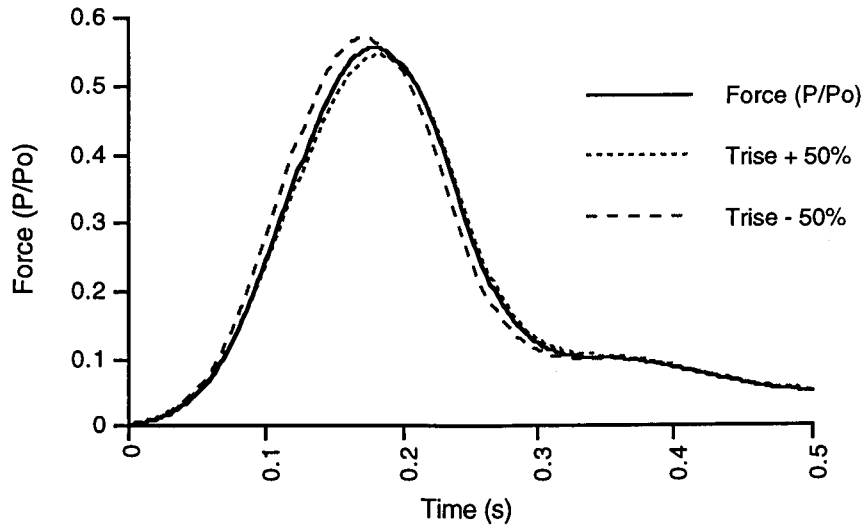

Figure A1: Model prediction of force for activation rise time constant +/- 50% of original.

A1.2 Deactivation Time Constant (τ_{fall})

Changes in deactivation time constant of +/- 50% of the initial value showed only a small effect on model predictions of muscle force (figure A2). The main effect in terms of force amplitude was on the falling phase of the contraction. The lowest time constant (ie. faster deactivation) resulted in a fastest increase in force production and also a fastest decrease or relaxation. The overall effects, however, were small compared with the large changes in the value of this parameter. The model was insensitive to small changes in the deactivation time constant

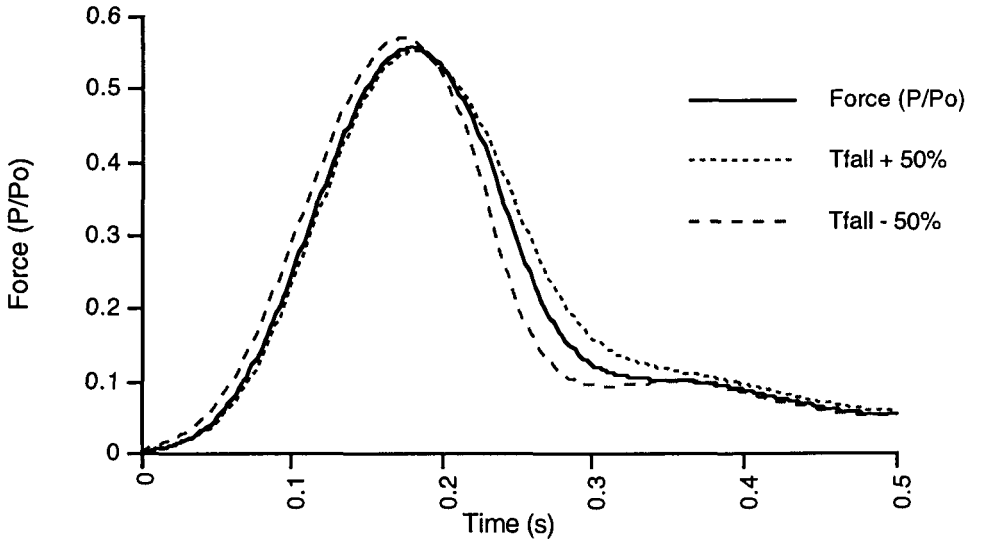

Figure A2: Model prediction of force for deactivation time constant +/- 50% of original.

A1.3 Fibre Stiffness (k_{SECf})

Changes in muscle fibre stiffness had a more pronounced influence on force compared with changes in the activation and deactivation parameters (figure A3). A 50% reduction in fibre stiffness had a dramatic effect on the model prediction of force, decreasing the force substantially. Although a 50% increase also had a noticable effect, the force prediction was increased by a smaller amount suggesting a non-linear effect with changes in fibre stiffness.

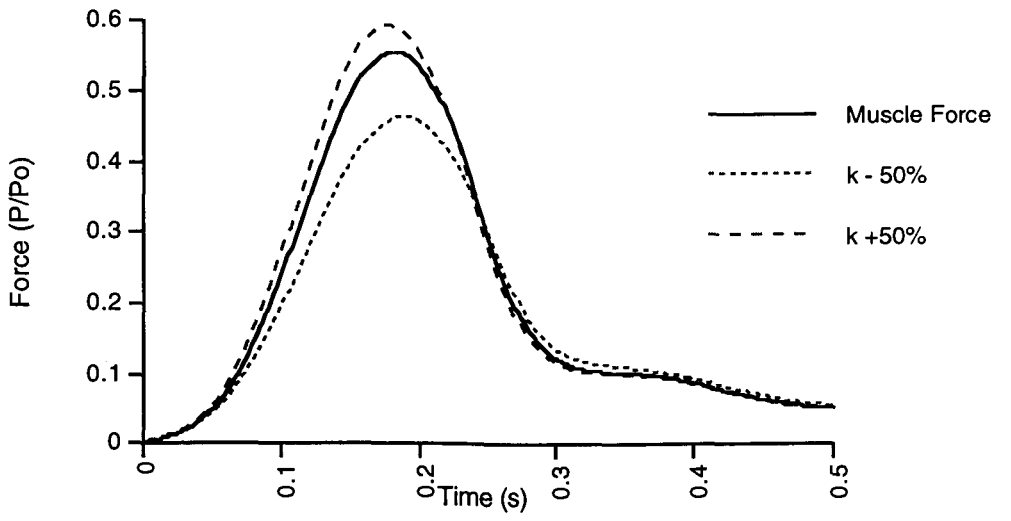

Figure A3: Model prediction of force for fibre stiffness +/- 50% of original.

This nonlinear influence was illustrated more clearly when the percent change in the fibre stiffness was compared with the percent change in peak force prediction (figure A4) over the entire range of changes. Changes in force output were larger for decreases in muscle stiffness than for increases in muscle stiffness. As the stiffness was reduced, the contractile component, in series, was able to shorten at a high velocity as it stretched the SECf. This higher velocity of shortening came at the expense of force, as predicted by the force-velocity relationship. With increased stiffness, the CC was less able to stretch the fibre SEC and contracted at a lower velocity approached thereby generating more force. The non-linear effects in terms of force amplitude are, then, a result of the shape of the force-velocity relationship. That is, changes in velocity of contraction do not result in linear changes in force. These values were summarized in table A1.

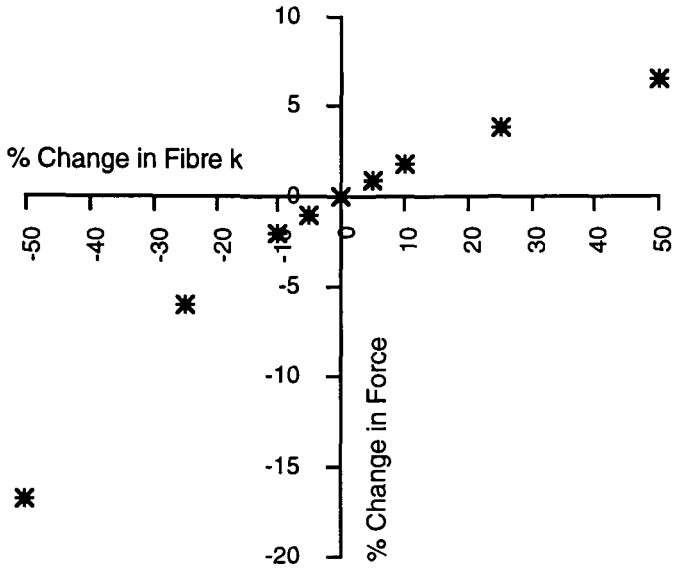

Figure A4. Percent change in peak force as a function of percent change in fibre stiffness.

Table A1 Changes in Peak Force as a Function of Changes in Fibre Stiffness

Fibre Stiffness	Peak Force (P/Po)	Percent Change
initial	0.557	0%
+ 5%	0.562	+0.89%
+ 10%	0.567	+1.8%
+ 25%	0.579	+3.9%
+ 50%	0.593	+6.5%
- 5%	0.552	-0.9%
- 10%	0.546	-2.0%
- 25%	0.524	-5.9%
- 50%	0.464	-16.7%

A1.4 Hill's Parameter *a*

Changes in force velocity parameters also effected the model predictions of force. Increases in Hill's parameter ***a*** resulted in decreases in force output and also a slower rise

in tension (figure A5). For increases in this parameter, the opposite changes were observed. This can be explained by examining the changes in the force-velocity relationship with changes in ***a***.. In the case of increased ***a*** (+50%) the force at any velocity was less than the initial value. For decreased ***a***, the opposite was true.

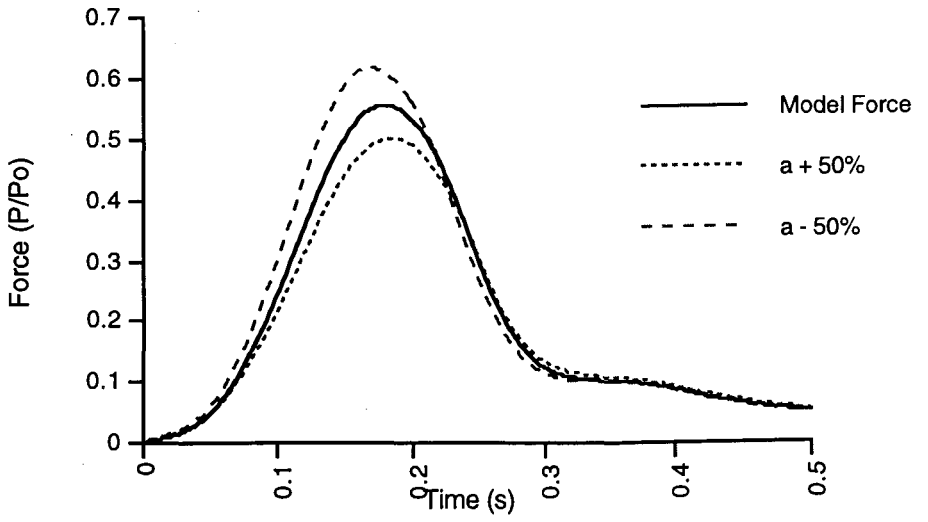

Figure A5. Model prediction of force for simulations using values of ***a*** +/- 50% of original.

Over the entire range of changes, there was a linear relationship between changes in ***a*** and changes in force. This is because the shape of the force-velocity relationship was preserved such that at any velocity the force was increased or decreased by the same amount for a given change in ***a***. These values were summarized in table A2.

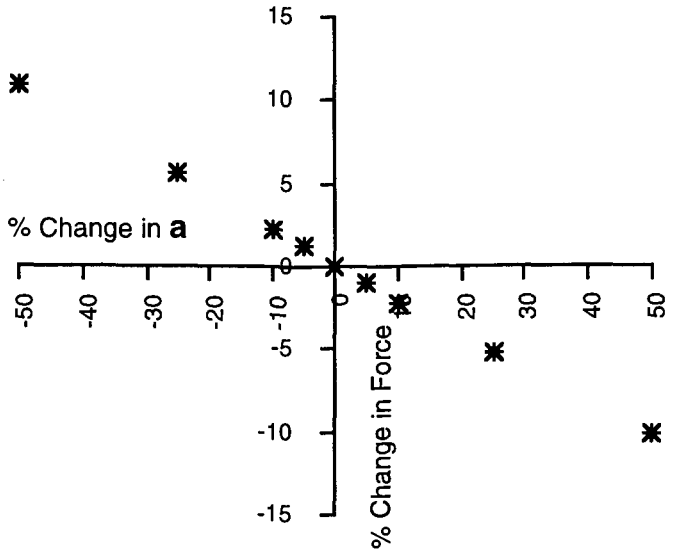

Figure A6. Percent change in peak force as a function of percent change in a.

Table A2 Changes in Peak Force as a Function of Changes in a

Hill's Parameter a	Peak Force (P/Po)	Percent Change
initial	0.557	0%
+ 5%	0.552	-0.9%
+ 10%	0.545	-2.2%
+ 25%	0.528	-5.2%
+ 50%	0.500	-10.2%
- 5%	0.564	+1.3%
- 10%	0.570	+2.3%
- 25%	0.588	+5.6%
- 50%	0.617	+10.8%

A1.5 Hill's parameter *b*

Changes in b had a profound effect of the model's prediction of force. For increases of 50% of the original value, the force increased. Decreases of 50% resulted in a dramatic and much larger drop in force than observed for increase of 50%. This large drop

suggested that there was a non-linear influence of changes in force as a function of changes in ***b***.

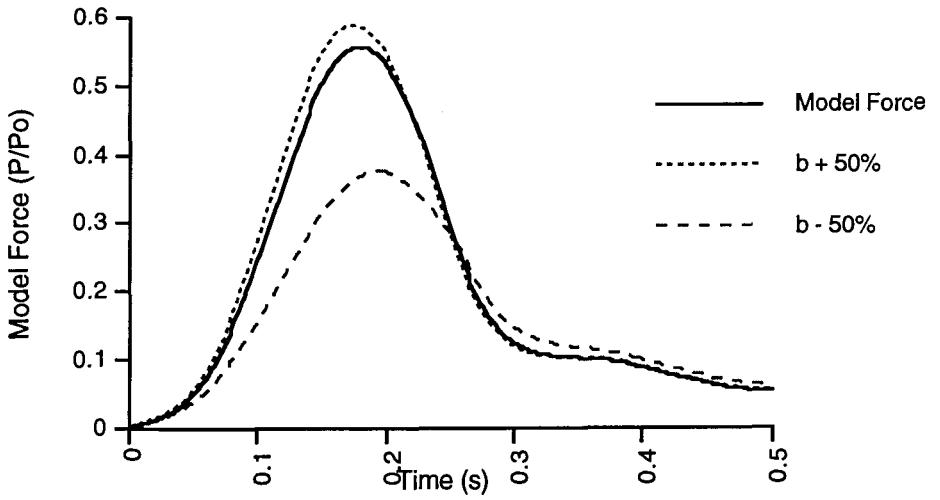

Figure A7. Model prediction of force for simulations using values of ***b*** +/- 50% of original.

The non-linear effect of changes in force as a function of changes in ***b*** are illustrated in figure A8. For increases in ***b*** , the force at any velocity was larger as predicted by the force-velocity relationship. The non-linear effect occured because changes in ***b*** not only shifted the force-velocity upward (increased ***b***) or downward (decreased ***b***), but also changed the concavity or curvature of the relationship. Low values of ***b*** resulted in high curvature or concavity of the force-velocity relationship. As a results greater changes in force for the same percentage change in ***b*** were observed for decreased values than for increased values of ***b*** . These values were summarized in table A3.

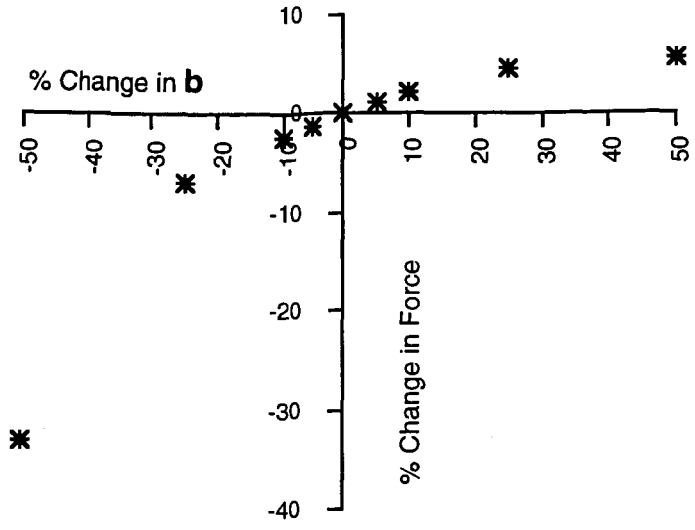

Figure A8. Percent change in peak force as a function of percent change in ***b***.

Table A3 Changes in Peak Force as a Function of Changes in b

Hill's Parameter b	Peak Force (P/Po)	Percent Change
initial	0.557	0%
+ 5%	0.563	+1.1%
+ 10%	0.569	+2.2%
+ 25%	0.582	+4.5%
+ 50%	0.588	+5.6%
- 5%	0.550	-1.3%
- 10%	0.544	-2.3%
- 25%	0.518	-7.0%
- 50%	0.374	-32.9%

A1.6 Summary

From this analysis, it is suggested that the model is most sensitive to changes in fibre stiffness, and parameters of the force-velocity relationship. Since the changes in force observed with changes in fibre stiffness as well as changes in ***a*** and ***b*** could be explained in terms of the force-velocity relationship, it is likely that the force-velocity relationship is

the dominate characteristic in this model. As a result, it is of utmost importance to ensure accurate assessment of the force-velocity characteristics of the muscles which are modelled using this protocol.

Chapter 6

References

Amis, A.A., Dowson, D., Wright, V. (1979). Muscle strengths and musculo-skeletal geometry of the upper limb. *Engineering in Medicine*, 8(1), 41-48.

An, K.N., Horii, E., Ryu, J. (1991) Muscle Function in in Biomechanics of the Wrist Joint. An, K., Berger, R.A., Cooney ,W.P. (eds). Springer-Verlag New York, Chapter 9 pp 157-169.

An, K.N., Hui, F.C., Morrey, B.F., Linscheid, R.L. & Chao, E.Y. (1981) Muscles across the elbow joint: a biomechanical analysis. *Journal of Biomechanics* , 14, 659-669.

An, K.N., Ueba, Y., Chao, E.Y., Cooney, W.P. & Linscheid, R.L. (1983) Tendon Excursion and moment arm of index finger muscles. *Journal of Biomechanics* , 16, 419-425.

Andrews, J.G. & Youm, Y. (1979) A biomechanical investigatino of wrist kinematics. *Journal of Biomechanics* , 12, 83-93.

Armstrong, T.J. & Chaffin, D.B. (1978) An investigation of the relationship between displacements of the finger and wrist joints and the extrinsic finger flexor tendons. *Journal of Biomechanics* , 11, 119-128.

Baildon, R.W.A., & Chapman, A.E. (1983) A new approach to the human muscle model. *Journal of Biomechanics,* 16(10), 803-809.

Baratta, R.V., Solomonow, M., Best, R., Zembo, M., Dambrosia, R. (1995). Architecture-based force-velocity models of load-moving skeletal muscles. *Clinical Biomechanics*, 10(3), 149-155.

Bernhang, A., Dehner, W., & Fogarty, C. (1974). Tennis elbow: a biomechanical approach. *Journal of Sports Medicine*, 2, 235-260.

Bernstein, N.A. (1967). The coordination and regulation of movements. Oxford, Pergamon.

Blackwell, J.R., & Cole, K.J. (1995). Wrist kinematics differ in expert and novice tennis players perfoming the backhand stroke: implications for tennis elbow. *Journal of Biomechanics*, 27(5), 509-516.

Brand, P.W., Beach, R.B. & Thompson, D.E. (1981). Relative tension and potential excursion of muscles in the forearm and hand. *Journal of Hand Surgery*, 6(3), 209-219.

Brumbaugh, R.B. (1982). An invivo study of normal wrist kinematics. *Journal of Biomechanical Engineering*, 104, 176-181.

Buchanan, T.S., Moniz, M.J., Dewald, J.P.A. & Rymer, W.Z. (1993). Estimation of muscle forces about the wrist joint during isometric tasks using an EMG coefficient method. *Journal of Biomechanics*, 26, 547-560.

Butler, D.L., Grood, E.S., Noyes, F.R. & Zernicke, R.F. (1979). Biomechanics of ligaments and tendons. *Exercise and Sport Science Reviews*, 6, 125-173.

Caldwell, G.E. & Chapman, A.E. (1987) Coordination of muscles controlling the human elbow. in Biomechanics XI-A de Groot et al (eds), pp 167-173, Free University Press, The Netherlands.

Caldwell, G.E. & Chapman, A.E. (1989). Applied muscle modelling: application of muscle specific models. *Computers in Biology and Medicine*, 19, 417-434.

Caldwell, G.E. (1987). Applied muscle models in prediction of forces at the elbow. PhD Thesis, Simon Fraser University, Canada.

Caldwell, G.E. (1995). Tendon elasticity and relative length: effects on the Hill two-component muscle model. *Journal of Applied Biomechanics*, 11, 1-24.

Caldwell, G.E. and Chapman, A.E. (1991). The general distribution problem: A physiological solution which includes antagonism. *Human Movement Science* , 10, 355-392.

Capaday, C., Forget, R., & Milner, T. (1994). A re-examination of the effects of instruction on the long-latency stretch reflex response of the flexor pollicis longus muscle. *Experimental Brain Research,* 100, 515-521.

Carlson, G.D., Botte, M.J., Josephs, M.S., Newton, P.O., Davis,, J.L.W. & Woo, S.L-Y. (1993). Morphologic and biomechanical comparison of tendons used as free grafts. *Journal of Hand Surgery*, 18A(1), 76-82.

Carter, R.R., Crago, P.E., & Gorman, P.H. (1993). Nonlinear stretch reflex interaction during co-contraction. *Journal of Neurophysiology*, 69(3), 943-952.

Chapman, A.E. (1985). The mechanical properties of human muscle. *Exercise and Sport Sciences Reviews* , 13, 443-501.

Chen J., Brubaker, C.E. & Sheth, P.N. (1988). Determination of attachment locations of human upper extremity muscles. ICAART, Montreal 138-139.

Close, R.I. (1972) Dynamic properties of mammalian skeletal muscle, *Physiological Reviews* 52, 129-199.

Cutts, A. (1988a). The range of sarcomere lengths in the muscles of the human lower limb. *Journal of Anatomy* , 160, 79-88.

Cutts, A. (1988b). Shrinkage of muscle fibres during the fixation of cadaveric tissue. *Journal of Anatomy*, 160, 75-78.

Cutts, A., Alenxander, R. McN., and Ker, R.F. (1991). Ratios of cross-sectional areas of muscle and their tendons in an healthy human forearm. *Journal of Anatomy*, 176, 133-137.

de Lange, A., Kauer, J.M.G. & Huiskes, R. (1985). Kinematic behaviour of the human wrist joint: a roentgen-stereophotogrammetric analysis. *Journal of Orthopaedic Research,* 3, 56-64.

Drinkwater, D.T. (1984). An Anatomically Derived Method for the Anthropometric Estimation of Human Body Composition. PhD Thesis, Simon Fraser University.

Ebashi, S. & Endo, E. (1968) Calcium and muscle contraction, *Progress in Biophysics.* 18, 123-183.

Edman, K.A.P. (1979). The velocity of unloaded shortening and its relation to sarcomere length and isometric force in vertebrate muscle fibres. *Journal of Physiol (Lond)* , 291, 143-159.

Edmondstone, M.A. (1993). Contribution of muscle to optimal performance in simulated overarm throwing. MSc thesis. Simon Fraser University.

Ettema, G.J.C. & Huijing, P.A. (1990) Architecture and elastic properties of the series elastic element of muscle-tendon complex. In Multiple Muscle Systems. Biomechanical and Movement Organization (J.M Winters and S.L-Y. Woo (eds). Springer-Verlag, New York, pp 57-68.

Faulkner, J.A., Claflin, D.R., McCully, K.K. (1986). Power output of fast and slow fibres from human skeletal muscles. in Human Muscle Power, Jones, N.L., N. McCartney, A.J. McComas (eds). Human Kinemtics, Champaign, Ill, USA, pp81-90.

Gans, C. (1982). Fibre architecture and muscle function. *Exercise and Sport Sciences Reviews*, 10, 160-207.

Gans, C. and Gaunt, A.S. (1991). Muscle architecture in relation to function. *Journal of Biomechanics* , 24, 53-65.

Garcia-Elias, M., Horii, E. & Berger, R.A. (1991). Individual Carpal Bone Motion. in Biomechanics of the Wrist Joint. An, K., Berger ,R.A., Cooney, W.P. (eds). Springer-Verlag New York, Chapter 4, pp 61-77.

Gordon, A.M., Huxley, A.F. & Julian, F.J. (1966). The variation in isometric tension with sarcomere length in vertegrade muscle fibres. *Journal of Physiology. (Lond)*, 184, 170-192.

Guimareas, A.C., Herzog, W., Allinger, T.L., and Zhang, Y.T. (1995). The EMG-force relationship of the cat soleus muscle and its association with contractile conditions during locomotion. *Journal of Experimental Biology*, 198, 975-987.

Hatcher, D.D. & Luff, A.R. (1986) The effect of initial length on the shortening velocity of cat hind limb muscles. *Pflugers Archives*, 407, 369-403.

Hatze, H. (1977) A myocybernetic control model of skeletal muscle. *Biological Cybernetics*, 25, 103-109.

Henneman, E., Somjen, G. & Carpenter, D.O. (1965). Functional significance of cell size in spinal motoneurons. *Journal of Neurophysiology*, 28, 560-580.

Herzog, W., Guimaraes, A.C., Anton, M.G. & Carter-Erdman, K.A. (1991). Moment-length relations of rectus femoris muscels of speed skaters/cyclists and runners. *Medicine and Science in Sports Exercise*, 23, 1289-1296.

Herzog, W., Leonard, T.R., Renaud, J.M., Wallace, J., Chaki ,G. & Bornemisza, S. (1992). Force-length properties and functional demands of cat gastrocnemius, soleus and plantaris muscles. *Journal of Biomechanics*, 25, 1329-1335.

Hill, A.V. (1950) The series elastic component of muscle. *Proceedings from the Royal Society of London.* B137, 273-280.

Hof, A.L. & van den Berg, J. (1981a) EMG to force processing I: An electrical analogue of the Hill muscle model. *Journal of Biomechanics*, 14, 747-758.

Hof, A.L., & van den Berg, J. (1981b) EMG to force processing II: estimation of parameters of the Hill muscle model for the human triceps srae by means of a calfergometer. *Journal of Biomechanics*, 14(11), 759-770.

Hoffer, J.A., Caputi, A.A., Pose, I.E. & Griffiths, R.I. (1989). Roles of muscle activity and load on the relationship between muscle spindle length and whole muscle length in the freely walking cat. *Progress in Brain Research*, 80, 75-85.

Hogfors, C., Sigholm, G. & Herberts, P. (1987). Biomechanical model of the human shoulder -I. Elements. *Journal of Biomechanics*, 20, 157-166.

Horii, E., An, K.N., Linscheid, R.L. (1993). Excursion of prime wrist tendons. *Journal of Hand Surgery*, 18A(1), 83-90.

Hsu, E.S., Patwardhan, A.G., Meade, K.P., Light, T.R. & Martin, W.R. (1993). Cross-sectional geometrical properties and bone mineral contents of the human radius and ulna. *Journal of Biomechanics* , 26, 1307-1318.

Huijing, P.A. & Woittiez, R.D. (1984). The effect of architecture on skeletal muscel performance: a simple planimetric model. *Netherlands Journal of Zoolology*, 34, 21-32.

Huijing, P.A. & Woittiez, R.D. (1985). Notes on planimetric and three-dimensional muscle models. *Netherlands Journal of Zoolology*, 35, 521-525.

Huxley, A.F. (1974). Review lecture: muscular contraction. *Journal of Physiology (London)*, 243, 1-23.

Huxley, A.V. (1957). Muscle structure and theories of contraction. *Progress in Biophysics Biophysiology and Chamistry*, 7, 255-318.

Ingelman, J.P. (1991). Biomechanical Comparison of backhand techniques used by novice and advanced tennis players: implications for lateral epicondylitis. Unpublished Master's Thesis. Simon Fraser University

Jensen, C., Vasseljen, O., Westgaard, R.H. (1993) The influence of electrode position on bipolar surface electromyography recordings of the upper trapezius muscle. *European Journal of Applied and Occupational Physiology*, 67(3), 266-273.

Jewel, B.R. & Wilkie, D.R. (1958). An analysis of the mechanical components in frog's striated muscle. *Journal of Physiology (London)*, 143, 515-540.

Kane, T.R. & Levison, D.A. (1985). Dynamics: Theory and Applications, McGraw-Hill Book Company, New York.

Kawakami, Y., Nakazawa, K., Fujimoto, T., Nozaki, D., Miyashita, M., and Fukunaga, T. (1994). Specific tension of elbow flexor and extensor muscles based on magnetic resonance imaging. *European Journal of Applied Physiology*, 68, 139-147.

Ker, R.F. (1981). Dynamic tensile properties of the plantaris tendon of sheep (ovis aries). *Journal of Experimental Biology*, 93, 283-302.

Kilbreath, S.L. & Gandevia, C. (1993). Neural and biomechanical specializations of human thumb muscles revealed by matching weights and grasping objects. *Journal of Physiology (London)*, 472, 537-556.

Koolstra, J.H., van Eijden, T.M.G.J. & Weijs, W.A. (1989). An iterative procedure to estimate muscle lines of action *in vivo*. *Journal of Biomechanics*, 22, 911-920.

Lambert, C.R., Gladden, L.B. & Stainsby, W.N. (1979). Length-dependent activation of in situcanine skeletal muscle. *American Journal of Physiology*, 237, C38-C42.

Lieber, R.L. & Brown, R.B. (1992). Quantitative method for comparison of skeletal muscle architecture properties. *Journal of Biomechanics*, 25(5), 557-560.

Lieber, R.L., Fazeli, B.M., Botte, M.J. (1990). Architecture of selected wrist flexor and extensor muscles. *Journal of Hand Surgery*, 15A, 244-250.

Lieber, R.L., Jocobson, M.D., Fazeli, B.M., Abrams, R.A. & Botte, M.J. (1992). Architecture of selected muscles of the arm and forearm: anatomy and implications for tendon transfer. *Journal of Hand Surgery*, 17A, 787-798.

Lieber, R.L., Loren, G.J., and Friden, J. (1994). In vivo measurement of human wrist extenor muscle sarcomere length changes. *Journal of Neurophysiology*, 17(3), 874-881.

Lieber, R.L., Woodburn, T.M. & Friden, J. (1991). Muscle damage induced by eccentric contractions of 25% strain. *Journal of Applied Physiology*, 70, 2498-2507.

Lieber, R.L., Woodburn, T.M., & Friden, J. (1991). Muscle damage induced by eccentric contraction of 25% strain. *Journal of Applied Physiology*, 70, 2498-2507.

Lin, D.C. & Rymer, W.Z. (1993). Mechanical properties of cat soleus muscle elicited by sequential ramp stretches: implication for control of muscle. *Journal of Neurophysiology*, 70(3), 997-1008.

Lindahl, O. & Lindgren, A.G.H. (1967). Cortical bone in man. *Acta Orthopaedica Scandinavica*, 38, 133-140.

Loren, G.J., and Lieber, R.L. (in press). Tendon biomechanical properties enhance human wrist muscle specialization. *Journal of Biomechanics,* 28, No. XX, XXX-XXX.

Loren, G.J., Shoemaker, S.D., Burkholder, T.J., Jacobson, M.D., Friden, J., and Lieber, R.L. (in press). Human wrist motors: biomechanical design and application to tendon transfers. *Journal of Biomechanics.*

MacIntosh, B.R., Herzog, W., Suter, E., Wiley, J.P., & Sokolosky, J. (1993). Human skeletal muscle fibre types and force:velocity properties. *European Journal of Applied Physiology.* 67, 499-506.

Mai, M.T. and Lieber, R.L. (1990) A model of semitendinosus muscle sarcomere length, knee and hip interaction in the frog hindlimb. *Journal of Biomechanics,* 23, 271-279.

Mcleish, R.D. & Charnely, . (1970) Abduction forces in the one-legged stance. *Journal of Biomechanics* , 3, 191-209.

Milner-Brown, H.S., Stein, R.B. & Yemm, R. (1973). The orderly recuirment of human motor units during voluntary isometric contractions. *Journal of Physiology (London),* 230, 359-370.

Morris, M., Jobe, F.W., Perry, J. (1989). Electromyographic analysis of elbow function in tennis players. *American Journal of Sports Medicine,* 17, 241-247.

Nathan, R.H. (1990) FNS of the upper limb: targeting the forearm muscles for surface stimulation. *Medicine and Biology in Engineering and Computing,* 28(3), 249-256.

Nathan, R.H. (1992). The isometric action of the forearm muscles *Journal of Biomedical Engineering*, 114, 162-169.

Otten, E. (1988) Concepts and models of functional architecture in skeletal muscle. *Exercise and Sports Sciences Reviews*, 16, 89-137.

Pandy, M.G., Anderson, F.C. & Hull, D.G. (1992). A parameter optimization approach for the optimal control of large-scale musculoskeletal systems. *Journal of Biomechanical Engineering*, 114, 450-458.

Pierrynowski, M.R. & Morrison, J.B. (1985). A physiological model for the evaluation of muscular forces in human locomotion: theoretical perspectives. *Mathematics in Biosciences* 75, 69-101.

Powell, P.L., Roy, R.R., Kanim, P., Bello, M. & Edgerton, V.R. (1984). Predictability of skeletal muscle tension from architectural determinations in guinea pig hindlimbs. *Journal of Applied Physiology*, 57, 1715-1721.

Rack, P.M.H. & Ross, H.F. (1984). The tendon of flexor pollicis longus: its effects on the muscular control of force and position at the human thumb. *Journal of Physiology*, 351, 99-110.

Rack, P.M.H. & Westbury, D.R. (1969). The effect of length and stimulus rate on tension in the isometric cat soleus muscle. *Journal of Physiology (London)*, 204, 443-460.

Riek, S. & Bawa, P. (1992). Recruitment of motor units in human forearm extensors. *Journal of Neurophysiology*, 68, 100-108.

Roetert, E.P., Brody, H., Dillman, C.J., Groppel, J.L. & Schultheis, J. M. (1995). The biomechanics of tennis elbow: An integrated approach. in Clinics in Sports Medicine: Racquet Sports. R.C. Lehman (ed). 14(1), W.B. Saunders Company, Philadelphia, PA, USA.

Ruby, L.K., Cooney, W.P., An, K.N., Linscheid, R.L. & Chao, E.Y.S. (1988). Relative motion of selected carpal bones: a kinematic analysis of the normal wrist. *Journal of Hand Surgery*, 13A, 1-10.

Sacks, R.D. & Roy, R.R. (1982). Architecture of hindlimb muscles of cats: functional significance. *Journal of Morphology*, 173, 185-195.

Savelberg, H.H.C.M., Kooloos, J.G.M., de Lange, A,. Huiskes, R. & Kauer, J.M.G. (1991) Human carpal ligament recruitment and three-dimensional carpal motion. *Journal of Orthopaedic Research*, 9, 693-704.

Savelberg, H.H.C.M., Otten, J.D.M., Kooloos, J.G.M., Huiskes, R. & Kauer, J.M.G. (1993). Carpal bone kinematics and ligament lengthening studied for the full range of joint movement. *Journal of Biomechanics*, 26, 1389-1402.

Sherif, M.H., Gregor, R.J., Liu, L.M., Roy, R.R. and Hager, C.L. (1983). Correlation of myoelectric activity and muscle force during selected cat treadmill locomotion. *Journal of Biomechanics*, 16, 691-701.

Sommer, H.J. & Miller, N.R. (1980). A technique for kinematic modeling of anatomical joints. *Journal of Biomechanical Engineering*, 102, 311-317.

Sutarno, C. G., & McGill, S.M. (1995). Isovelocity investigation of the lengthening behaviour of the erector spinae muscles. *European Journal of Applied Physiology*, 70, 146-153.

Toft, R. & Berme, N. (1980). A biomechanical analysis of the joints of the thumb. *Journal of Biomechanical*, 13, 353-360.

van den Bogert, A.J., Hartman, W., Schamhardt, H.C., and Sauren, A.A.H.J. (1988). *In vivo* relationship between force, EMG and length change in deep digital flexor muscle of the horse. In Biomechanics, XI-A, A.P. Hollander, P.A. Huijing and G.J. van Ingen Schenau (eds), pp. 68-74. Amsterdam: Free University of Amsterdam.

Veeger, H.E.J., van der Helm, F.C.T., van der Woude, L.H.V., Pronk, G.M. & Rozendal, R.H. (1991). Inertia and muscle contraction parameters for musculoskeletal modelling of the shoulder mechanism. *Journal of Biomechanics*, 24, 615-629.

Wilkie, D.R. (1950). The relation between force and velocity in human muscle. *Journal of Physiology (London)*, 110, 249-269.

Winters, J.M. & Stark, L. (1985). Analysis of fundamental movement patterns through the use of in depth antafonistic muscle models. *IEEE Transactions in Biomedical Engineering*, BME-32, 826-839.

Winters, J.M. (1990). Hill-based muscle models: A systems engineering perspective, in Multiple Muscle Systems. Part I: Muscle Modeling, Springer-Verlag, Winters, J.M. & Woo, S.L-Y (eds), pp 69-93.

Woittiez, R.D., Huijing, P.A., Boom, H.B.K., Rozendal, R.H. (1984). A three-dimensional muscle model: a quantified relation between form and function of skeletal muscles. *Journal of Morphology*, 182, 95-113.

Wood, J.E., Meek, S.G. & Jacobsen, S.C. (1989a). Quantitation of human shoulder anatomy for prosthetic arm control-I. surface modelling. *Journal of Biomechanics* , 22, 273-292.

Wood, J.E., Meek, S.G. & Jacobsen, S.C. (1989b). Quantitation of human shoulder anatomy for prosthetic arm control-II anatomy matrices. *Journal of Biomechanics*, 22, 309-325.

Zajac, F.E. (1989). Muscle and tendon: properties, models, scaling, and application to biomechanics and motor control. In CRC Critical Reviews in Biomedical Engineering (Edited by Bourne, J.R.), Vol 17, No 4, pp359-411. CRC Press, Boca Raton, USA.

Zajac, F.E. (1992). How musculotendon architecture and joint geometry affect the capacity of muscles to move and exert force: a review with application to arm and forearm tendon transger design. *Journal of Hand Surgery*, 17, 799-804.

Zuurbier, C.J. & Huijing, P.A. (1992). Influence of muscle geometry on shortening speed of fibre, aponeurosis and muscle. *Journal of Biomechanics*, 25, 1017-1026.